Multiparametric Quantitative MRI of the Liver

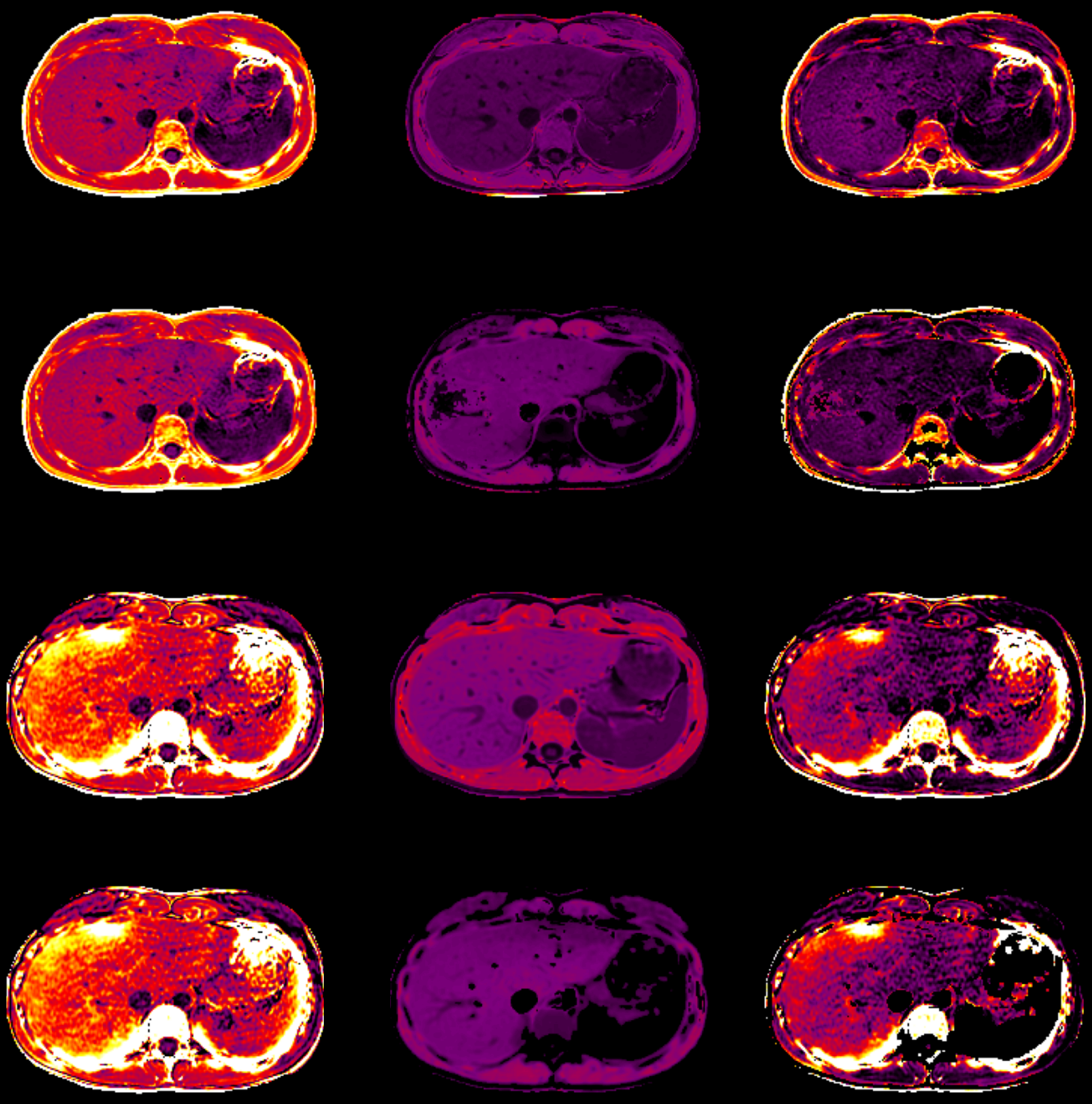

Msc. Thesis Technical Medicine

Inge Bosch

Multiparametric Quantitative MRI of the Liver

Master Thesis Report

by

Inge Bosch

Student number: 4853571

14 August 2025

Thesis in partial fulfilment of the requirements for the joint degree of Master of Science in

Technical Medicine

Leiden University; Delft University of Technology; Erasmus University Rotterdam

Master thesis project (TM30004; 35 ECTS)

Department:	Dept. of Biomechanical Engineering, TU Delft
Track:	Imaging and Interventions
Project Duration:	February, 2025 – August, 2025
Supervisors:	
Technical supervisor:	Dr. Esther Warnert
Medical Supervisor:	Dr. Roy Dwarkasing

Thesis committee members:

Prof. dr. ir. Juan Hernandez Tamames (chair)	*TU Delft & EMC*
UD. dr. ir. Esther Warnert	*Erasmus MC*
Dr. Roy Dwarkasing	*Erasmus MC*

Universiteit Leiden

TU Delft

Erasmus Universiteit Rotterdam

Preface

Dear reader,

Here it is, my master's thesis. Not just the end of 26 weeks of research, but this marks the end of my time as a student. These seven years of studying were wonderful years in which I've grown both professionally and personally.

I've always felt completely at home in Delft in the Technical Medicine program, and I've enjoyed the fun and the people around it even more. From the start, I found myself surrounded by lovely friends. From late-night study sessions and dinners to parties until morning, while still showing up at 8:30 lectures in Delft, Leiden, or Rotterdam. After my gap year contributing to Project MARCH, I chose the Imaging and Interventions track, and to this day, I'm happy with that decision. Medical imaging fascinates me, how we can diagnose and treat people without even touching them. Isn't that amazing? I still want to learn a lot more in this field.

During my master's, I had the opportunity to rotate through four different hospital departments, and each inspired me in its own way. Here, I've learned a lot of clinical and technical skills, from assisting at open-heart surgeries to building machine learning models, from doing outpatient clinics to writing scientific papers. As the cherry on top, I seized the chance to do my final elective internship abroad. I spent three months in Nepal, an experience I can honestly say was one of the best of my life. Together with Alex, I cycled every day with views of 8000-meter peaks to the hospital in this stunning yet primitive country, trying to contribute to healthcare there.

I conducted this master's thesis at the Radiology Department of Erasmus MC, focusing on liver MRI. MRI is the technique I find most fascinating, and most challenging at the same time. I deliberately chose a topic that would push me one more time on the technical side: researching a new technique within MRI. As Mika said, "Impossible is just a really big challenge." And with those encouraging words, I started this project under the guidance of Esther and Roy. They are the first people I want to thank. Thank you, Esther, for your positivity and for all the long meetings where we could brainstorm about complex MRI phenomena, but also laugh a lot and enjoy the process. I've learned much from you. And thank you, Roy, for your trust and the medical expertise you brought to my project. I'm also grateful to all the others who contributed their time and effort to this project.

I want to thank my fellow graduates; without you, this journey would have been far less fun. Daily lunches at 12:00 and coffee runs to "het mannetje". A special thanks to Elisa for listening to all my thoughts and for always celebrating the wins together.

Lastly, I want to thank my family and friends for their love and support, not just during my thesis, but throughout the past seven years. A special thanks to my parents, housemates, and, of course, to Martijn. Thank you for all your hugs and support.

I've truly enjoyed working on this thesis and am grateful to have contributed to this topic.

With pride, I present to you my master thesis. Enjoy reading!

Inge Bosch
Rotterdam, August 2025

Executive Summary

The assessment of functional liver tissue is of growing clinical importance in predicting post-operative outcomes and optimizing liver-directed therapies. Quantitative Blood Oxygen Level Dependent (qBOLD) imaging offers a non-invasive MRI-based method to measure tissue oxygenation via the R2′ relaxation parameter. R2′ is defined as the difference between R2* and R2, and reflects magnetic field inhomogeneities caused by deoxyhemoglobin, among other factors.

This research explores the feasibility of estimating R2′ in the liver using a multiparametric qBOLD (MqBOLD) approach under free-breathing conditions. Two MRI sequences, one for R2 and one for R2* mapping, were optimized and applied at 1.5 T and 3 T. A cohort of five healthy volunteers was scanned to evaluate image quality and relaxation rates across field strengths and breathing techniques.

Results showed that R2′ mapping is feasible using an MqBOLD approach under predominantly free-breathing conditions, without apparent motion artifacts. The mean R2′ values in homogeneous liver parenchyma were 12.7 ± 2.8 s^{-1} at 1.5 T and 24.6 ± 4.8 s^{-1} at 3 T. Both 1.5 T and 3 T proved suitable for R2′ mapping. While 1.5 T offered better image quality, 3 T provided more reliable quantitative results and greater patient comfort.

As a proof of concept, the MqBOLD protocol was successfully integrated into a routine clinical liver MRI scan protocol for a patient with neuroendocrine liver metastasis. The additional scan time was under three minutes, and the resulting relaxation maps showed contrast between tumor and healthy liver tissue.

In conclusion, this research establishes the feasibility of R2′ mapping in the liver using a multiparametric MRI approach under mostly free-breathing conditions. It presents a foundation for non-invasive liver oxygenation imaging, with the potential to evolve into a clinically applicable tool for functional liver assessment.

Contents

Nomenclature

List of Abbreviations

4DMR	Four Dimensional Magnetic Resonance
BH	Breath-Hold
BOLD	Blood Oxygenation Level Dependent
DWI	Diffusion-Weighted Imaging
FB	Free-Breathing
FIESTA	Fast Imaging Employing Steady-State Acquisition
FOV	Field-of-View
FSPGR	Fast Spoiled Gradient Echo
GE	General Electric
GRE	Gradient-Echo
IDEAL-IQ	Iterative Decomposition of water and fat with Echo Asymmetry and Least-squares estimation – Iron Quantification
LAVA FLEX	Liver Acquisition with Volume Acceleration – Flexible
MqBOLD	Multi-Parametric Quantitative Blood Oxygenation Level Dependent
MRI	Magnetic Resonance Imaging
NaN	Not a Number
PE	Phase Encoding
qBOLD	Quantitative Blood Oxygenation Level Dependent
R2’	R2prime
ROI	Region-of-Interest
SI	Superior-Inferior
SMART2Map	Smooth Motion-Assisted Rapid T2 Mapping
SNR	Signal-to-Noise Ratio
T2’	T2prime

List of Symbols

$B0$	Field Strength
T	Tesla

List of Figures

List of Tables

1 Introduction

One of the main challenges in imaging diagnostics of liver (patho)physiology is to obtain an accurate measurement of functional rather than structural tissue volume. The latter, for instance, fails to accurately assess treatment response in liver tumors [1]. Furthermore, the volume of functional liver tissue remaining after partial resection is highly correlated with post-hepatectomy liver failure [2]. However, the current clinical use of testing clearance of indocyanine green from the blood plasma after intravenous injection can only assess the function of the liver globally and is therefore limited in predicting post-hepatectomy liver failure. The alternative, i.e., CT-volumetry, only takes into account the remaining volume after liver resection and does not take into account liver function at all. Accurate determination of functional liver volume remains challenging in clinical practice, as no reliable and feasible monitoring technique is currently available [1][3].

A potential biomarker of tissue function is the local level of oxygenation, as oxygen is key to well-functioning liver tissue. Lack of oxygen, i.e., hypoxia, is an early sign of reduced tissue functioning and causes damage to healthy liver tissue. Moreover, in liver tumors, hypoxia stimulates tumor growth and makes tumors resistant to treatment [4]. Hence, increasing levels of hypoxia are associated with poor outcomes in liver tumors [5], and reoxygenation of tissue is seen either in successfully treated tumors or is of interest as a potentiator of current and novel treatment regimes. Therefore, having a reliable biomarker of liver oxygen levels as a functional index is of great clinical interest. Still, a technique to acquire such an imaging biomarker is currently not available for routine clinical use in liver diagnostics.

An important step forward in this area is the application of quantitative blood-oxygenation level-dependent (qBOLD) magnetic resonance imaging (MRI), which has been used in the brain to measure oxygen content. This method is based on the estimation of R2prime (R2′), which represents the mesoscopic transverse relaxation rate of water protons. This rate depends on the amount of local deoxyhemoglobin [6]. Currently, qBOLD techniques are optimized and validated for use in the brain [7]. However, the feasibility of qBOLD in the liver has previously been published [8].

A robust implementation of qBOLD is multi-parametric qBOLD (MqBOLD), which involves separately acquiring R2 and R2* maps to estimate R2′. R2′ is a component of the effective transverse relaxation rate (R2*), which reflects the combined effects of intrinsic spin-spin interactions (R2) and magnetic field inhomogeneities (R2′). R2′ can be seen as the difference between R2* and R2 [9]. Since R2′ cannot be directly measured, it is estimated by subtracting R2 from R2*, both of which are acquired separately.

For MqBOLD imaging to be effective in the liver, it is essential to adapt and optimize MRI acquisition techniques to account for the physiological and structural characteristics of hepatic tissue. Using MqBOLD imaging for the liver could enhance the non-invasive assessment of liver function and physiology, hereby providing a valuable tool for clinical diagnostics and treatment planning [8]. One important aspect to overcome for accurate estimation of R2′ for MqBOLD imaging is the respiratory motion of the liver. While this can be done by acquiring MRI data during breath-holds (BH), free-breathing (FB) approaches are more favorable to optimize patient compliance and comfort. Another important aspect is the impact of the field strength used for image acquisition. To obtain optimal data for fitting R2′, the signal must be measurable and accurate. Therefore, a high SNR is required, with a minimal number of artifacts occurring in the images. The impact of using different field strengths on the estimation of R2′ must be understood to select the optimal field strength.

This thesis aims to answer the following research question: Can the R2′ relaxation rate be accurately estimated in the liver using MqBOLD MRI under FB conditions, and which field strength yields the most accurate estimation?

This thesis addresses the research question through the following structure:

Chapter I presents the literature review I wrote in advance of my thesis, which explores the optimal and most feasible approach for estimating R2′ in the liver. It focuses on the most suitable MRI sequences, breathing approaches, and field strengths, based on current literature. This chapter also includes a detailed description of the MRI sequences used in this study. **Chapter II** outlines the methodology of the proof-of-concept study. It begins with a preliminary scan of a single volunteer, during which the scan protocol was developed and optimized. This is followed by scanning a cohort of five healthy volunteers to assess whether R2′ can be accurately estimated in the liver during FB, and to determine the optimal field strength for this imaging protocol. Finally, patient scans were performed to investigate the contrast in R2′ values between healthy and abnormal liver tissue. **Chapter III** presents the results of the study, while **Chapter IV** provides the discussion and conclusions drawn from the findings.

Part I

Background

2

Literature Review

Note: This literature review was originally conducted as part of a separate course (TM30003) and is included here as background information.

Free-Breathing R2' Measurement in the Liver

Inge T. Bosch, Roy S. Dwarkasing, Esther A.H. Warnert

Abstract

Accurate assessment of functional liver volume is of clinical interest in predicting treatment response and avoiding post-hepatectomy liver failure. Quantitative Blood Oxygen Level Dependent (qBOLD) imaging offers a non-invasive way to measure tissue oxygenation by fitting R2', a parameter related to local deoxyhemoglobin levels. This review explores the optimal strategy for measuring R2' in the liver using free-breathing MRI techniques. Among various methods, multi-parametric qBOLD with a self-gated free-breathing approach emerges as the most feasible technique. This approach could improve the clinical assessment of liver function and aid in treatment planning for liver diseases.

1. Introduction

One of the main challenges in imaging diagnostics of liver (patho)physiology is to obtain accurate measurement of functional rather than structural tissue volume. The latter is failing to accurately assess treatment response in liver tumors (1). Furthermore, the volume of functional liver tissue remaining after partial resection is highly correlated with post-hepatectomy liver failure (2). However, the current clinical use of testing clearance of indocyanine green from the blood plasma after intravenous injection can only assess function of the liver globally and is therefore limited in predicting post-hepatectomy liver failure. The alternative, i.e. CT-volumetry, only takes into account the remaining volume after liver resection and not liver function. Accurate determination of functional volume therefore remains difficult in clinical routine because clinically feasible and reliable monitoring of tissue function for the liver is currently not available (1,3).

A potential biomarker of tissue function is the local level of oxygenation, as oxygen is key to well-functioning liver tissue. Lack of oxygen, i.e. hypoxia, is an early sign of reduced tissue functioning and causes damage to healthy liver tissue. Moreover, in liver tumors hypoxia stimulates tumor growth and makes tumors resistant to treatment (4). Hence, increasing levels of hypoxia in liver tumors are associated with poor clinical outcome (5), and reoxygenation of tissue is seen either in successfully treated tumors or is of interest as a potentiator of current and novel treatment regimes. Having a reliable biomarker of liver oxygen levels as a functional index is therefore of great clinical interest, but a technique to acquire such an imaging biomarker is currently unavailable for routine clinical use in liver diagnostics.

An important step forward in this area is the application of qBOLD imaging, which has been used in the brain to measure oxygen content. This method is based on the measurement of R2', which represents the mesoscopic transverse relaxation rate. This parameter depends on the amount of local deoxyhemoglobin (6). Currently, qBOLD techniques are optimized and validated for use in the brain (7). However, the feasibility of qBOLD in the liver has previously been published (8).

For qBOLD imaging to be effective in the liver, it is essential to adapt and optimize MRI acquisition techniques to account for the physiological and structural characteristics of hepatic tissue. Using qBOLD imaging for the liver could enhance the non-invasive assessment of liver function and physiology, providing a valuable tool for clinical diagnostics and treatment planning (8). One important aspect to overcome for accurate measurement of R2′ for qBOLD imaging is the respiratory motion of the liver. While this can be done by acquiring MRI data during breath holds, free-breathing approaches are more favorable to optimize patient compliance and comfort. Another important aspect to investigate is the impact of field strength (1.5T or 3T) on the estimation of R2′ in the liver. Where higher field strength in general leads to an increase in SNR in MR images, it also comes with increased senstitivty to field inhomogeneities that affects the measured transverse relaxation rates. To choose the most optimal field strength for R2′ measurements in the liver, the impact of using the different field strengths has to be understood. This literature review aims to explore the optimal approach for measuring R2′ in the liver, in terms of MRI sequence, breathing approach, and field strength.

2. Background

2.1 Anatomy and function of the liver

The liver is the largest internal organ in the body, consisting of eight segments across two main lobes, and is positioned in the abdominal cavity, directly beneath the diaphragm (9,10). The liver is essential for maintaining homeostasis through macronutrient metabolism, blood regulation, detoxification, and protein synthesis, including glucose storage, lipid metabolism, and nitrogen waste elimination (11).

The liver accounts for 20% of total body oxygen consumption and has a more complex circulation than other organs, because of its dual blood supply (12). The combined hepatic blood perfusion rate is ~1.1 ml/g/min, which is 2-3 times the amount of the brain (13,14). 75%-80% of the blood entering the liver is partially deoxygenated, nutrient-rich venous blood supplied by the portal vein. The remaining 20–25% oxygen-rich blood is delivered by the hepatic artery (12). While the portal vein carries partly deoxygenated blood and the hepatic artery supplies fully oxygenated blood (15), hepatic oxygenation depends almost equally on both vessels (12). The oxygen- and nutrient-rich blood is mixed and distributed throughout the liver via capillaries, called sinusoids. The deoxygenated blood drains into central veins, which converge into hepatic veins. The liver has a major role as a blood volume reservoir, as it can fit up to one-fifth of the body's total blood volume (9,16).

To maintain vital functions, blood flow to the liver and the hepatic oxygenation status have to be kept on a high level (17). Normal partial pressure of oxygen (pO2) in the liver ranges between 30-40 mmHg in healthy tissue (18–20). A reduced oxygenation status, defined as hypoxia when pO2 drops below 10 mmHg (20), can indicate cellular dysfunction and has been linked to various liver pathologies (8,21). For example, hepatocellular carcinoma (HCC) is characterized by regional hypoxia due to rapid tumor growth that outpaces the formation of

functional blood vessels (18). Hypoxia in the liver can alter cellular metabolism, impair function, and promote disease progression (4).

2.2 Oxygen properties in MR signal

Oxygen is transported in the blood, which primarily consists of plasma and erythrocytes. Water molecules in plasma are detectable by MRI as bulk water, which accounts for 90% of the blood volume. Oxygen binds to hemoglobin, a protein in erythrocytes composed of four subunits, each containing a heme iron that can bind one oxygen molecule, enabling each hemoglobin to carry four oxygen molecules. Heme iron in the ferrous state not only allows oxygen binding but also provides magnetic properties relevant for MRI (22,23).

Oxygen binds to hemoglobin, forming oxyhemoglobin. In tissues, oxygen is released from the hemoglobin to meet metabolic demands. After release of the oxygen molecules, the hemoglobin is referred to as deoxyhemoglobin (24). When blood is removed from the circulation, hemoglobin undergoes oxidative denaturation to form methemoglobin, which contains iron in the ferric state (23).

Important in MRI are the properties of hemoglobin. Oxyhemoglobin does not possess any unpaired electrons. Deoxyhemoglobin contains four unpaired electrons and methemoglobin of five, giving them paramagnetic properties. This affects the relaxation time of water molecules in MRI (23).

2.3 Respiratory motion in MRI

A challenge in MRI of the abdomen is the periodic motion associated with respiratory movement, which gives motion artifacts (25). The respiratory cycle, lasting about 4–5 seconds at rest, causes significant movement of structures like the diaphragm, directly impacting abdominal motion (26). The movement of the abdominal structures (e.g. the liver) is non-rigid (27). However, it is known that the largest effect is in the displacement along the superior-inferior direction. Therefore, this is the direction in which the motion artifacts should be mostly minimized (28).

3. Literature search method

3.1 Search strategy

A systematic search for this review was performed in January 2025 in the following databases: Medline, Embase, Web of Science Core Collection, Cochrane Central Register of Controlled Trials, and Google Scholar. The search was conducted by combinations of the following terms: "R2'", "R2 prime", "qBOLD", "quantitative BOLD", and "qBOLD liver". Full details of the search strategy are provided in Appendix A.

After evaluation of the titles and abstracts, the full text of the non-preliminary eliminated studies was evaluated. Selected studies were further assessed for their fit to the inclusion and exclusion criteria. Studies investigating qBOLD or R2′ MRI of the thorax or abdomen were

included. Snowballing was applied by manually evaluating the reference lists of each included study to avoid missing relevant studies.

3.2 Eligibility criteria

The following inclusion criteria were applied: studies conducted on the abdomen or thorax of either humans or animals. Studies focusing on T2′/R2′ or qBOLD were included, as well as those investigating R2. T2′ represents the reversible transverse relaxation time, the inverse of R2′.

The exclusion criteria were as follows: studies focusing exclusively on the brain; studies investigating singularly R2* instead of R2 and R2′; studies utilizing techniques other than MRI; and studies not conducted on humans or animals.

3.3 Results

The initial search yielded 529 studies. After screening titles and abstracts, 431 studies were excluded due to irrelevance, leaving 98 studies for full-text evaluation. Following this assessment, ten studies met the inclusion criteria and were included as the core literature for this review.

These ten core studies served as the foundation for further literature exploration through snowballing. The core studies are highlighted in the reference section for clarity.

4. Findings

4.1 Principles of Quantitative BOLD and R2′ Mapping

An MR signal is generated by applying radiofrequency pulses that rotate the proton magnetic moment into the transverse plane relative to the main magnetic field. In the transverse plane, the loss of phase coherence among spins is referred to as transverse relaxation. T2 relaxation time is the time it takes for transverse magnetization to decay to a set fraction of its initial value. Phase differences are influenced by local magnetic fields, resulting in diamagnetic and paramagnetic relaxation (23). Oxygenated hemoglobin has diamagnetic properties, meaning the transverse relaxation of fully oxygenated blood is dominated by spin-spin relaxation effects, which come from microscopic variations. However, deoxygenated hemoglobin is paramagnetic and has a strong effect on transverse relaxation. It causes differences in precession frequencies of spins present in or around deoxygenated hemoglobin pools, caused by mesoscopic inhomogeneities (23).

Blood Oxygen Level Dependent (BOLD) MRI uses the deoxygenated hemoglobin as an endogenous paramagnetic contrast agent (8). Paramagnetic contrast agents reduce the relaxation times of the water protons in a concentration dependent manner. In regions with a higher concentration of paramagnetic contrast agent, the MRI contrast increases (29). The paramagnetic properties of deoxygenated hemoglobin lead to dephasing of hydrogen spins, and thus a stronger signal (8).

This BOLD technique has been applied to provide non-invasive qualitative measurements of tissue oxygenation (8). However, BOLD does not provide direct quantitative measurements of blood oxygenation (30). BOLD signal is influenced by parameters other than blood oxygenation, such as regional blood volume, blood flow, and tissue composition (8). Because BOLD signal is unable to separate the contribution of blood oxygenation, an increased signal can be caused by either an increased blood volume or decreased blood oxygenation (31).

Unlike conventional BOLD, which can only reflect relative changes in blood oxygenation, qBOLD enables absolute measurements of tissue oxygen metabolism (30). qBOLD has proven to be a promising technique for measuring baseline oxygenation parameters in a broad range of pathologies, such as in the brain, breasts, liver and kidneys (31,32).

qBOLD oxygenation parameter measurements are based on fitting R2′ signal, the mesoscopic transverse relaxation rate. R2' plays a crucial role in quantifying tissue oxygenation, as it specifically reflects the magnetic field inhomogeneities caused by local inhomogeneities, partly due to the presence of paramagnetic deoxygenated hemoglobin. R2′ is a component of the effective transverse relaxation rate (R2*), which reflects the combined effects of intrinsic spin-spin interactions (R2) and magnetic field inhomogeneities (R2′). R2′ can simply be seen as the difference between R2* and R2 (33).

The original qBOLD model is based on the theory of nuclear magnetic resonance (NMR) signal behavior in magnetically inhomogeneous tissues described by Yablonsky and Haacke (33). They described that while the underlying mechanism of microscopic relaxation (T1 and T2) relies on quantum principles, relaxation in biological systems, such as the human body, is also affected by static field inhomogeneities. These inhomogeneities arise from factors like paramagnetic blood vessels, natural iron deposits in the liver, and deoxyhemoglobin in the blood. Unlike microscopic relaxation, NMR signal formation under static field inhomogeneities can be modeled using a macroscopic framework that accounts for the spatial distribution of the magnetic field. R2′ reflects the contribution to signal relaxation due to local field inhomogeneities and can be described as the product of the nuclear gyromagnetic ratio and the field change within the voxel volume of interest (33).

The original qBOLD model described by He & Yablonski (6) relies on the assumption of randomly oriented blood vessels for accurately assessing tissue oxygenation. The liver's microvasculature differs significantly from the microvasculature of the brain, for which the original qBOLD model was designed (34). In the brain, the predominantly isotropic and randomly oriented vasculature leads to uniform magnetic field inhomogeneities, enabling a direct relationship between qBOLD signal changes and deoxyhemoglobin concentration. In contrast, the liver's more organized vascular structure, especially near major vessels, leads to anisotropic magnetic field distributions, complicating qBOLD signal interpretation (8).

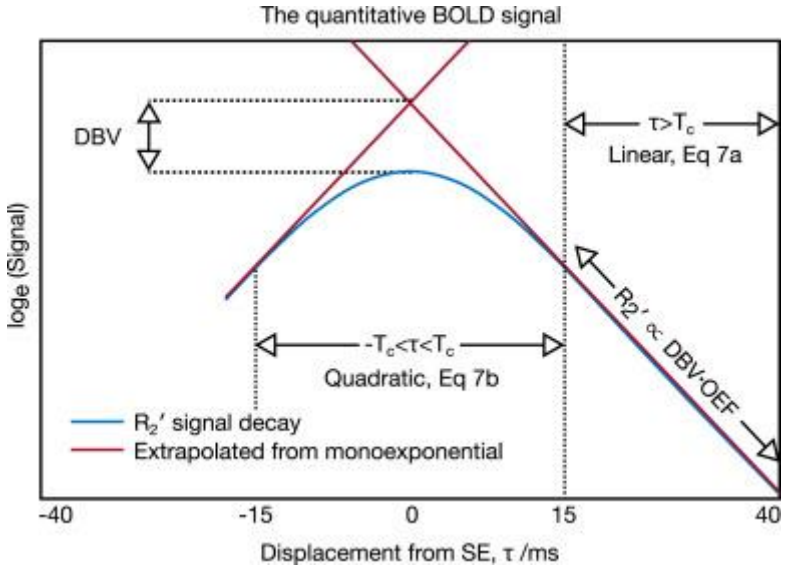

Figure 1: The qBOLD signal. Reprinted from Stone et al. (7)

Traditionally, BOLD models are unable to separate the contributions of blood oxygenation level and blood volume to the transverse signal decay (31). In the brain, it is known that the R2′-weighted signal behaves differently in two different regimes of spin echo displacement time (τ): the short τ and long τ timescales, as visualized in Figure 1 (7). For the long τ timescale, the measured R2′-signal amplitude is linearly exponential. However, for the short τ timescale, the R2′-signal decays with a quadratic exponential profile. In both timescales, R2′ decay is superimposed on the underlying R2 decay of tissue, which is affected by the blood volume. By distinguishing the linear and quadratic regimes, the contribution of the blood volume to the R2′ signal can be disentangled, thereby allowing for more accurate oxygenation assessments (7).

There are two main methods to measure R2′. The first approach involves a direct measurement of R2′. The second approach is by measuring R2 and R2* separately and taking the difference between the two.

4.1.1 Method 1: Direct measurement of R2′

Direct measurement of the R2′ signal relies on its echo time (TE)-dependent behavior, as previously described. This relationship is influenced by factors such as the volume fraction of field-creating structures, the magnetic field strength, and the magnetic susceptibility difference between tissues (33).

4.1.1.1 GESSE sequence

The sequence used by He & Yablonski (6) to perform qBOLD MRI is the Gradient Echo Sampling of Spin Echo (GESSE) technique, visualized in Figure 2a. Here, for every phase encoding step, a spin echo signal is produced and sampled with many very rapid gradient echo readouts before and after the echo time. Thus, GESSE has a fixed spin echo moment and changes the gradient echo time (6). Due to the many gradient echo readouts, high temporal resolution is gained. The phase data of GESSE can be used to determine R2′ directly (35).

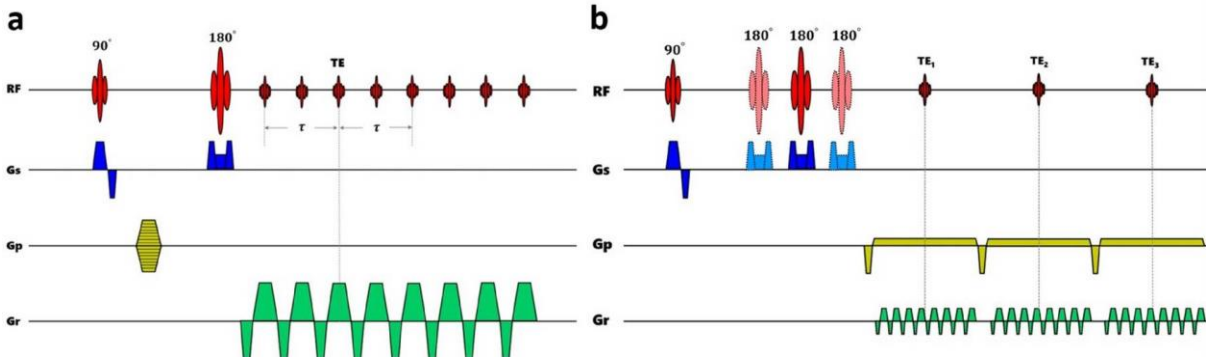

Figure 2: qBOLD sequences (a) GESSE; (b) ASE. Reprinted from Li et al. (36)

4.1.1.2 ASE sequence

The asymmetric spin echo (ASE) sequence is visualized in Figure 2b. In contrast to GESSE, ASE has a fixed gradient echo time and changes the spin echo moment by shifting the position of the 180° pulse in time (36). This way every acquisition happens in the same timeframe after the excitation, and R2 can be considered as a constant weighting due to the fixed echo time (37). Using ASE, R2′ can directly be measured in a relatively short acquisition time (38).

4.1.2 Method 2: indirect measurement of R2′

4.1.2.1 Multi-parametric qBOLD

In multi-parametric quantitative BOLD (MqBOLD), the R2, and R2* relaxation parameters and the blood volume are acquired separately (39). R2 and R2* maps display the pixelwise relaxation rate (Hz), in which the intensity of each voxel is the output of a calculation performed independently at each corresponding spatial pixel from a series of input images acquired with increasing TE (40). They are created by fitting the signal intensity of all echo times at each pixel to a mono-exponential decay curve using a maximum likelihood expectation maximization algorithm. Parametric maps can be automatically generated by the MRI scanner during image acquisition (41,42).

T2 is the inverse of R2 and defined as the time in milliseconds by which the transverse magnetization has decayed to 37% of the original value. For T2 transverse relaxation time mapping, multiple images with increasing T2 preparation times are employed to generate a transverse relaxation curve. A long repetition time is used to allow complete T1 relaxation, effectively minimizing the effect of T1 relaxation to confound T2 estimates. The T2 map value reflects the calculated T2 relaxation time at each pixel (40). T2 mapping can be achieved by using spin echo sequences such as: Turbo Spin Echo (TSE), multi-echo spin echo, or T2-prepared Balanced steady-state free precession (bSSFP) (42).

T2* is the inverse of R2* and is defined as the decay time in transverse magnetization due to the combined effect of field inhomogeneities and spin dephasing. T2* quantification is performed using GRE imaging, where multiple echoes are collected following each excitation

pulse until transverse magnetization fully decays. Quantifying the T2* is done by pixel-wise fitting of signal intensity for each pixel within the multi echo GRE image series (42).

In the MqBOLD approach, R2′ is derived using: R2′ = R2* - R2. However, the blood volume cannot directly be measured from the R2′ signal as in direct qBOLD measurements. Therefore, a separate perfusion scan has to be used to enable differentiation of the local oxygen information and the blood volume (43). In figure 3 an overview of MqBOLD is given as an example.

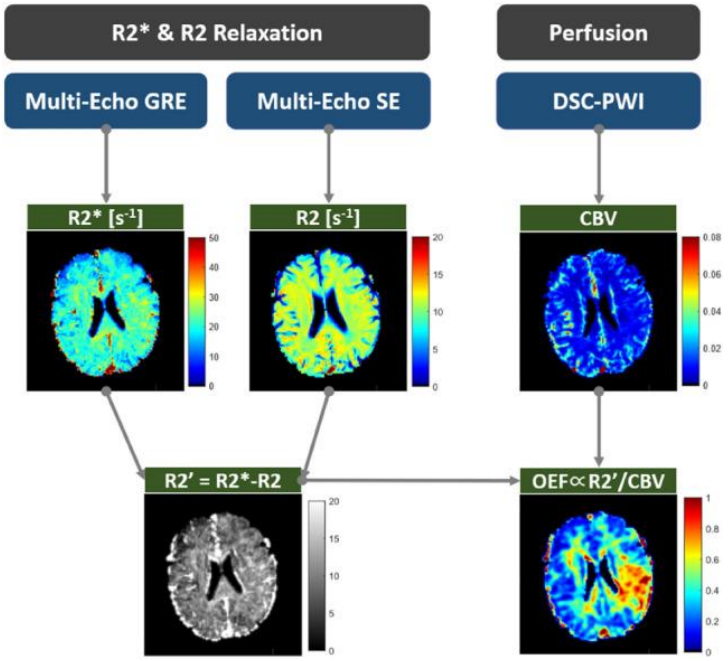

Figure 3: Example overview of the MqBOLD approach. Reprinted from Li et al. (36)

4.2 Field strength analysis

The field strength of the MRI scanner significantly impacts the accuracy and feasibility of R2*, and hence R2′, and BOLD-based measurements. This is due to its effect on local inhomogeneities in the main magnetic field, which in turn affect relaxation rates, and required shimming and echo times. Multiple studies have demonstrated that R2* increases linearly with field strength, which necessitates shorter echo times at higher fields to accurately quantify R2* (44).

For instance, Storey et al. (44) compared liver images and R2* maps by scanning the same patient with two different field strengths, 1.5T and 3T. They found that the liver exhibits a higher R2* at 3T than at 1.5T. R2* increases linearly with field strength. The apparent scaling of R2* with field strength means that shorter echo times are needed to quantify R2* at stronger fields (44). Similarly, Alam et al. (37) concluded that 1.5T remains the preferred field strength for R2* in clinical practice, as there are no clear advantages for using 3T (37).

Silvennoinen et al. (45) further investigated the dependence of blood R2 and R2* on oxygen saturation at 1.5T and 4.7T. They found that qBOLD effects at higher field strengths become

increasingly difficult, particularly in gradient echo sequences, which exhibit poorer spatial quality at low oxygenation levels compared to spin echo sequences. Importantly, their study showed that the oxygenation dependence of R2 and R2' is similar at both low and high field strengths, with R2' increasing only slightly as oxygenation decreases (45).

4.3 Breathing approach

4.3.1 Breath-holds

To overcome the limitation of respiratory motion, using a breath-hold for image acquisition remains a key component in liver MRI to reduce artifacts. The required duration for a single breath-hold typically is 15-20 seconds (46). End-expiration is mostly used because it represents the longest motionless phase in the respiratory cycle. However, inadequate breath-holding still leads to artifacts (47). Failed breath-holding can produce substantial image blurring, resulting in degraded image quality and/or image misregistration (46). Subsequently, patients with diminished breath-hold capacity present a challenge to the breath-holding approach (48,49). Besides, breath-holding leads to increased vascular CO2 levels and thus vasodilation, thereby causing an elevation in R2 and R2*, and therefore a change in BOLD signal (50). The MRI resolution is often sacrificed to shorten the acquisition time to the limit of the patient's breath-hold (49,51).

4.3.2 Free-breathing

Another method to overcome respiratory motion artifacts is to use an image acquisition that is compatible with free-breathing. One free-breathing approach is to use a sequence with a short acquisition time such that the extent of respiratory motion is negligible. An image acquisition time window of 0.5 to 1 second is required to "freeze" the respiratory motion (28).

A second free-breathing approach relies on a surrogate signal of respiratory motion. This can consist of respiratory triggering or gating techniques. Patients can breathe normally during an MRI examination. Data can be either collected at the same phase during the respiratory cycle (triggering) or acquired continuously and selected retrospectively (gating) (46).

The correlation between the surrogate signal and actual respiratory motion must be accurate, especially in the superior-inferior direction, which requires a high signal frequency for sufficient sampling (28). There are multiple methods to measure the motion surrogate signal.

One is a respiratory bellow, which expands/contracts during inflation/deflation generating breathing waveforms that enable respiratory gating. However, this gives an oversimplification showing only an indirect and qualitative breathing pattern (52).

A second possibility is using dedicated navigator readout lines or echoes interleaved with the imaging acquisition. Here, tracking of the diaphragm is possible by using a readout line along the superior-inferior direction. This is a direct and quantitative measurement, however requiring a slight increase in the acquisition time (28).

A third option is self-gating or self-navigation, where the surrogate signal to measure the respiratory motion is directly estimated from the acquired imaging data. Eliminating the need for additional intermediate navigation scans. This is only possible using a specific read-out, namely non-Cartesian k-space trajectories, because they continuously sample the center of k-space, which allows for detection of respiratory motion (53).

5. Discussion

Accurately fitting R2′ is the first step in quantifying oxygenation non-invasively in the liver and thus in obtaining accurate measurement of functional tissue volume. This literature review explored the optimal qBOLD approach for measuring R2′ in the liver using a free-breathing approach. Several acquisition strategies were evaluated, including GESSE and ASE that directly estimate R2′, and an MqBOLD-compatible approach, in which R2′ is fitted through separately mapping R2 and R2*. For the latter, an additional perfusion measurement is needed to enable differentiation of the local oxygen information and the blood volume. Field strength and respiratory motion were identified as key factors affecting the measurement of R2′ in the liver.

Among the discussed techniques, MqBOLD, using a free-breathing approach, appears the most promising for R2′ mapping in the liver, while no conclusion can be drawn for the optimal field strength. In contrast to direct qBOLD approaches, MqBOLD estimates a single parameter per acquisition, reducing the demand on signal-to-noise ratio. This is advantageous in hepatic imaging, where susceptibility to respiratory motion artifacts is challenging. Moreover, MqBOLD leverages existing non-EPI MRI sequences that are already available for liver imaging. Although MqBOLD requires accurate registration between the scans and requires perfusion mapping for translating the R2′ map to oxygenation, it currently represents the most robust and feasible approach for non-invasive R2′ quantification in the liver.

5.1 Comparison of Direct and Indirect qBOLD Approaches

Assessing oxygenation using GESSE and ASE requires a high signal to noise ratio (SNR), because of the high demand in the multi-parameter fitting of the qBOLD model (54). In addition, Sedlacik and Reichenbach conducted a phantom study (55) demonstrating that simultaneously quantifying oxygenation and blood volume could result in large variations because these parameters have an interdependent influence on the BOLD signal. However, by fixing one of these parameters beforehand, the other could be estimated with greater accuracy (55).

When using GESSE, every gradient echo is sampled at a different time point from the excitation pulse. Therefore, the signal is weighted by both R2′ and R2, necessitating correction. An additional disadvantage of acquiring one phase encoding step per TR is the long acquisition time, adding the risk of patient movement between TRs, causing motion artifacts. Besides, a longer acquisition time makes clinical implementation more challenging (36).

Unlike GESSE, ASE acquires spin-echo signals with asymmetrically shifted echo times, allowing for improved separation of R2 and R2′ contributions (6). The ASE sequence combined with an echo planar imaging (EPI) readout method reduces scanning time compared to GESSE, partly overcoming the problem of motion sensitivity due to the long acquisition (38). For this reason, ASE is more widely used in clinical research than GESSE (36). However, while EPI-based acquisitions are commonly used in brain imaging, their application in liver imaging presents additional challenges (6). The proximity of the liver to the lungs can lead to increased susceptibility artifacts due to air-tissue interfaces, while abdominal motion during free-breathing introduces additional artifacts that EPI does not effectively compensate for, making it less suitable for hepatic imaging (56).

Compared to ASE and GESSE, fitting R2 and R2* separately as in MqBOLD does not require additional optimizing or development of MRI sequences, but mostly combines already available sequences for the liver. However, adjustments might be needed to obtain similar acquisition strategies between sequences, for example in terms of breathing approach. MqBOLD is less dependent on a high SNR than direct qBOLD measurements, because only one parameter per acquisition must be fit. This allows for higher spatial resolution images, what makes MqBOLD a relatively straightforward and clinically accessible method for oxygenation measurements. However, to accurately measure oxygenation from the R2′ signal, MqBOLD relies on additional accurate perfusion data to estimate blood volume, which currently requires a contrast agent injection, making MqBOLD a partially invasive method (36). Furthermore, MqBOLD requires a registration step, as it involves multiple MRI scans for quantitative analysis. The separate acquisitions must be accurately registered to prevent motion-induced artifacts that could affect results. To ensure accurate registration, all scans should ideally be acquired using similar acquisition strategies. Combining different methods, such as free-breathing, breath-hold, 3D, and 2D sequences, can introduce spatial inconsistencies that complicate the registration process and reduce the reliability of the quantitative analysis (57).

Comparing ASE, GESSE and MqBOLD, MqBOLD is currently selected as the preferred approach for measuring R2′, based on its suitability for liver imaging. R2 and R2* sequences are currently available for liver imaging. Additionally, unlike ASE and GESSE which are commonly implemented with EPI-based readouts, both R2* and R2 mapping sequences rely on non-EPI acquisitions, which are more robust for liver imaging. Non-EPI techniques are less susceptible to macroscopic field inhomogeneities, thereby reducing signal drop-out and distortions that are common in hepatic imaging due to susceptibility differences at air-tissue interfaces (56). Although non-EPI readouts could theoretically be combined with ASE or GESSE, such implementations have not yet been optimized for liver R2′ mapping. By leveraging and optimizing existing non-EPI sequences, MqBOLD provides a practical and clinically feasible option for R2′ measurement in the liver.

5.2 Field strength analysis

Based on current literature, no definitive conclusion can be drawn regarding the optimal field strength for R2' measurements. While it is known that R2* signal and SNR increase with field strength, making high-field imaging theoretically attractive, clinical studies have not demonstrated a clear advantage. Moreover, higher field strengths are associated with an increased risk of artifacts, such as air-tissue susceptibility artifacts. Since no comparative studies have been conducted on low versus high field strength for R2′ measurement in the liver, no clear conclusion can be made based on existing literature (44,45,58).

5.3 Breathing approach

This article discusses multiple breathing approaches, including several free-breathing methods. These free-breathing approaches allow extension of the acquisition time, which can enhance SNR and thus allow for improved anatomical detail (59). However, one of the limitations is the relatively long scan time (60). Among the available free-breathing techniques, self-gating or self-navigation appears to be the most optimal, as it eliminates the need for external respiratory monitoring via belts or additional navigator scans. A study of Zhong et al. (61) found that their free-breathing stack-of-radial self-gating method corrects the respiratory motion bias and enables accurate R2* quantification of liver (61). Additionally, a study of Kee et al. (62) compared breath-holding with a Cartesian K-space read-out, free-breathing with a Cartesian read-out and free-breathing with a non-Cartesian read-out for R2* mapping of the liver. This study concludes that free-breathing with non-Cartesian read-out enabled motion-robust, ungated, and free-breathing R2* mapping of the liver, with comparable R2* measurements and image quality to breath-holding with Cartesian read-out, and better image quality than free-breathing with Cartesian read-out (62). However, implementing a free-breathing approach remains technically more challenging than breath-hold imaging.

5.4 Translating R2′ signal to oxygenation

There are challenges in the translation step from R2' signal to determining oxygenation. The qBOLD model considers a single extravascular tissue compartment and assumes that BOLD measurement is only associated with deoxygenated blood. However, there are multiple influencing factors other than blood oxygenation including hepatic blood volume, and intrinsic liver tissue parameters such as iron concentration. The hepatic iron concentration can modulate the magnetic susceptibility difference between hepatic venous blood and hepatic tissue. When not considered, this can influence the estimation of oxygenation (8).

Additionally, it is known that microvasculature in the liver differs from the microvasculature in the brain, for which the original qBOLD model was designed (8). Wengler et al. (8) addressed this challenge by proposing a hepatic qBOLD model that accounts for the unique vascular architecture of the liver. Through Monte Carlo simulations, they identified significant estimation biases due to the non-random vessel orientation and high blood volume fraction in hepatic tissue. To mitigate these biases, they developed calibration curves to correct the

estimations, enabling more accurate non-invasive mapping of hepatic blood volume and oxygenation in human subjects (8).

5.5 Thesis proposal

The recommended approach for measuring R2′ in the liver based on literature is through separately measuring R2 and R2* using self-gated free-breathing acquisition strategies. Nevertheless, the accuracy of R2′ measurement in the liver using this approach, as well as the optimal field strength for this measurement, remains uncertain. Therefore, this thesis aims to answer the following research question: Can the R2′ relaxation rate be accurately measured in the liver using a MqBOLD approach, while allowing free-breathing, and what is the optimal field strength for this measurement?

To map R2, a multiple spin echo sequence, and for R2*, a multi echo GRE sequence, will be implemented. Accurate R2' mapping is required for qBOLD modeling. However, adaptation of the qBOLD model to go from R2' to oxygen extraction fraction of liver tissue is required. This includes addressing the violation of one of the assumptions of the qBOLD model, namely the non-randomly oriented vasculature of the liver. very challenging due to the breathing motion, non-randomly oriented vasculature and high blood vessel density/high blood volume in the liver.

The primary aim is to measure the R2′ relaxation rate in the liver as a first step toward developing reliable, quantitative liver oxygenation measurements. The measured R2-, R2*- and R2′-values will be compared with values found in literature and evaluated on homogeneity within regions. Measuring R2′ offers a way to assess oxygenation non-invasively and could serve as a foundation for further research in functional liver imaging. The focus remains on R2′ mapping, while parameters such as deoxygenated blood volume (DBV) and oxygen extraction fraction (OEF) are beyond the current scope.

To address the investigation of the most optimal field strength for R2′ mapping of the liver, a comparative study will be conducted by scanning healthy volunteers on both 1.5T and 3T, using the same scan protocol. The comparison will include signal-to-noise evaluations in the R2 map and the R2* map, as well as interscan variability to evaluate repeatability of the scans. Additionally, qualitative assessment by a radiologist will be done to evaluate image interpretability and artifact presence. This approach allows for a direct comparison, enabling conclusions about the optimal field strength for R2′ measurement.

It is hypothesized that R2′ can be measured in the liver using a self-gating free-breathing acquisition strategy. To evaluate accurateness of the R2′ measurement, evaluation must be done of the R2′ parameter, the SNR, artifacts and motion robustness. During image processing significant challenges will arise due to respiratory motion and susceptibility artifacts. Besides, differences in image acquisition parameters between R2 and R2* map scans will complicate image registration, necessary for creating the R2′ map. Additionally, it is expected that 1.5T will yield better results than 3T, as the shorter T2* decay at 3T reduces the available imaging

window, leading to a lower SNR in images acquired with the same TE. Furthermore, 1.5T is expected to produce fewer artifacts, improving the robustness of the measurement.

5.6 Limitations

This review was limited to investigating qBOLD/R2′ techniques in the human liver. Unfortunately, the available literature is limited, as only three studies have specifically addressed this topic. Therefore, literature of qBOLD/R2′ for the brain and other organs in the abdomen and thorax were included, as well as preclinical studies.

6. References

1. Gregory J, Dioguardi Burgio M, Corrias G, Vilgrain V, Ronot M. Evaluation of liver tumour response by imaging. JHEP Rep Innov Hepatol. 2020 Jun;2(3):100100.

2. Guglielmi A, Ruzzenente A, Conci S, Valdegamberi A, Iacono C. How much remnant is enough in liver resection? Dig Surg. 2012;29(1):6–17.

3. Khan AS, Garcia-Aroz S, Ansari MA, Atiq SM, Senter-Zapata M, Fowler K, et al. Assessment and optimization of liver volume before major hepatic resection: Current guidelines and a narrative review. Int J Surg Lond Engl. 2018 Apr;52:74–81.

4. Muz B, de la Puente P, Azab F, Azab AK. The role of hypoxia in cancer progression, angiogenesis, metastasis, and resistance to therapy. Hypoxia. 2015 Dec 11;3:83–92.

5. Zou B, Liu X, Zhang B, Gong Y, Cai C, Li P, et al. The Expression of FAP in Hepatocellular Carcinoma Cells is Induced by Hypoxia and Correlates with Poor Clinical Outcomes. J Cancer. 2018 Sep 7;9(18):3278–86.

6. He X, Yablonskiy DA. Quantitative BOLD: Mapping of Human Cerebral Deoxygenated Blood Volume and Oxygen Extraction Fraction: Default State. Magn Reson Med Off J Soc Magn Reson Med Soc Magn Reson Med. 2007 Jan;57(1):115–26.

7. Stone AJ, Blockley NP. A streamlined acquisition for mapping baseline brain oxygenation using quantitative BOLD. NeuroImage. 2017 Feb 15;147:79–88.

8. Wengler K, Wang J, Serrano Sosa M, Gumus S, He A, Hussain S, et al. Mapping hepatic blood oxygenation by quantitative BOLD (qBOLD) MRI. Magn Reson Med. 2019 May;81(5):3272–82.

9. O'g'li AJM, Qizi HSU, O'g'li MMB, O'g'li SXE, O'g'li SAR. LIVER ANATOMY, HISTOLOGY AND PHYSIOLOGY. Intellect Educ Technol Solut Innov Digit TOOLS. 2022 Nov 17;1(11):8–11.

10. Liver: Anatomy and Functions [Internet]. 2019 [cited 2024 Dec 20]. Available from: https://www.hopkinsmedicine.org/health/conditions-and-diseases/liver-anatomy-and-functions

11. Trefts E, Gannon M, Wasserman DH. The liver. Curr Biol CB. 2017 Nov 6;27(21):R1147–51.

12. Vollmar B, Menger MD. The Hepatic Microcirculation: Mechanistic Contributions and Therapeutic Targets in Liver Injury and Repair. Physiol Rev. 2009 Oct;89(4):1269–339.

13. Lassen NA. Cerebral blood flow and oxygen consumption in man. Physiol Rev. 1959 Apr;39(2):183–238.

14. Cramer T, Vaupel P. Severe hypoxia is a typical characteristic of human hepatocellular carcinoma: Scientific fact or fallacy? J Hepatol. 2022 Apr;76(4):975–80.

15. Rappaport AM. Hepatic blood flow: morphologic aspects and physiologic regulation. Int Rev Physiol. 1980;21:1–63.

16. Eipel C, Abshagen K, Vollmar B. Regulation of hepatic blood flow: The hepatic arterial buffer response revisited. World J Gastroenterol WJG. 2010 Dec 28;16(48):6046–57.

17. Vaupel P, Multhoff G. Blood Supply and Oxygenation Status of the Liver: From Physiology to Malignancy. Adv Exp Med Biol. 2022;1395:263–7.

18. Chiu DKC, Tse APW, Xu IMJ, Di Cui J, Lai RKH, Li LL, et al. Hypoxia inducible factor HIF-1 promotes myeloid-derived suppressor cells accumulation through ENTPD2/CD39L1 in hepatocellular carcinoma. Nat Commun. 2017 Sep 11;8(1):517.

19. Vaupel P, Höckel M, Mayer A. Detection and characterization of tumor hypoxia using pO2 histography. Antioxid Redox Signal. 2007 Aug;9(8):1221–35.

20. Vaupel P, Flood AB, Swartz HM. Oxygenation Status of Malignant Tumors vs. Normal Tissues: Critical Evaluation and Updated Data Source Based on Direct Measurements with pO2 Microsensors. Appl Magn Reson. 2021 Oct 1;52(10):1451–79.

21. Ba ZF, Wang P, Koo DJ, Cioffi WG, Bland KI, Chaudry IH. Alterations in tissue oxygen consumption and extraction after trauma and hemorrhagic shock. Crit Care Med. 2000 Aug;28(8):2837.

22. Rhodes CE, Denault D, Varacallo MA. Physiology, Oxygen Transport. In: StatPearls. Treasure Island (FL): StatPearls Publishing; 2025.

23. Ghugre NR, Wright GA. Myocardial BOLD imaging with T2 relaxation. Open Med Imaging J. 2012;6(SPEC.ISS.1):18–30.

24. Schaller C. Structure and Reactivity in Organic, Biological, and Inorganic Chemistry. LibreTexts; 2019. (V; vol. Reactivity in Organic, Biological, and Inorganic Chemistry).

25. Maniam S, Szklaruk J. Magnetic resonance imaging: Review of imaging techniques and overview of liver imaging. World J Radiol. 2010 Aug 28;2(8):309–22.

26. van Heeswijk RB, Bonanno G, Coppo S, Coristine A, Kober T, Stuber M. Motion compensation strategies in magnetic resonance imaging. Crit Rev Biomed Eng. 2012;40(2):99–119.

27. Batchelor PG, Atkinson D, Irarrazaval P, Hill DLG, Hajnal J, Larkman D. Matrix description of general motion correction applied to multishot images. Magn Reson Med. 2005 Nov;54(5):1273–80.

28. Shih SF, Wu HH. Free-breathing MRI techniques for fat and R2* quantification in the liver. Magn Reson Mater Phys Biol Med. 2024 Aug 1;37(4):583–602.

29. Pérez-Mayoral E, Negri V, Soler-Padrós J, Cerdán S, Ballesteros P. Chemistry of paramagnetic and diamagnetic contrast agents for Magnetic Resonance Imaging and Spectroscopy: pH responsive contrast agents. Eur J Radiol. 2008 Sep 1;67(3):453–8.

30. He X, Zhu M, Yablonskiy DA. Validation of Oxygen Extraction Fraction Measurement by qBOLD Technique. Magn Reson Med Off J Soc Magn Reson Med Soc Magn Reson Med. 2008 Oct;60(4):882–8.

31. Alzaidi AA, Panek R, Blockley NP. Quantitative BOLD (qBOLD) imaging of oxygen metabolism and blood oxygenation in the human body: A scoping review. Magn Reson Med. 2024;92(5):1822–37.

32. Stadlbauer A, Zimmermann M, Bennani-Baiti B, Helbich TH, Baltzer P, Clauser P, et al. Development of a Non-invasive Assessment of Hypoxia and Neovascularization with Magnetic Resonance Imaging in Benign and Malignant Breast Tumors: Initial Results. Mol Imaging Biol. 2019;21(4):758–70.

33. Yablonskiy DA, Haacke EM. Theory of NMR signal behavior in magnetically inhomogeneous tissues: The static dephasing regime. Magn Reson Med. 1994;32(6):749–63.

34. McCuskey RS. The hepatic microvascular system in health and its response to toxicants. Anat Rec Hoboken NJ 2007. 2008 Jun;291(6):661–71.

35. Dickson JD, Ash TWJ, Williams GB, Harding SG, Carpenter TA, Menon DK, et al. Quantitative BOLD: the effect of diffusion. J Magn Reson Imaging JMRI. 2010 Oct;32(4):953–61.

36. Li H, Wang C, Yu X, Luo Y, Wang H. Measurement of Cerebral Oxygen Extraction Fraction Using Quantitative BOLD Approach: A Review. Phenomics. 2022 Dec 5;3(1):101.

37. Blockley NP, Griffeth VEM, Simon AB, Buxton RB. A review of calibrated blood oxygenation level-dependent (BOLD) methods for the measurement of task-induced changes in brain oxygen metabolism. NMR Biomed. 2013 Aug;26(8):987–1003.

38. An H, Lin W. Impact of intravascular signal on quantitative measures of cerebral oxygen extraction and blood volume under normo- and hypercapnic conditions using an asymmetric spin echo approach. Magn Reson Med. 2003 Oct;50(4):708–16.

39. Prasad PV, Li LP, Hack B, Leloudas N, Sprague SM. Quantitative Blood Oxygenation Level Dependent Magnetic Resonance Imaging for Estimating Intra-renal Oxygen Availability Demonstrates Kidneys Are Hypoxemic in Human CKD. KI Rep. 2023;8(5):1057–67.

40. Lota AS, Gatehouse PD, Mohiaddin RH. T2 mapping and T2* imaging in heart failure. Heart Fail Rev. 2017 Jul 1;22(4):431–40.

41. Rossello X, Lopez-Ayala P, Fernández-Jiménez R, Oliver E, Galán-Arriola C, de Molina-Iracheta A, et al. R2 prime (R20) magnetic resonance imaging for post-myocardial infarction intramyocardial haemorrhage quantification. Eur Heart J Cardiovasc Imaging. 2020;21(9):1031–8.

42. Topriceanu CC, Pierce I, Moon JC, Captur G. T2 and T2∗ mapping and weighted imaging in cardiac MRI. Magn Reson Imaging. 2022 Nov 1;93:15–32.

43. Christen T, Lemasson B, Pannetier N, Farion R, Segebarth C, Rémy C, et al. Evaluation of a quantitative blood oxygenation level-dependent (qBOLD) approach to map local blood oxygen saturation. NMR Biomed. 2011 May;24(4):393–403.

44. Storey P, Thompson AA, Carqueville CL, Wood JC, de Freitas RA, Rigsby CK. R2* Imaging of Transfusional Iron Burden at 3T and Comparison with 1.5T. J Magn Reson Imaging JMRI. 2007 Mar;25(3):540–7.

45. Silvennoinen M j., Clingman C s., Golay X, Kauppinen R a., van Zijl P c. m. Comparison of the dependence of blood R2 and R on oxygen saturation at 1.5 and 4.7 Tesla. Magn Reson Med. 2003;49(1):47–60.

46. Nepal P, Bagga B, Feng L, Chandarana H. Respiratory Motion Management in Abdominal MRI: *Radiology* In Training. Radiology. 2023 Jan;306(1):47–53.

47. Vu KN, Haldipur AG, Roh ATH, Lindholm P, Loening AM. Comparison of End-Expiration Versus End-Inspiration Breath-Holds With Respect to Respiratory Motion Artifacts on T1-Weighted Abdominal MRI. Am J Roentgenol. 2019 May;212(5):1024–9.

48. Chavhan GB, Babyn PS, Vasanawala SS. Abdominal MR Imaging in Children: Motion Compensation, Sequence Optimization, and Protocol Organization. RadioGraphics. 2013 May;33(3):703–19.

49. Young PM, Brau AC, Iwadate Y, Vasanawala S, Daniel BL, Tamrazi A, et al. Respiratory Navigated Free Breathing 3D Spoiled Gradient-Recalled Echo Sequence for Contrast-Enhanced Examination of the Liver: Diagnostic Utility and Comparison With Free Breathing and Breath-Hold Conventional Examinations. Am J Roentgenol. 2010 Sep;195(3):687–91.

50. Zhang K, Triphan SMF, Wielpütz MO. Navigator-based motion compensation for liver BOLD measurement with five-echo SAGE EPI and breath-hold task. NMR Biomed. 2024;

51. Paling MR, Brookeman JR. Respiration artifacts in MR imaging: reduction by breath holding. J Comput Assist Tomogr. 1986;10(6):1080–2.

52. Madore B, Hess AT, van Niekerk AMJ, Hoinkiss DC, Hucker P, Zaitsev M, et al. External Hardware and Sensors, for Improved MRI. J Magn Reson Imaging. 2023;57(3):690–705.

53. Grimm R, Bauer S, Kiefer B, Hornegger J, Block T. Optimal Channel Selection for Respiratory Self-Gating Signals.

54. Ulrich X, Yablonskiy DA. Separation of Cellular and BOLD Contributions to T2* Signal Relaxation. Magn Reson Med. 2016 Feb;75(2):606–15.

55. Sedlacik J, Reichenbach JR. Validation of quantitative estimation of tissue oxygen extraction fraction and deoxygenated blood volume fraction in phantom and in vivo experiments by using MRI. Magn Reson Med. 2010 Apr;63(4):910–21.

56. Hori M, Murakami T, Kim T, Kanematsu M, Tsuda K, Takahashi S, et al. Single breath-hold T2-weighted MR imaging of the liver: value of single-shot fast spin-echo and multishot spin-echo echoplanar imaging. AJR Am J Roentgenol. 2000 May;174(5):1423–31.

57. Darzi F, Bocklitz T. A Review of Medical Image Registration for Different Modalities. Bioengineering. 2024 Aug 2;11(8):786.

58. Alam MH, Auger D, McGill LA, Smith GC, He T, Izgi C, et al. Comparison of 3 T and 1.5 T for T2* magnetic resonance of tissue iron. J Cardiovasc Magn Reson. 2016 Jul 8;18(1):40.

59. Low RN, Alzate GD, Shimakawa A. Motion suppression in MR imaging of the liver: comparison of respiratory-triggered and nontriggered fast spin-echo sequences. AJR Am J Roentgenol. 1997 Jan;168(1):225–31.

60. Chandarana H, Block TK, Rosenkrantz AB, Lim RP, Kim D, Mossa DJ, et al. Free-Breathing Radial 3D Fat-Suppressed T1-Weighted Gradient Echo Sequence: A Viable Alternative for Contrast-Enhanced Liver Imaging in Patients Unable to Suspend Respiration. Invest Radiol. 2011 Oct;46(10):648.

61. Zhong X, Armstrong T, Nickel MD, Kannengiesser SAR, Pan L, Dale BM, et al. Effect of respiratory motion on free-breathing 3D stack-of-radial liver relaxometry and improved quantification accuracy using self-gating. Magn Reson Med. 2020;83(6):1964–78.

62. Kee Y, Sandino CM, Syed AB, Cheng JY, Shimakawa A, Colgan TJ, et al. Free-breathing mapping of hepatic iron overload in children using 3D multi-echo UTE cones MRI. Magn Reson Med. 2021;85(5):2608–21.

Appendix A

R2 prime liver
Narrative
Trials: ja

Database searched	Platform	Years of coverage	Records	Records after duplicates removed
Medline ALL	Ovid	1946 - Present	205	190
Embase	Embase.com	1971 - Present	235	73
Web of Science Core Collection*	Web of Knowledge	1975 - Present	363	183
Cochrane Central Register of Controlled Trials	Wiley	1992 - Present	2	1
Additional Search Engines: Google Scholar**			100	87
Total			**905**	**534**

*Science Citation Index Expanded (1975-present) ; Social Sciences Citation Index (1975-present) ; Arts & Humanities Citation Index (1975-present) ; Conference Proceedings Citation Index- Science (1990-present) ; Conference Proceedings Citation Index- Social Science & Humanities (1990-present) ; Emerging Sources Citation Index (2005-present)
**Google Scholar was searched via "Publish or Perish" to download the results in EndNote.

No other database limits were used than those specified in the search strategies

Medline
((((r2 OR r-2) ADJ3 (prime*)) OR ((quantit*) ADJ3 (bold*)) OR qbold OR q-bold).ab,ti,kf.)

Embase
((((r2 OR r-2) NEAR/3 (prime*)) OR ((quantit*) NEAR/3 (bold*)) OR qbold OR q-bold):ab,ti,kw)

Web of Science
(TS=(((r2 OR r-2) NEAR/2 (prime*)) OR ((quantit*) NEAR/2 (bold*)) OR qbold OR q-bold))

Cochrane CENTRAL
((((r2 OR "r" NEXT/1 "2") NEAR/3 (prime*)) OR ((quantit*) NEAR/3 (bold*)) OR qbold OR "q" NEXT/1 bold):ab,ti,kw)
Google Scholar
'r2 prime'|'r 2 prime'|'quantitative|q bold'|qbold liver

3

MRI Sequences

A detailed description of sequences and breathing strategies used in this study is provided below.

3.1. Quantitative MRI

R2 Mapping

SMART2Map: For R2 mapping (the inverse of T2), the Smooth Motion-Assisted Rapid T2 Mapping (SMART2Map) sequence was used. SMART2Map is a ”Work In Progress” developed by GE Healthcare, designed primarily for cardiac T2 mapping. SMART2Map is based on a 2D fast gradient echo pulse sequence and includes integrated T2 quantification and reconstruction modules. The technique supports both BH and FB acquisitions. In BH mode, imaging is performed at end-expiration, acquiring one slice per BH. In the FB mode, respiratory triggering is achieved via a surrogate signal from a respiratory belt, and imaging is also performed at the end of the expiration phase.

SMART2Map provides the choice between two readout strategies: T2-preparation-based Fast Imaging Employing Steady-State Acquisition (FIESTA) and Fast Spoiled Gradient Echo (FSPGR). FIESTA refers to General Electric’s (GE) implementation of a balanced steady-state gradient echo sequence [10]. FSPGR is a GE’s version of a fast spoiled gradient echo sequence.

Although SMART2Map has been developed and optimized for cardiac imaging, it has not been validated for liver applications.

R2* Mapping

IDEAL-IQ: For R2* mapping (the inverse of T2*), the IDEAL-IQ sequence was used. IDEAL-IQ is a GE-optimized, multi-echo gradient-echo (GRE) sequence designed for liver imaging. It provides whole-liver 3D coverage in a single BH, enabling quantitative R2* estimation.

By assuming equal T2* for water and fat within a voxel, the algorithm introduces a ”complex field map” to account for B0 inhomogeneities and exponential T2* decay. This map is iteratively refined using least-squares estimation, allowing the extraction of R2* from the imaginary component while correcting source images for both B0 and T2* effects.

3.2. Structural Imaging

4D MRI

For anatomical images and an insight into liver motion during scanning, the four-dimensional magnetic resonance imaging (4DMR) sequence was used. Also, a “Work in Progress” from GE. 4DMR is a T1-weighted sequence using stack-of-spirals spatial encoding for self-gated, continuous 3D FB acquisition. During reconstruction, the acquired data is retrospectively gated into multiple respiratory-correlated phases, producing both respiratory-resolved and respiratory-compensated 3D volumes.

This sequence had not previously been used at Erasmus Medical Center. As such, its implementation in this study also served as a means to evaluate the self-gating technique and be able to retrieve information about the respiratory motion of the subjects.

Standard Clinical Sequences

In addition to 4DMR, conventional structural imaging sequences with a short acquisition time were used to complement the quantitative data. These sequences are currently used in clinical settings:

- **Coronal T2-weighted scan**: Provides high soft-tissue contrast and anatomical orientation.
- **Axial LAVA-FLEX**: A dual-echo, fat–water separated gradient-echo sequence performed during a single BH; used for dynamic contrast-enhanced imaging.
- **Axial Diffusion-Weighted Imaging (DWI)**: Captures water molecule diffusion properties, often used to assess tissue integrity and pathology.
- **Axial FIESTA (Ungated)**: A balanced Steady-State Free Precession sequence that provides high signal for fluid-filled structures and strong tissue contrast.

3.3. Breathing Strategies During MRI

Breath-Hold

End-of-expiration BHs were used based on literature study, which can be found in section 2. For the BH sequences, auditory communication was used to coordinate the BH timing. Therefore, breathing cycles were monitored using the respiratory belt. The MRI operator used the breathing information to time scan initiation.

Auditory prompts instructed volunteers: “Breathe in,” “Breathe out,” and “Hold your breath.” At scan completion, “Relax” was played. Some sequences consisted of a single BH other of a series of five BHs. For a series of five BHs, volunteers were allowed three normal breaths between BHs, ensuring comfort.

Free-Breathing and Self-Gating

- **Respiratory Belt Gating:** FB scans used respiratory gating to acquire images during the end-expiration phase. The scan time is therefore reliant on the breathing pace and pattern of the subject. A higher breathing pace resulted in a shorter scan time. Data were acquired in segments across cycles until complete.
- **Self-Gating:** For the 4DMR sequence, data acquisition was continuous. Retrospective reconstruction yielded ten respiratory phases and one motion-compensated image.

Part II

Methods

4

MRI Hardware and Subject Positioning

Experiments were conducted at the Department of Radiology & Nuclear Medicine at Erasmus Medical Center on MRI scanners from GE: The SIGNA™ Artist 1.5 T and the SIGNA™ Premier 3 T. Both scanners operated on the same software version (MR30.1RO1). Subjects were asked to remove their shoes and change into metal-free clothing. Subjects were positioned supine with feet first on the scanner bed (see Figure 4.1a), with the liver aligned to the scanner isocenter. The GE AIR™ body coil was placed on the abdomen, centered over the liver, and secured between the arms and torso (Figure 4.2a). For respiratory gating, the ”Adult Bellow for MRI Respiratory Gating” was placed around the abdomen (Figure 4.2b and 4.2c). BH sequences were coordinated through auditory instructions. For cardiac gating, the Fiber Optic Finger Probe from GE HealthCare was attached to the left index finger (Figure 4.2d). To enhance comfort and minimize motion, subjects were provided with earplugs, a head pillow, and leg support. An emergency squeeze ball was placed in the right hand for communication during the scan. The scan landmark was set at the level of the liver before the subject was slid into the scanner.

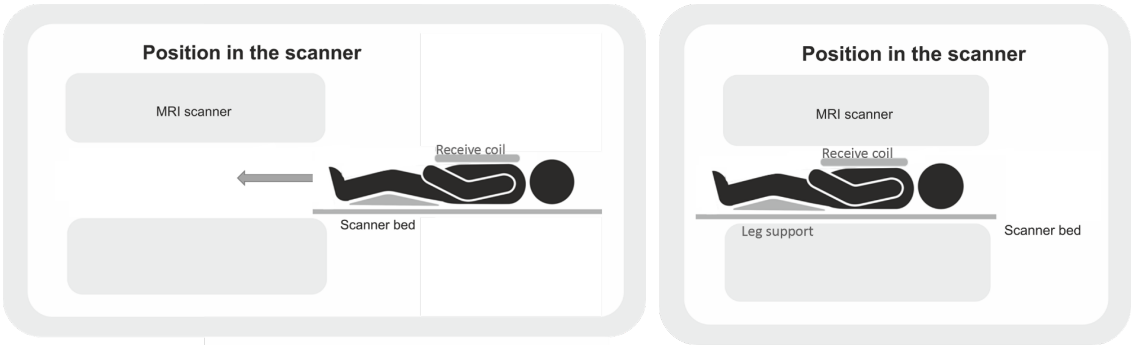

(a) Subject positioning on the scanner table.

(b) Scan position in the MRI scanner with liver centered.

Figure 4.1: Subject positioning in the MRI scanner, showing alignment of the liver with the scanner isocenter.

(a) AIR body coil.

(b) Respiratory belt.

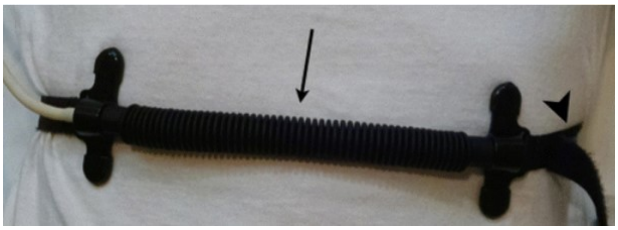

(c) Respiratory belt (around the abdomen).

(d) Fiber Optic Finger Probe.

Figure 4.2: Illustration of hardware accessories for quantitative liver MRI acquisition.

5

Protocol Development and Optimization

This section describes the development and optimization of the imaging protocol for SMART2Map and IDEAL-IQ sequences. Additionally, the applicability of SMART2Map and 4DMR sequences for liver imaging and displacement assessment was evaluated.

Therefore, a series of pilot scans in a healthy volunteer was conducted. Beginning with the default settings provided by the manufacturer, GE, we repeated each sequence several times, adjusting one parameter at a time to observe its impact on image quality and scan duration, as described in the following section.

5.1. Feasibility of SMART2Map and 4DMR for Hepatic Imaging

As described in section 3, the SMART2Map and 4DMR sequences had not previously been implemented at Erasmus Medical Center. Moreover, SMART2Map was not designed and optimized for liver imaging but for cardiac imaging. Accordingly, both sequences were first evaluated in a healthy volunteer. The 4DMR images were evaluated for their suitability in assessing liver motion. The images acquired with SMART2Map were assessed by visual inspection and quantitative analysis for anatomical detail, T2 relaxation times, and presence of artifacts.

5.2. Optimization of Acquisition Parameters

Field-of-View and Scan Time

The field of view (FOV) was optimized, balancing scan time with sufficient anatomical coverage and image quality. This was done separately for the 2D, 3D, and 4D sequences.

- For the 2D acquisitions, multiple breath-held, single-slice scans were evaluated. Various parameters were iteratively adjusted, including different scan planes, slice thicknesses, inter-slice spacing, BH durations, and recovery time between acquisitions. A maximum BH duration of 20 seconds was used.
- 3D sequences, including structural imaging and localizers, were reviewed for scan coverage and timing efficiency (e.g., BH duration and scan time). The acquisitions already adhered to clinical quality standards.
- For the 4D acquisition, the FOV was optimized to fully cover the liver throughout all phases of the respiratory cycle, while avoiding unnecessary oversampling of surrounding areas.

To guide consistent liver coverage over all sequences, FOV guidelines were defined in consultation with an abdominal radiologist. Alternative FOVs were explored to mitigate susceptibility artifacts, particularly from air-filled adjacent structures like the lungs and bowel.

Voxel Size

To achieve high spatial resolution, while ensuring a high SNR and maintaining anatomical detail, multiple voxel sizes were tested. An important requirement was choosing the same voxel size for all sequences, allowing creation of a difference map with as few post-processing steps as possible. The images were evaluated for artifacts, contrast, and SNR.

Slice Thickness
Literature was assessed to choose the optimal slice thickness.

Echo Times
The mapping sequences use different echo times to obtain relaxation maps. To evaluate the influence of the echo times, multiple options were tested. The SNR as well as the goodness-of-fit ($R2^2$) of the images were compared.

B0 Shimming
To improve B0 field homogeneity across the FOV, standard B0 shimming was performed before each scan. The shimming volume was defined to cover the entire FOV.

Scans were acquired both with and without shimming to assess its impact on image quality. These images were reviewed by an experienced abdominal radiologist.

5.3. Improving R2* imaging
The IDEAL-IQ sequence, originally developed for liver imaging and provided as a product scan for fat and iron quantification, was evaluated for its potential in R2* quantification. Sequence parameters were optimized in collaboration with MRI research associate Piotr Wielopolski.

6

Healthy Volunteer Study

Five healthy volunteers (1 male, 4 female; mean age 23 +/- 4 years) were scanned using the protocol described in Table 6.1. Each volunteer was scanned first on the 3 T scanner and immediately following on the 1.5 T scanner. The scan parameters were refined as described in section 5. The scan parameters used can be found in section 10.

Table 6.1: Liver qBOLD imaging protocol.

	Protocol Liver MqBOLD	**Plane**	**Breathing method**
1	Localizer	3D	BH | Single
2	Cor T2	Coronal	BH | Single
3	Ax LAVA-FLEX	Axial	BH | Single
4	Ax DWI	Axial	FB
5	Ax Fiesta Ungated	Axial	BH | Single
6	T2map 4 echoes - Reference	Axial	BH | Per slice
7	SMART2Map (FIESTA)	Axial	BH | Per slice
8	SMART2Map (FIESTA)	Axial	FB | Gated
9	SMART2Map (FSPGR)	Axial	BH | Per slice
10	SMART2Map (FSPGR)	Axial	FB | Gating
11	IDEAL-IQ	3D	BH | Single
12	4DMR	3D	FB | Self-gated

Ethical Approval
The scans were performed under ethical approval of the local review board (NL47429.078.13). Written informed consent was obtained from each recruited subject.

Healthy Volunteers
Healthy volunteers were recruited through the Imaging Trial Bureau at Erasmus Medical Center. Exclusion criteria included standard MRI contraindications (e.g., claustrophobia, metallic implants), discomfort during BH (e.g., due to asthma), and known hepatic or systemic diseases.

Workflow
All volunteers signed an informed consent form before participation (Appendix C) and completed an MRI screening form (Appendix D). The form was reviewed by MRI-certified staff and discussed with the participant.

The set-up of the experiment proceeded as described in section 4. Once the setup was complete, the subject was placed into the scanner (see Figure 4.1b), and the scan protocol was initiated (Table 6.1). The scan protocol on 3 T lasted approximately 35 minutes, after which the process was repeated on the 1.5 T scanner. The total experiment per subject took around 90 minutes.

7

Image Processing

Following data acquisition from all volunteers, the raw datasets were initially stored in DICOM format. These DICOM files were converted to NIfTI format to enable image visualization and further processing. The computation of the R2′ map required a series of image processing steps, which are described in this chapter. All processing steps were implemented in Python (version 10.3.2) using Visual Studio Code as the development environment. The scripts used are provided in Appendix B.

7.1. Computation of R2 and R2* Maps

Relaxation maps were generated by fitting signal intensities across echo times using the raw T2-weighted data and T2*-weighted data. An example of the fitting process is shown in Fig. 7.1.

A Python script performed voxel-wise exponential fitting of signal intensities across echo times to generate T2 and T2* maps (Figure 7.1 A - B). T2 and T2* relaxation times were estimated using the following equation:

$$S(t_e) = S_0 \cdot e^{-\frac{t_e}{T2}}$$

where $S(t_e)$ is the signal at echo time t_e, S_0 the initial signal, and T_2 (or T_2^*) the relaxation time corresponding to a 63% signal decay post-excitation.

R2 and R2* values (in s^{-1}) were computed as the inverse of T2 and T2* relaxation times, respectively, after converting milliseconds to seconds, using the following equation:

$$R2 = \frac{1}{T2/1000}$$

An example of the R2 conversion is shown in Figure 7.1 C - D.

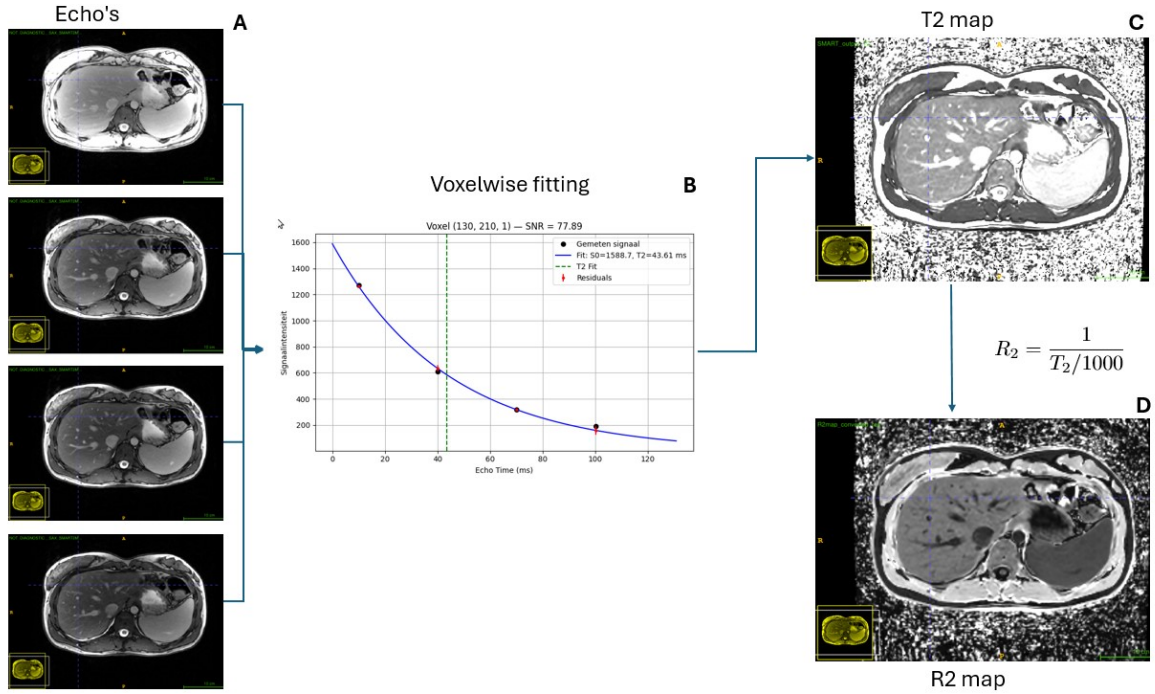

Figure 7.1: Overview of the R2 and R2* mapping pipeline, including exponential fitting of multi-echo signals and map conversion.

7.2. Computation of R2′ Maps

The R2′ difference map was computed using voxel-wise subtraction (an example is shown in 7.2). The following formula was used:

$$R2' = R2^* - R2$$

The computation of difference map values was constrained to voxels where values were available from both maps. In cases of missing data, a NaN (Not a Number) value was assigned. Before subtraction, R2 and R2* maps were spatially aligned through resampling of the R2 map with the R2* map as reference. This was done in Visual Studio Code using the script in Appendix B.

To reduce background noise, a binary mask of the abdominal region was generated from the structural axial FIESTA scan using intensity thresholding.

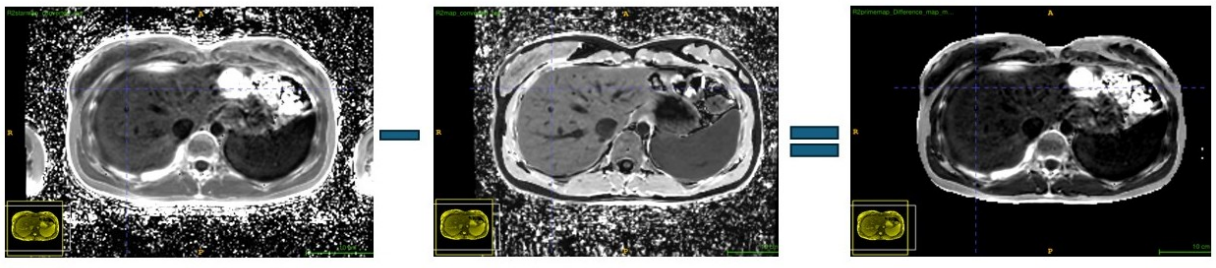

Figure 7.2: Voxel-wise computation of the R2′ map via subtraction of aligned R2* and R2 maps.

8

Image Analysis

8.1. Relaxation Rates

The R2, R2*, and R2′ relaxation rates were determined for each subject at both field strengths. Three regions of interest (ROIs) were manually placed within homogeneous liver tissue using ITK-SNAP (v4.0.2), as illustrated in Figure 8.1. This was done for the R2 maps (acquired through SMART2Map and the conventional 4-echo sequences), the R2* map (acquired via the IDEAL-IQ sequence), and the computed R2′ difference map. The same ROIs were applied across all maps to ensure consistency. The mean value of the three ROIs was calculated for each relaxation rate. The relaxation rates were compared within and between subjects, as well as between field strengths. All statistical analyses were performed with a significance level set at $p < 0.05$.

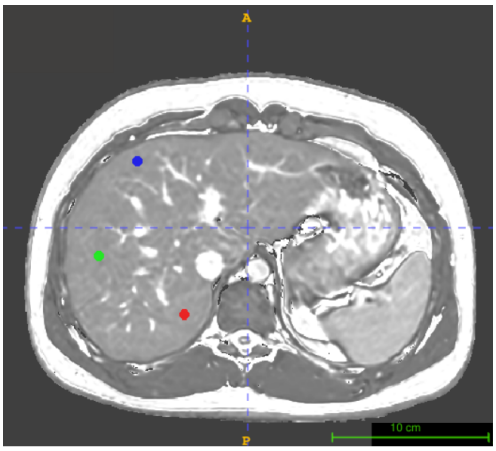

Figure 8.1: Representative ROI placement within homogeneous liver tissue for quantification of relaxation rates.

8.2. Evaluation of SMART2Map Performance

The SMART2Map sequence offers multiple options in the breathing and read-out method as described in chapter 3. For each SMART2Map sequence variant (FIESTA BH, FIESTA FB, FSPGR BH, FSPGR FB, the goodness-of-fit and T2 relaxation times were compared.

Goodness-of-fit was quantified using the coefficient of determination (R^2), with values > 0.85 considered high. The analysis was performed at both 1.5 T and 3 T field strengths across two regions: the entire liver (Figure 8.2a) as well as an ROI placed within homogeneous liver tissue (Figure 8.2c). Both regions were segmented once per volunteer and applied across all sequence variants to ensure consistency.

T2 relaxation times were extracted from the same ROIs as described above. Mean T2 values were compared across all SMART2Map sequence variants at both field strengths. A repeated measures ANOVA was conducted to test for statistical differences in T2 values between sequence variants. To assess the effect of breathing method (BH vs. FB), a post-hoc test with Bonferroni correction was applied.

Based on this analysis and the visual quality of the images, the optimal SMART2Map sequence variant was selected for the following analyses. In cases where no clear performance advantage was observed between sequences, the FB variant was preferred.

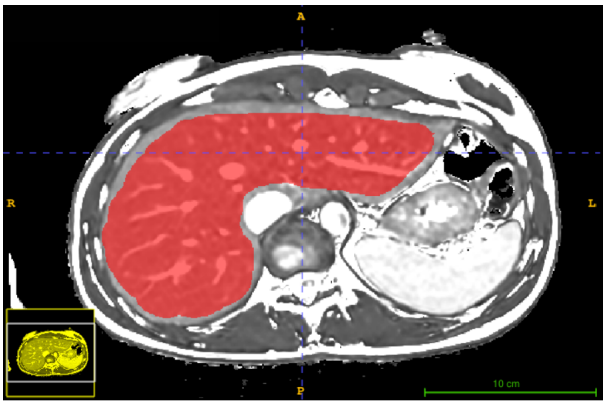

(a) Whole Liver Segmentation on T2 Image.

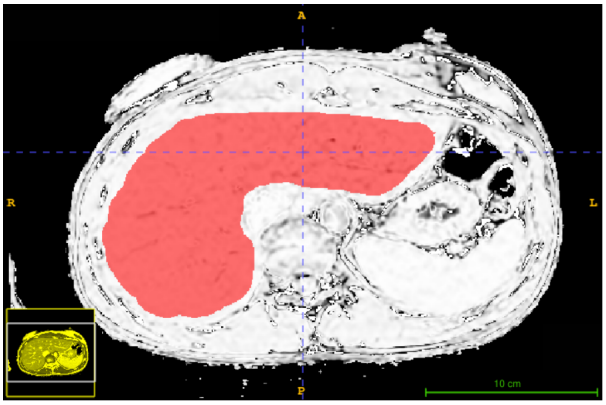

(b) Whole Liver Segmentation on R^2 Image.

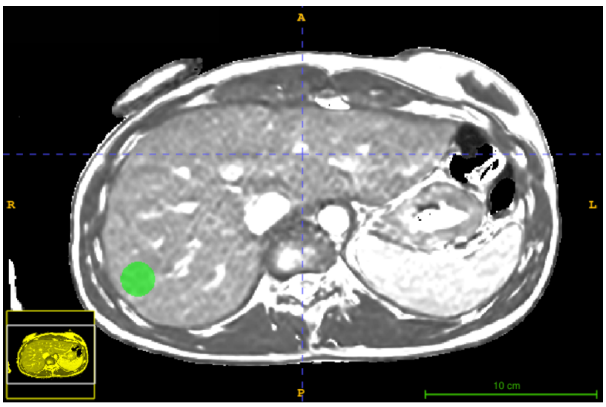

(c) ROI Segmentation on T2 Image.

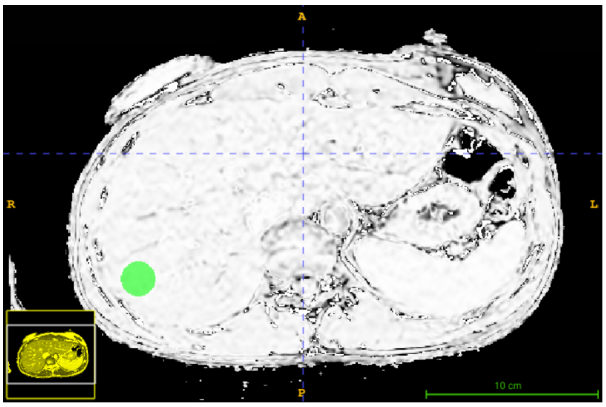

(d) ROI Segmentation on R^2 Image.

Note: Both green ROIs have a diameter of 30 mm.

Figure 8.2: Segmentation examples for whole-liver and ROI-based analysis on T2 and R^2 maps.

SMART2Map vs. Standard T2 Mapping

To validate SMART2Map performance, T2 values were compared with those obtained from a conventional T2 mapping sequence, the T2map 4-echo sequence. For this comparison, the same placement of ROIs as shown in Figure 8.1 was used. The mean T2 values within these ROIs were statistically compared using a paired t-test. This analysis was conducted for both 1.5 T and 3 T datasets. No significant differences in T2 values were expected between the two methods.

8.3. Comparative Analysis: 1.5 T vs 3 T

Quantitative Comparison of Relaxation Parameters

To assess the impact of magnetic field strength on relaxation rate measurements, the R2, R2*, and R2′ relaxation values determined as described in section 8.1, were compared between 1.5 T and 3 T. A paired t-test was performed to assess whether significant differences in relaxation rates exist between the two field strengths. This comparison was conducted using R2 values obtained from both the SMART2Map sequence and the conventional T2 mapping sequence.

Signal-to-Noise Comparison

To address the effect of the field strength on the protocol and the R2′ values, the SNR of the R2 and R2* images between field strengths was compared seperately. The SNR was calculated as:

$$SNR = \frac{\mu_{\text{ROI}}}{\sigma_{\text{background}}}$$

Where μ_{ROI} is the mean signal in a homogeneous ROI within the liver, and $\sigma_{\text{background}}$ represents the standard deviation of background noise. The ROI of the background is located outside the body and avoids pockets of systematic noise. An example of the ROI placement is shown in 8.3. The SNR was obtained within the separate echo images of the IDEAL-IQ and SMART2Map acquisitions on both 1.5 T and 3 T.

SNR values were considered high > 100. SNR values across field strengths were compared using a paired t-test. In addition, qualitative assessments were performed by a radiologist.

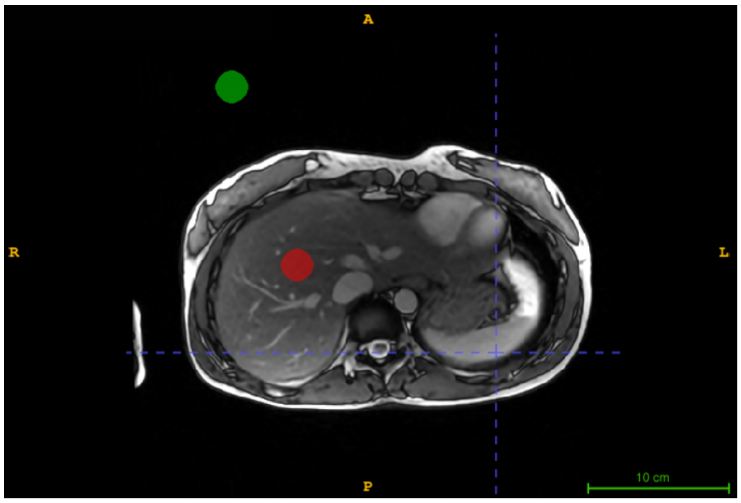

Note: Green label is for background noise. Red label is an ROI in the liver.

Figure 8.3: ROI placement strategy used to calculate SNR in liver and background regions across echo times.

8.4. Quantification of Hepatic Motion

The 4DMR scan captures ten phases of the breathing cycle. Respiration-induced liver motion was quantified by comparing the position of the liver between the full inspiration phase and the full expiration phase (see Figure 8.4a and 8.4b).

In ITK-SNAP, anatomical landmarks were annotated in the coronal view. Liver translation was measured using the annotation tool between corresponding landmarks across respiratory phases. Superior-inferior (SI) displacement was measured between the most cranial (segment VIII) and caudal (segment VI) liver landmarks.

A paired t-test was conducted to evaluate differences in displacement between cranial and caudal liver regions.

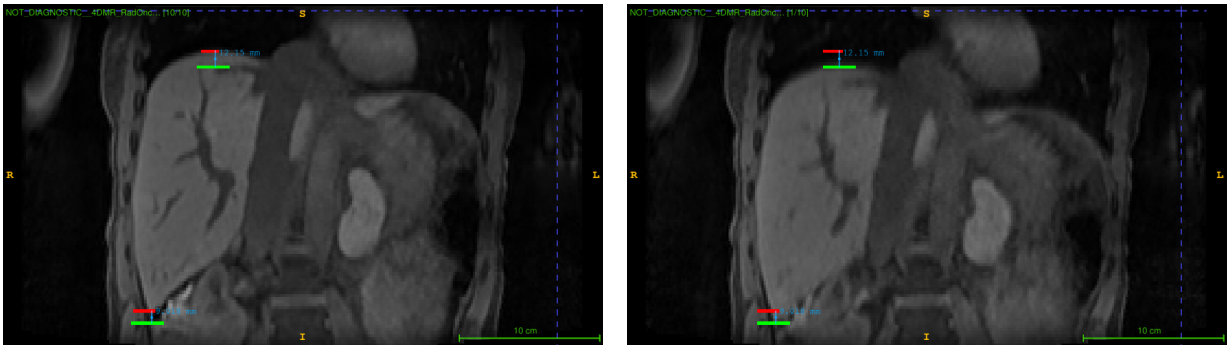

(a) End of Expiration.

(b) End of Inspiration.

Figure 8.4: Respiration-induced liver displacement measured in ITK-SNAP using 4DMR images.

Assessing Motion-Related Discrepancies Between BH and FB Scans

To evaluate the impact of motion between BH and FB acquisitions, a voxel-wise subtraction was performed between the SMART2Map FIESTA-FB and FIESTA-BH maps. A threshold of ±10 intensity units was applied to the resulting difference map. This cutoff was empirically determined on the typical intensity contrast between liver tissue and surrounding structures, ensuring that only substantial deviations are highlighted. The resulting binary map visualizes regions where motion-induced discrepancies exceed this threshold. Particular attention was given to the liver boundaries, where motion is most likely to be seen.

9

Patient Scanning

To evaluate the clinical feasibility of the MqBOLD method, a patient scan was performed using the proposed MqBOLD protocol integrated into the routine imaging workflow. The primary objective was to determine whether the MqBOLD approach can detect measurable differences in the R2′ relaxation rate between healthy and abnormal liver tissue.

A single patient (male, 52 years old) diagnosed with a neuroendocrine liver tumor was scanned following the procedure described in Section 4. Since the scan was integrated into the standard clinical protocol, the patient was positioned head-first in the scanner, following routine practice.

Imaging was performed on a 3 T PET/MR scanner during the pre-contrast phase of a dedicated liver protocol. Specifically, the SMART2Map FIESTA-FB and the IDEAL-IQ sequences from the liver qBOLD protocol (Table 6.1) were acquired. Detailed imaging parameters for these sequences are provided in Section 10.3.

Image processing followed the pipeline described in Section 7. The R2, R2*, and R2′ relaxation rates were calculated for ROIs placed in homogeneous liver tissue and compared to those obtained from healthy volunteers included in this study. Additional ROIs were placed within the tumor tissue, and the corresponding relaxation rates were compared to those of the homogeneous liver tissue.

A visible contrast between the tumor and healthy liver tissue is expected in R2, R2*, and R2‘ relaxation maps. No differences are expected between the homogeneous liver tissue of the patient and that of the healthy volunteers.

Part III

Results

10

Protocol Refinement

10.1. Assessment of Sequence Usability

Both SMART2Map and 4DMR sequences were successfully acquired during the friendly volunteer phase. The 4DMR images effectively captured liver motion, while the SMART2Map sequences provided clear anatomical detail, consistent R2 relaxation rates, and were free of significant artifacts.

10.2. Field-of-View Selection in the Liver

For the 2D sequences, five axial slices were acquired within the liver. The superior FOV boundary was aligned with the diaphragm. A slice thickness of 5 mm and an inter-slice gap of 5 mm was chosen to optimize contrast, SNR, and anatomical coverage. As a result, the FOV extended from the outer edge of the diaphragm to 50 mm inferiorly (see Figure 10.1).

This FOV was used for the 2D sequences (scans 6–10 in Table 6.1). For the 3D sequences (scans 2-5 and 11), the entire liver was covered. The 4D sequence (scan 12) also covered the entire liver, including a wide inferior margin of 5 cm.

For the 2D-BH sequences, five slices corresponded with five separate BHs. Acquisition of multiple slices per breath-hold was avoided, as it showed contrast variation between the first slice and subsequent slices (Figure in appendix A.2).

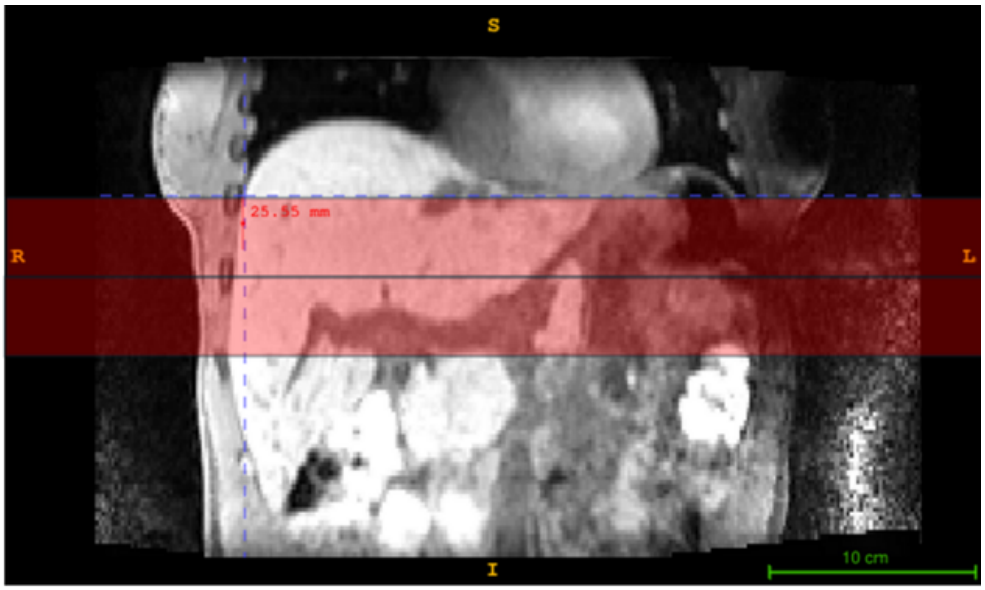

Figure 10.1: Field of view used for 2D sequences, indicated in red on a structural image.

10.3. Finalized Imaging Protocol

The recommended protocol is presented in Table 10.1 and includes optimized scan parameters for the R2, R2*, and structural imaging sequences.

Table 10.1: Optimized pulse sequence parameters for R2, R2*, and structural imaging.

Parameter	R2 MRI	R2* MRI	Structural MRI
Type of Sequence	Balanced steady-state gradient echo sequence	Multi-echo gradient-echo	T1 stack-of-spirals
Sequence name	SMART2MAP	IDEAL-IQ	4DMR
Scan Mode	2D	3D	4D
Breathing approach	Respiratory triggered FB	BH	Self gating
TR (ms)	3.7	8.1	-
No. of echoes	4	6	-
First TE value (ms)	0	1.26	-
Echo space (ms)	15	1.6	-
Flip angle	35	4.0	12.0
Matrix size	256x256	256x256	256x256
Slice thickness (mm)	5	5	2.2
No. of slices	5	32	45
Spacing (mm)	5	5	-
Voxel size (mm^3)	1.4x1.4x5	1.4x1.4x5	1.56x1.56x2.2
Shimming	Yes	Yes	Yes
Acceleration factor	2.0	2.0	1.0
Scan time (min:sec)	1:45	0:17	5:21

11

Healthy Volunteer Study

Five healthy volunteers were included in this study. Three out of five participants completed the full scanning protocol, while two underwent a shortened version due to time constraints or software availability issues.

11.1. Relaxation Maps Visualization

Figure 11.1 presents a single slice of the R2, R2*, and R2′ relaxation maps obtained using the proposed liver MqBOLD protocol. The maps are shown for both 1.5 T and 3 T field strengths, including R2 maps acquired via SMART2Map and conventional mapping sequences, as well as the computed R2′ maps. Figure 11.2 presents the total coverage of the liver.

Relaxation rates were generally lower at 1.5 T compared to 3 T. Furthermore, at 1.5 T the R2 and R2′ maps obtained using the conventional and SMART2Map show noticeable differences, whereas at 3 T, the values in the different R2 and R2′ maps appear more similar.

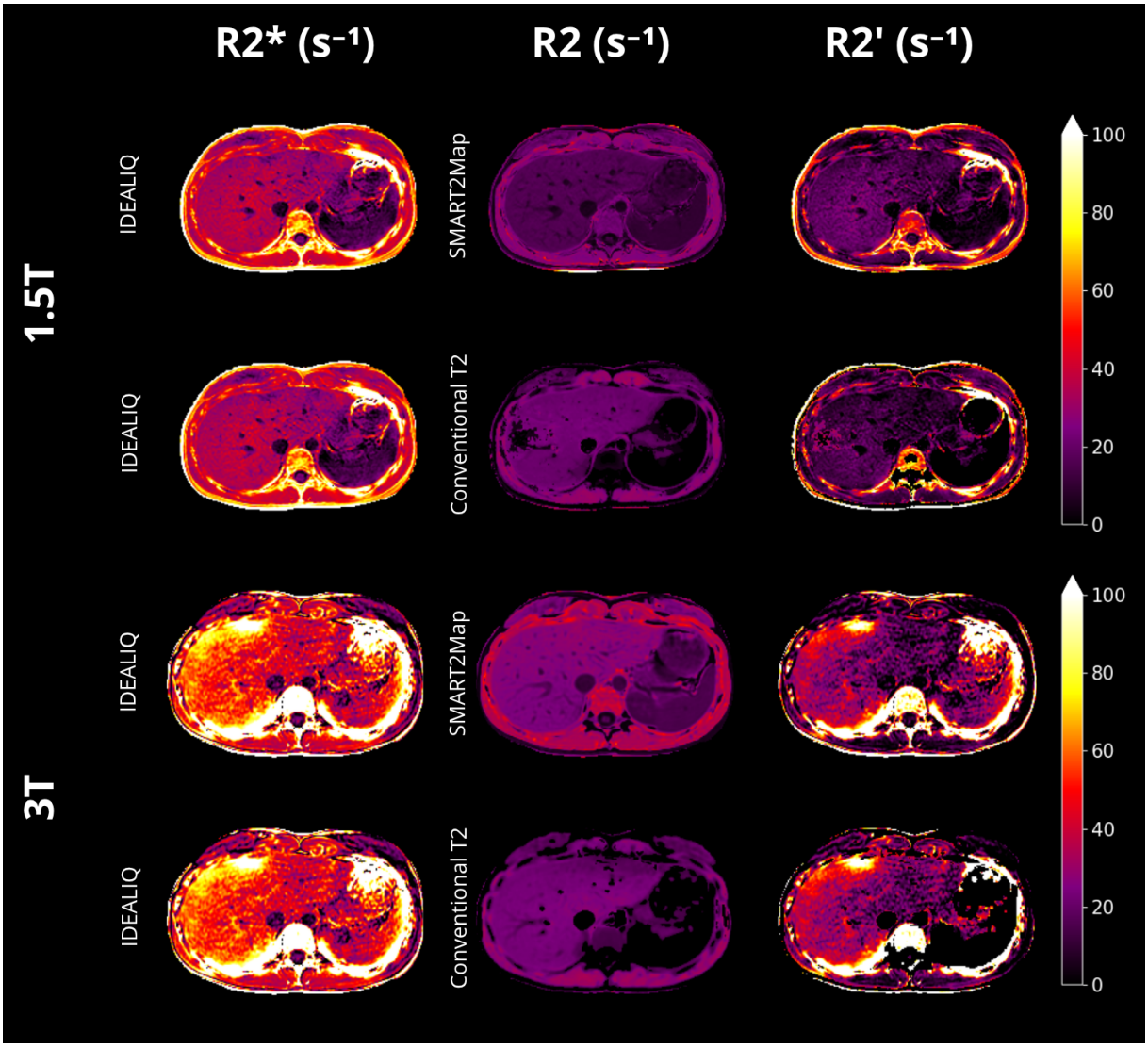

Note: The same R2 map was used for both SMART2Map and conventional T2 mapping at each field strength.

Figure 11.1: Colored relaxation maps: R2*, R2 (SMART2Map), reference R2 (4-echo), and derived R2′ maps in one volunteer at both 1.5 T and 3 T.

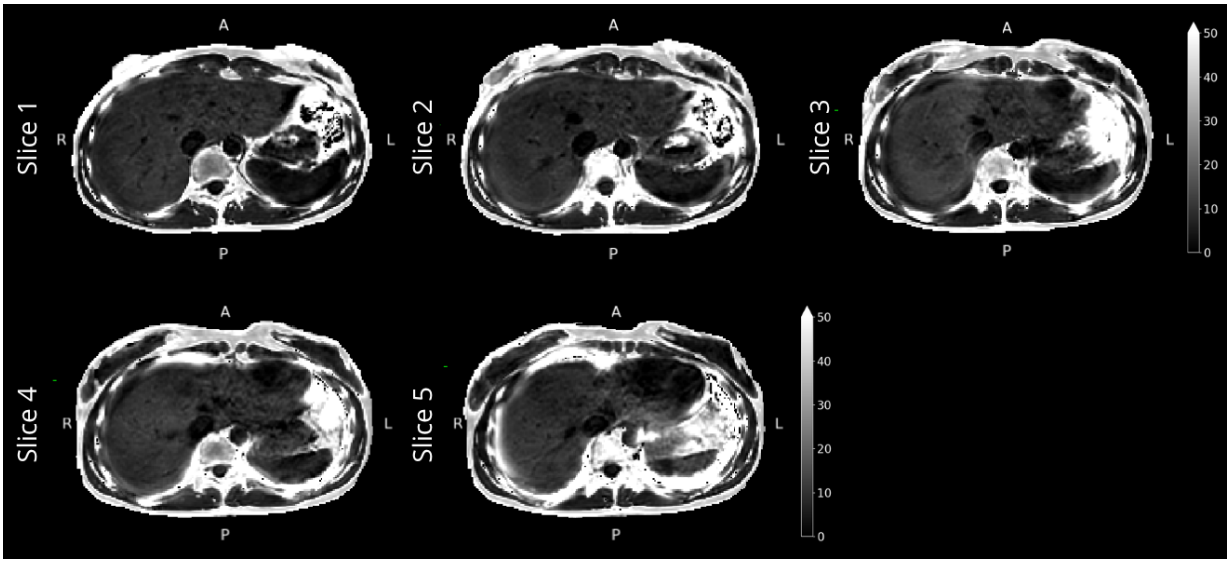

Figure 11.2: Representative slices of the R2′ map in the liver at 1.5 T.

11.2. Assessment of SMART2Map Sequence Quality

Goodness-of-Fit

Mean R^2 values exceeded 0.85 across all SMART2Map sequences in both whole-liver and ROI-based analyses. Figure A.4 shows an example of a binary map of R^2 images from all sequences on 1.5 T, where areas with R^2 values above 0.85 are highlighted in white. Visually, the FIESTA sequences showed a greater proportion of high R^2 voxels compared to the FSPGR sequences. An example for 3 T can be found in Appendix A.

The mean R^2 values are summarized in Figure 11.4. Overall, the 3 T shows higher mean R^2 values than the 1.5 T images. The R^2 values in the FIESTA-sequence images were higher than those in the FSPGR-sequence images for both field strengths. For all sequences on both field strengths, the difference in R^2 values measured in the ROIs between FB and BH was negligible.

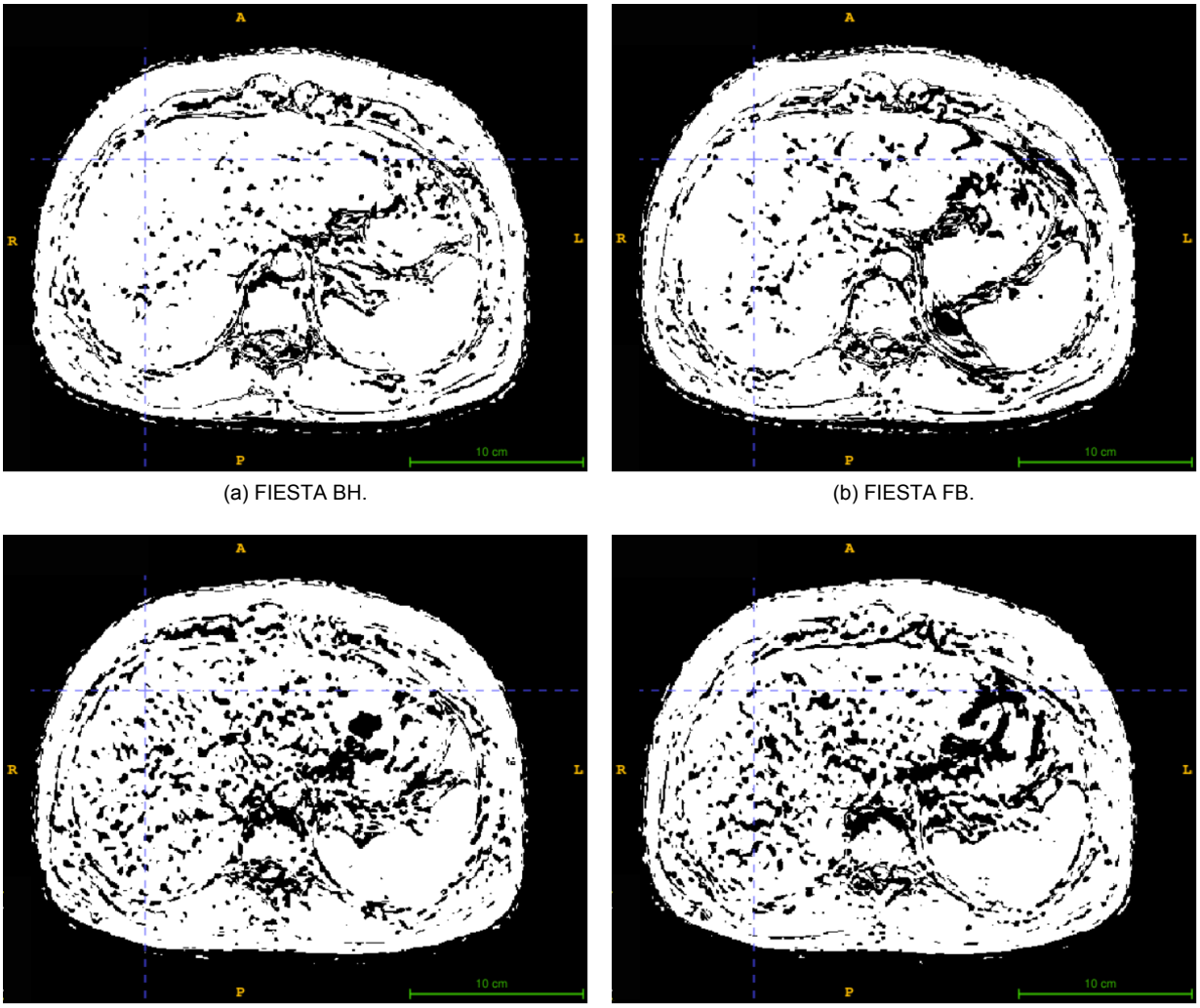

(a) FIESTA BH.

(b) FIESTA FB.

(c) FSPGR BH.

(d) FSPGR FB.

Note: Cut-off value 0.85

Figure 11.3: Comparison of R^2 binary masked goodness-of-fit maps across SMART2Map variants at 1.5 T.

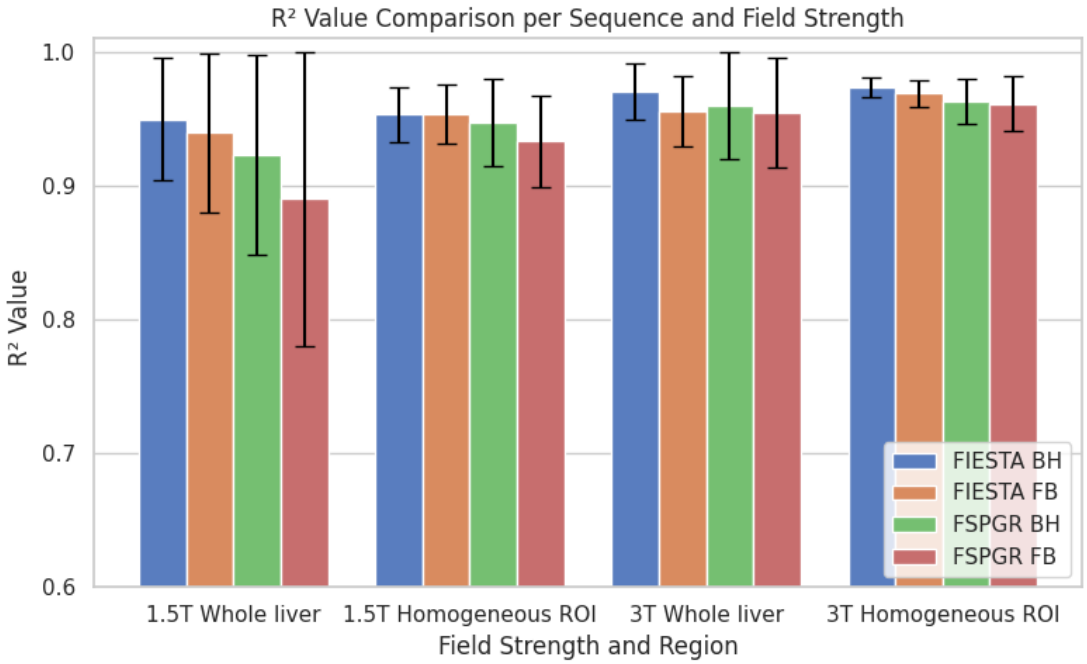

Figure 11.4: Boxplot comparison of whole-liver and ROI R^2 values between SMART2Map sequences at 1.5 T and 3 T.

T2 Relaxation Times

In Figure 11.5, as a representation, a single slice is shown, acquired with all four SMART2Map sequence options on 1.5 T (an example for 3 T images can be found in Appendix A). No apparent differences are observed between the FB and the BH acquisitions. However, the FSPGR images appear to be noisier than the FIESTA images.

The mean T2 relaxation times in the homogeneous ROI varied across the sequences as shown in Figure 11.6 for 3 T scans and Figure 11.7 for the 1.5 T scans. A repeated measures ANOVA showed no statistical differences in mean T2 values across the four sequences for both field strengths ($p=0.16$). However, a paired t-test revealed a significant difference in T2 values between 1.5 T and 3 T across all sequences ($p<0.003$).

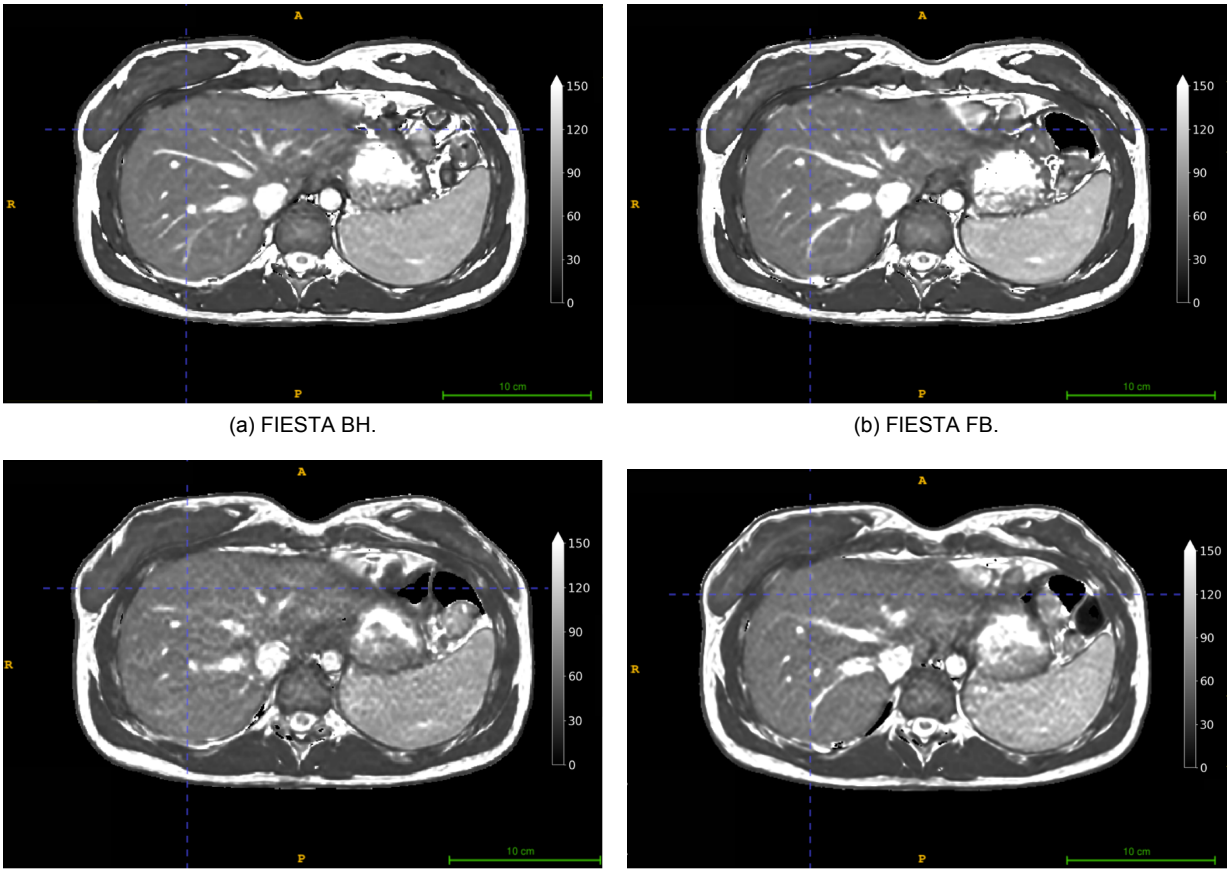

(a) FIESTA BH.

(b) FIESTA FB.

(c) FSPGR BH.

(d) FSPGR FB.

Figure 11.5: Example slice of T2 maps across SMART2Map variants at 1.5 T.

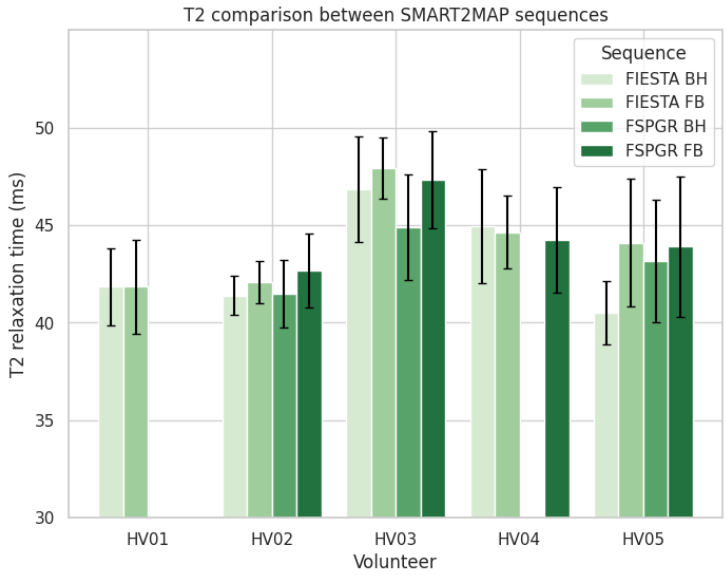

Figure 11.6: Boxplot comparison of T2 relaxation times across SMART2Map sequence variants on 3 T within a homogeneous ROI.

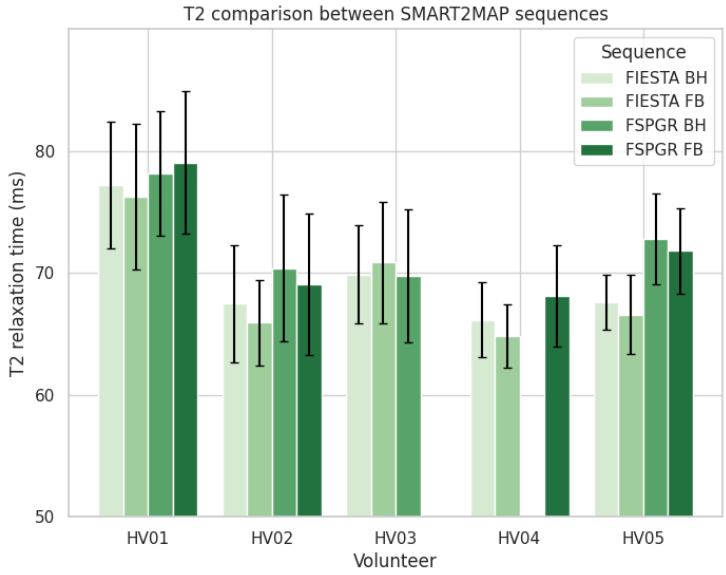

Figure 11.7: Comparison of T2 relaxation times across SMART2Map sequence variants on 1.5 T within a homogeneous ROI.

Comparing SMART2Map to Reference

Figure 11.8 displays an example representing the T2 maps acquired with the conventional 4-echo sequence and the SMART2Map FIESTA-FB sequences at 1.5 T and 3 T. The conventional sequence (Fig. 11.8a) demonstrates good image quality within the liver parenchyma. However, areas outside the liver show signal voids. In contrast, the SMART2Map sequence (Fig. 11.8b) shows good image quality across the entire slice, without the presence of signal voids.

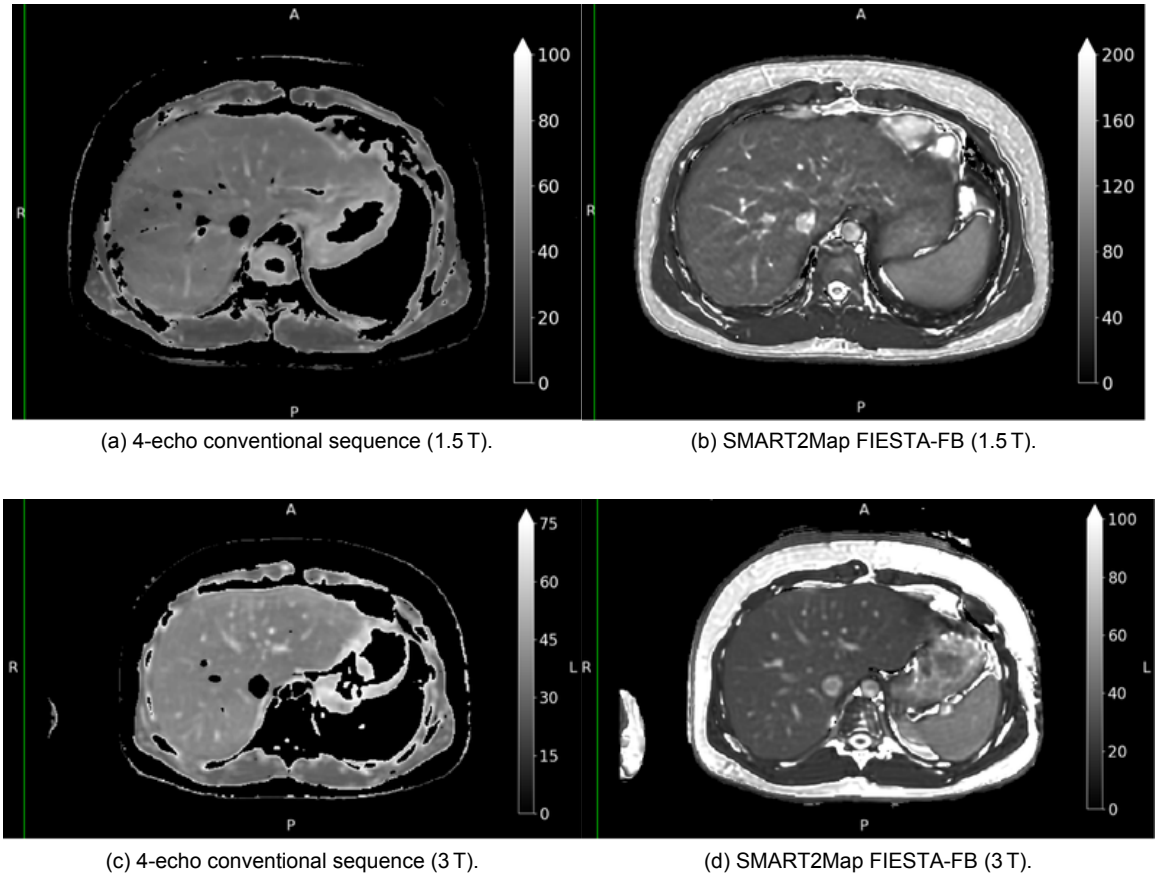

(a) 4-echo conventional sequence (1.5 T). (b) SMART2Map FIESTA-FB (1.5 T).

(c) 4-echo conventional sequence (3 T). (d) SMART2Map FIESTA-FB (3 T).

Intensity range: (a) 0-100 (b) 0-200 (c) 0-75 (d) 0-100

Figure 11.8: T2 maps acquired with the conventional 4-echo sequence and the SMART2Map FIESTA-FB sequences on 1.5 T and 3 T.

A paired t-test comparing T2 relaxation times between the SMART2Map and conventional 4-echo T2 mapping sequences revealed a significant difference at 1.5 T (p=*0.003*), with SMART2Map yielding higher T2 values. In contrast, no significant difference was observed at 3 T (p=*0.389*). The mean T2 values are visualized in Figure 11.9. The T2 relaxation times per volunteer can be found in Appendix A.

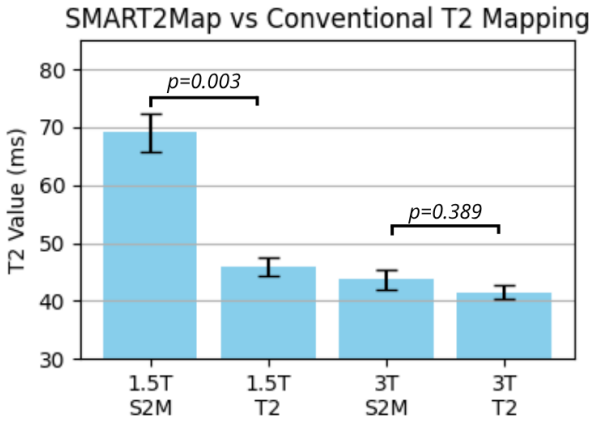

S2M = SMART2Map; T2 = T2map 4 echoes sequence

Figure 11.9: Comparison between T2 values from SMART2Map (FB FIESTA) and the conventional 4-echo T2 mapping sequence.

11.3. Comparative Analysis: 1.5 T vs 3 T

Artifacts and Visual Inspection

Figures 11.8 shows an example of the T2 maps on both field strengths. Visually, no clear differences in image quality were observed between the two field strengths. The conventional 4-echo sequence images show similar signal voids on both 1.5 T and 3 T.

Image quality differences were observed in the R2* maps. The 1.5 T images show more anatomical detail compared to the 3 T images. In both R2′ and R2* maps, a banding artifact was observed (see Figure 11.10). At 1.5 T, this artifact is primarily visible along the SI direction, with a bandwidth of approximately 12 mm. At 3 T, the effect is also present along the anterior-posterior axis, with a narrower bandwidth of around 4 mm.

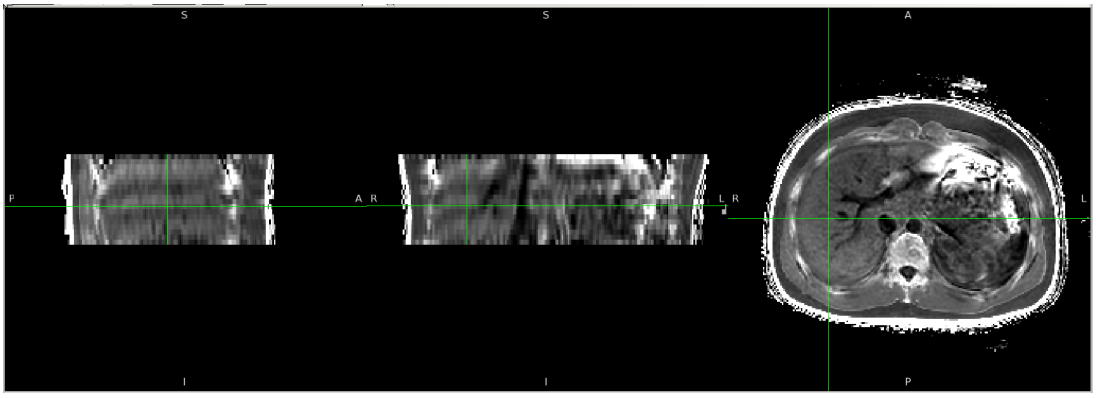

(a) 1.5 T.

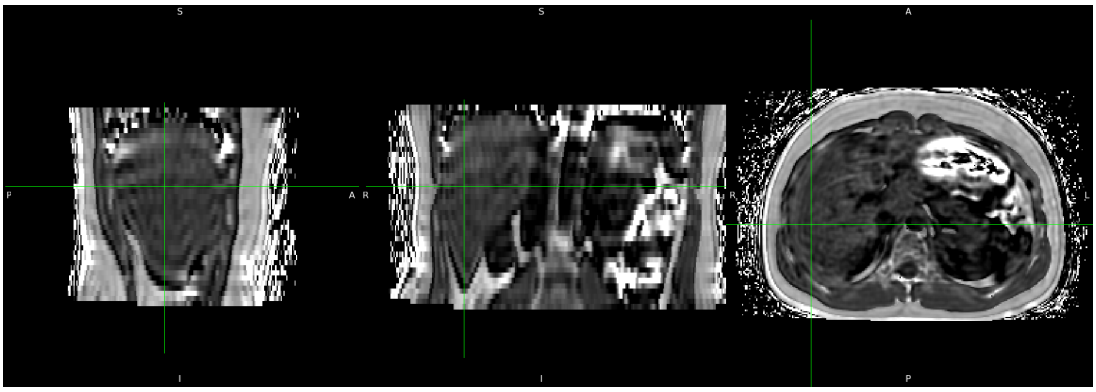

(b) 3 T.

Figure 11.10: Banding artifact observed in R2* maps, primarily in SI and AP directions, specific to IDEAL-IQ.

Relaxation Rates Dependence on Field Strength

In this section, we present the results of R2* (IDEALIQ), R2 (SMART2Map at 3 T, T2map 4-echoes at 1.5 T), and the computed R2′ relaxation rates. Appendix A provides an overview of all relaxation rates acquired. Figure 11.11 visualizes the relaxation rates per volunteer in a similar ROI for the two field strengths. Table 11.1 provides an overview of the mean relaxation rates over three ROIs. Statistically significant differences were observed between R2, R2*, and R2′ relaxation rates at 1.5 T and 3 T. The largest absolute difference was found in the R2* (14.65 s^{-1}).

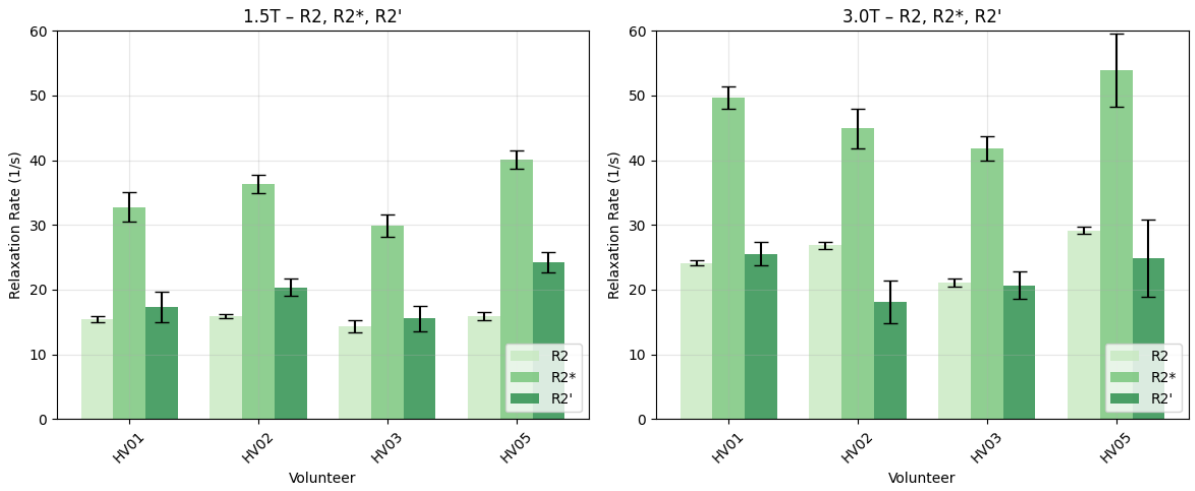

(a) Relaxation rates (T2map 4 echoes & IDEAL-IQ), 1.5 T.

(b) Relaxation rates (SMART2Map & IDEAL-IQ), 3 T.

Figure 11.11: Comparison of R2, R2* and R2′ relaxation rates within a homogeneous ROI, obtained using the 4-echo T2map sequence at 1.5 T and the SMART2Map FIESTA-FB sequence at 3 T.

Table 11.1: Mean relaxation metrics (R2, R2*, R2′) at 1.5 T and 3 T including statistical comparisons.

Metric	1.5T (mean ± std)	3.0T (mean ± std)	p-value
R2	21.54 ± 1.72	24.39 ± 1.96	0.002
R2*	34.28 ± 3.58	48.93 ± 4.65	0.000
R2′	12.74 ± 2.84	24.55 ± 4.80	0.000

Note: Relaxation rates in s^{-1}. 1.5 T R2 values are obtained from the 4echo conventional T2map sequence, the 3 T R2 values are obtained from the SMART2Map Fiesta FB sequence.

Image Quality Dependence on Field Strength

Figures 11.12 and 11.13 show the SNR across echo times for R2* and R2-weighted images, respectively. Overall, the mean SNR values are considered high (> 100), except for the fourth echo time in the R2 images at 3 T.

As shown in Figure 11.12, the mean SNR of the R2* images is consistently higher at 3 T compared to 1.5 T across all echo times (paired t-test: *p=0.01*). The SNR curve for the R2* images remained relatively stable across echo times. In contrast, Figure 11.13 shows a decreasing trend in SNR for the R2 images as echo time increases. While the SNR values at 1.5 T and 3 T are overall similar, the decline is steeper at 3 T. A paired t-test revealed no statistically significant difference in SNR between field strengths for the R2 images (*p=0.46*).

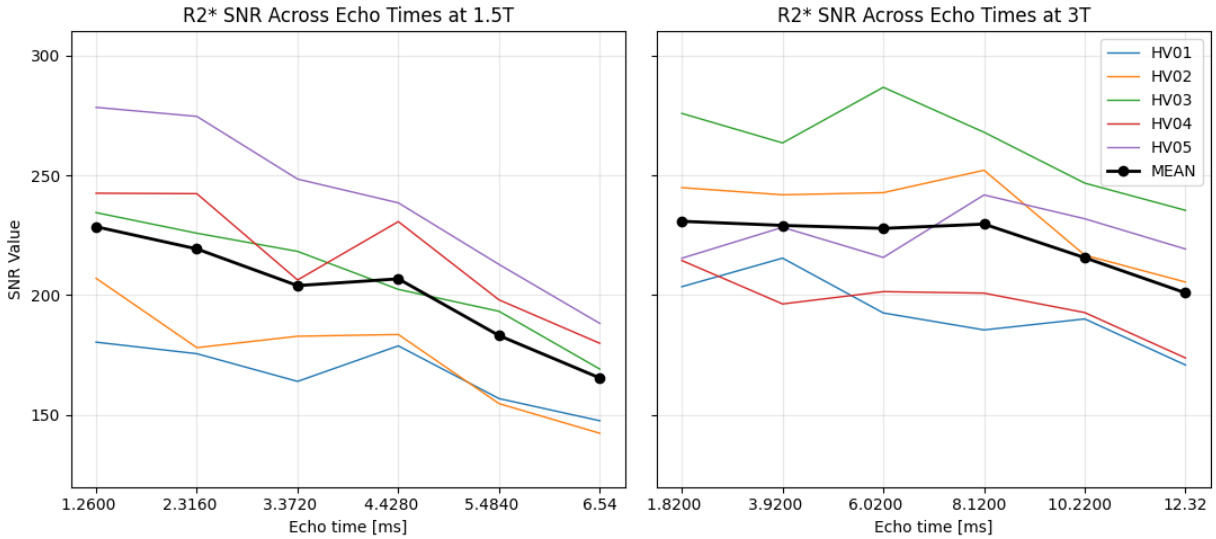

Figure 11.12: Comparison of mean SNR across echo times in R2* weighted images at 1.5 T and 3 T.

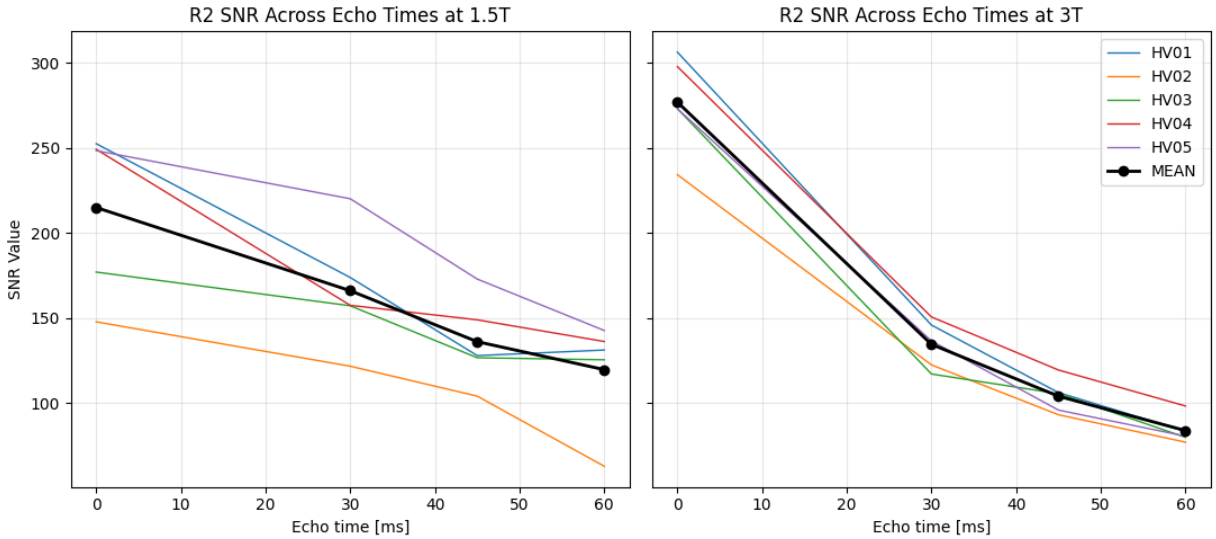

Figure 11.13: Comparison of mean SNR across echo times in R2 weighted images at 1.5 T and 3 T.

11.4. Motion-Related Image Variability

Motion between acquisitions was minimal, as confirmed by an abdominal radiologist, who reviewed the images and assessed liver displacement to be negligible. The degree of overlap is demonstrated in Figure 11.14.

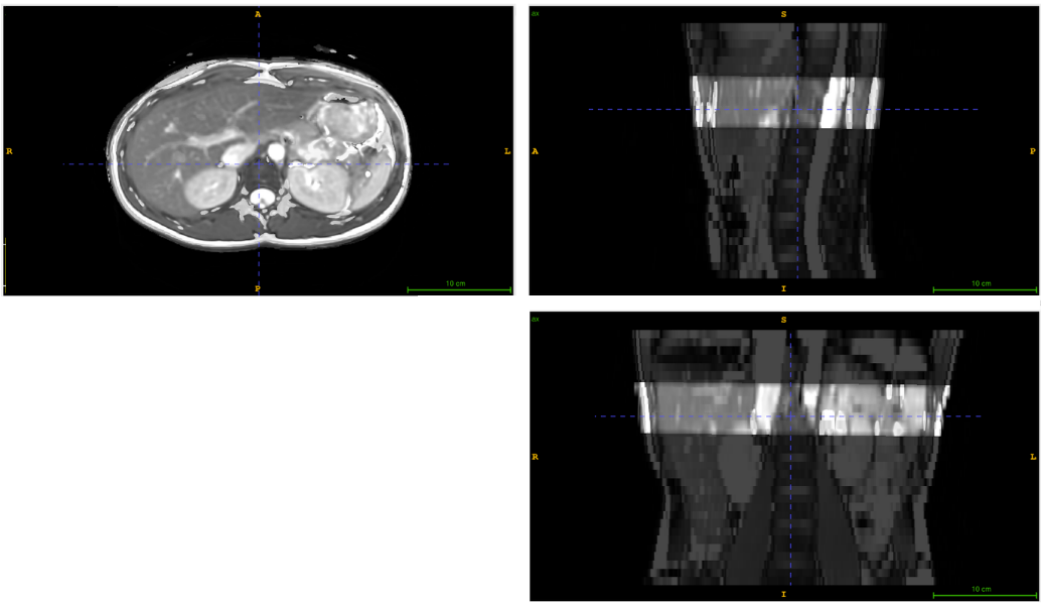

Figure 11.14: Overlay images from different sequences, demonstrating spatial alignment.

FB vs. BH in Practice

T2 maps obtained from both BH and FB acquisitions demonstrated comparable image quality, with no visible motion artifacts in the liver. Figure 11.15 illustrates an example of a well-performed and a poorly performed BH. In this study, however, only well-performed BHs were observed. The subtraction map in Figure 11.16 shows one slice per volunteer to demonstrate the similarity between the FB and BH SMART2Map images. Minimal blue regions were observed at the liver edges, indicating negligible respiratory motion effects. Highlighted regions primarily corresponded to blood vessels and fat tissue.

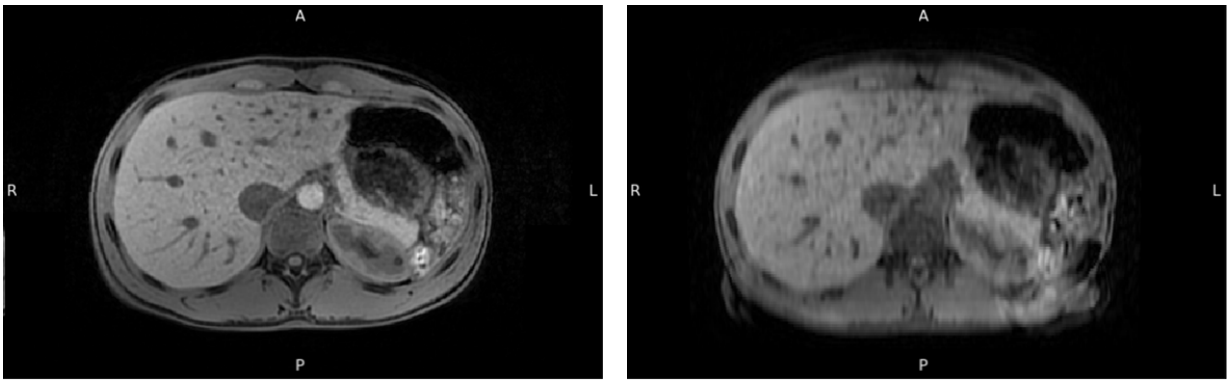

(a) (b)

Figure 11.15: Examples of breath-hold performance: (a) well-executed BH without motion artifacts; (b) poorly executed BH with visible motion artifacts.

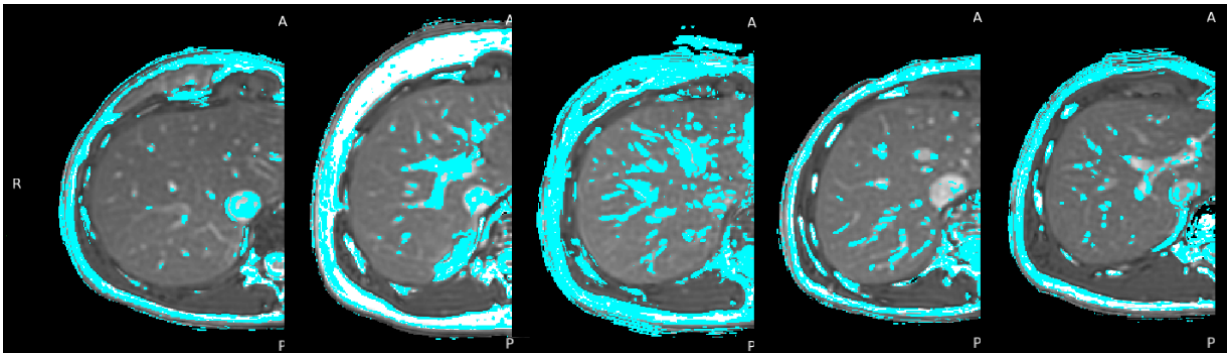

Figure 11.16: Subtraction maps for all volunteers showing similarity between BH and FB R2 maps; blue areas indicate differences.

Respiratory Motion

Table 11.2 summarises the measured cranial and caudal liver displacements for all volunteers.

Cranial displacement was consistently greater than caudal displacement, except for one measurement. The displacement values are different between the field strengths for all volunteers. The mean cranial displacement was 11.0 mm. The mean caudal displacement was 7.7 mm. Normality of displacement data was confirmed using the Shapiro–Wilk test.

A paired t-test revealed a statistically significant difference between cranial and caudal liver displacement ($p = 0.0085$).

Table 11.2: Respiratory displacement of cranial and caudal liver positions.

Field strength	Volunteer	Cranial Displacement [mm]	Caudal Displacement [mm]
1.5T			
	HV02	11.0	11.3
	HV03	20.0	12.0
	HV04	8.5	8.0
	HV05	8.7	4.1
3T			
	HV01	3.0	2.0
	HV02	9.0	6.5
	HV03	11.0	8.0
	HV04	17.6	11.2
	HV05	10.5	6.6
	Mean	**11.0**	**7.7**

12

Patient Scanning

A single patient was included. The additional scan time introduced by the MqBOLD sequences was less than three minutes. The resulting relaxation maps are shown in Figure 12.1, where visible contrast can be observed between healthy liver tissue and tumor tissue in the R2, R2*, and R2′ maps.

Quantitative analysis of these maps revealed clear differences between tumor and healthy liver tissue. The corresponding relaxation rates are summarized in Table 12.1. In homogeneous liver tissue, the mean R2 value was 25.2 ± 1.18, whereas in the tumor region it was lower, at 17.5 ± 1.19. R2* values were relatively similar between liver (75.3 ± 6.85) and tumor (80.1 ± 6.64). However, R2′ values were notably higher in the tumor (62.6 ± 7.21) compared to liver tissue (50.1 ± 6.95).

The R2 value in the patient's liver tissue was consistent with the R2 found in the healthy volunteers at 3.0 T (R2: 24.6 ± 2.06, R2*: 49.5 ± 6.29, R2′: 25.0 ± 6.16). In contrast, the R2* value in the liver was approximately 1.5 times higher than the reference.

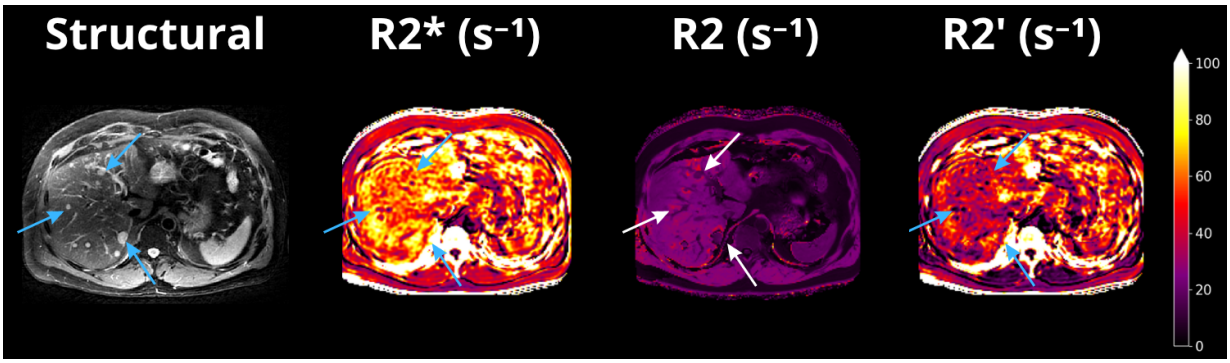

Figure 12.1: Patient relaxation maps acquired on a 3T MRI scanner. The left image shows a T2-weighted structural reference scan, while the middle and right images represent quantitative relaxation maps. Arrows indicate tumor tissue in the liver.

Table 12.1: Mean ± standard deviation of R2, R2*, and R2′ relaxation rates (in s^{-1}) measured in liver and tumor tissue of a single patient. Values are compared to reference relaxation rates obtained from five healthy volunteers scanned at 3.0 T.

Tissue	**R2 (s^{-1})**	**R2* (s^{-1})**	**R2′ (s^{-1})**
Liver	25.20 ± 1.18	75.30 ± 6.85	50.10 ± 6.95
Tumor	17.46 ± 1.19	80.05 ± 6.64	62.58 ± 7.21
Healthy Volunteers (3.0T)	24.57 ± 2.06	49.54 ± 6.29	24.97 ± 6.16

Part IV

Concluding Matter

13

Discussion

This study is the first to demonstrate the feasibility of multiparametric qBOLD imaging using FB acquisitions for estimating R2′ relaxation rates in the human liver. By optimizing R2* and R2 mapping sequences and applying them at both 1.5 T and 3 T, we show that non-invasive assessment of R2′ values can be achieved within clinically acceptable scan times. These findings mark an initial step in using R2′ relaxation rate as a marker for liver function. Additionally, the study addresses key practical challenges, including the breathing approach and identifying the optimal field strength for accurate measurement.

Relaxation Rates

Overall, the R2 and R2* found in this study are largely in line with the literature. Table 13.1 presents an overview of reported R2 and R2* relaxation rates in the liver from various studies, all based on healthy volunteers or control groups.

At 1.5 T, our mean hepatic R2 value was 21.5 s^{-1}, which corresponds well with previously reported values by de Bazelaire et al., and Merkle et al., who reported values of 21.7 and 23.0 s^{-1}, respectively [11][12]. At 3 T, the mean R2 value found was 24.5 s^{-1}, also corresponding with reported values, such as 23 s^{-1} [12] and 29.4 s^{-1} [11]. These findings confirm that our R2 measurements at both field strengths are consistent with established reference values.

Our mean measured R2* relaxation rates were 34.3 s^{-1} at 1.5 T and 48.9 s^{-1} at 3 T. These findings correspond well to the study by Kritsaneepaiboon et al., who reported R2* values of 32.3 and 49.8 s^{-1} at 1.5 T and 3 T, respectively [13]. Higher R2 values have been reported in other studies, particularly at 3 T, which may reflect differences in sequence parameters, ROI placement, or post-processing techniques [14][8].

Notably, no literature values were found for R2′, and therefore, no reference range is currently available for this parameter. However, assuming that the studies reporting R2 and R2* measured these parameters at the same anatomical location, R2′ values can be estimated as the difference between the two. For example, Wengler et al. reported R2 and R2* values of 34.9 s^{-1} and 63.4 s^{-1} at 3 T, yielding an estimated R2′ of 28.5 s^{-1}[8]. Similarly, Kritsaneepaiboon et al. reported values of 19.7 s^{-1} and 49.8 s^{-1} at 3 T, resulting in an R2′ of 30.1 s^{-1}[13]. At 1.5 T, their reported values of 18.3 s^{-1} and 32.3 s^{-1} yield an R2′ of 14.0 s^{-1}. In our study, we found mean R2′ values of 24.6 s^{-1} at 3 T and 12.8 s^{-1} at 1.5 T. These findings are broadly in line with the estimates derived from previous studies.

It is important to note that the reported relaxation values in the literature show considerable variability, indicating a lack of consensus regarding standard hepatic relaxation rates. This heterogeneity likely reflects differences in acquisition protocols.

The T2 relaxation times acquired with the SMART2Map sequence at 3 T were consistent with expectations based on literature values. However, the relaxation times measured at 1.5 T were higher than expected (Appendix A). When compared to the reference 4-echo T2 sequence, the SMART2Map values at 1.5 T showed poor agreement. Based on literature values (Table 13.1) and theoretical expectations, namely T2 is independent of B0, the 4-echo T2 sequence values are considered to provide more accurate results at 1.5 T [12] [15]. The elevated T2 values observed with SMART2Map at 1.5 T are likely due to sequence-specific effects such as T1 shine-through or fluid suppression within the liver. These factors

could interfere with accurate T2 estimation, but the exact cause remains unclear and requires further investigation.

In contrast to theoretical expectations, the article by Bazelaire et al., published shortened T2 times at 3 T compared to 1.5 T. They explain this phenomenon: ”T2 relaxation time can be shortened by the diffusion of water around magnetic molecules, such as hemoglobin in deoxygenated blood. Such effects increase with the field strength” [11].

Given its more consistent performance at 1.5 T compared to literature, the 4-echo reference sequence is preferred in this study, despite the reliance on BHs. For 3 T, the SMART2Map FB sequence is selected as the preferred option.

Table 13.1: Reference relaxation rates (R2, R2*) reported in existing literature.

		R2 [s^{-1}]		R2* [s^{-1}]	
	# slices	**1.5T**	**3.0T**	**1.5T**	**3.0T**
de Bazelaire CM., 2004 [11]	1	21.7	29.4		
Merkle EM., 2006 [12]	?	23.0	23.0		
Storey P., 2007 [14]	1			39.2	69.1
Kritsaneepaiboon S., 2017 [13]	1	18.3	19.7	32.3	49.8
Wengler K., 2019 [8]	1		34.9		63.4
Present study	5	21.5	24.4	34.3	48.9

Relaxation rates are in s^{-1}. R2 and R2* literature values for 1.5 T and 3 T. T2 and T2* values were converted to R2 and R2* values.

SMART2Map Sequence Selection

Both SMART2Map acquisitions' read-out methods for R2 mapping, FSPGR, and FIESTA provide acceptable results. However, upon visual inspection, the quality of the FIESTA acquisition was higher.

The absence of differences in quality between BH and FB acquisitions in this study is likely due to the inclusion of healthy volunteers, all of whom were able to perform consistent and well-executed BHs. In patient populations, however, BH performance is often more variable. Figure 11.15a shows a well-executed BH with no motion artifacts, while 11.15b shows a poorly executed BH with visible motion artifacts. This artefact can be avoided when using an FB sequence.

Another downside of the BH sequence is the longer scan time. An option would be to perform the SMART2Map sequence across multiple slices within a single BH. However, this resulted in signal variation, likely due to incomplete T1 relaxation between acquisitions (Figure in Appendix A.2).

To account for the potential impact of motion artifacts in clinical settings, and in line with the study's objective of maximizing patient comfort while maintaining image quality, the FB-FIESTA sequence was selected as the preferred method for R2 mapping.

Field Strength Considerations

In terms of visual image quality, 1.5 T was preferred over 3 T. R2 mapping showed comparable quality and SNR at both field strengths. For R2*, the visual quality was better at 1.5 T, although the SNR was slightly lower. Nevertheless, both field strengths provided sufficiently high SNR for reliable analysis of both R2 and R2* maps.

Despite the superior image quality at 1.5 T, SMART2Map did not yield the expected quantitative results at this field strength. As a result, the conventional R2 mapping sequence was used instead. This sequence was less desirable due to the presence of signal voids and the lack of an FB acquisition option. In contrast, at 3 T, SMART2Map performed well quantitatively and supported FB acquisition, although the overall image quality was slightly lower.

These findings highlight a trade-off between image quality, patient comfort, and quantitative performance. If visual clarity is important, 1.5 T may be preferred, if robust quantitative mapping and patient comfort are prioritized, 3 T is more suitable.

Scan Coverage

A key strength of this study is the use of multiple slices across the liver, rather than relying on a single mid-slice, as is common in many of the studies in the literature (Table 13.1). This approach improves spatial coverage and provides a more representative assessment of liver tissue. However, a FOV of five slices in the liver was used, which still does not cover the entire anatomical liver region. It covers approximately one-third of the liver in the SI direction.

After optimizing the protocol, only two sequences have to be used to create an R2′ map: an R2 map sequence and an R2* map sequence. This results in a total scan time of approximately two minutes for five slices. Expanding the field of view to include the entire liver would be feasible within a clinically acceptable scan time of around five minutes.

Occurrence and Handling of Non-Physical Values

A small number of negative values are observed in the calculated R2′ maps. Theoretically, such values should not occur, as R2′ relaxation is a component of R2* relaxation. Consequently, the R2′ relaxation rate cannot exceed the R2* relaxation rate. When this does occur, it indicates an error or artifact in the data.

Upon evaluating the spatial distribution of these negative values, they are consistently located at vessel walls, bowel, or skin. A plausible explanation for this observation is the presence of subtle motion artifacts. These artifacts can result in misalignment between corresponding voxels in the two scans used to compute the difference map. For example, a voxel located on the vessel wall in one scan may be misaligned with a voxel in the liver parenchyma in the other, leading to erroneous subtraction values.

Additionally, if the scans differ in spatial resolution, partial volume effects may contribute to erroneous values in the R2′ map. In regions with complex anatomical boundaries, a single voxel may represent a mixture of tissues in one scan but predominantly a single tissue type in the other. This mismatch in tissue composition between corresponding voxels can lead to artificially high or low values in the resulting difference map.

Such artifacts are difficult to correct due to the inevitable short time interval between the two acquisitions required for difference mapping. Even when performed within the same scan session, slight motion between scans is almost unavoidable. As a result, this limitation is inherent in the current method and must be acknowledged. Additionally, values in the difference map near sharp anatomical boundaries, such as vessel walls, should be interpreted with caution, as they may not be reliable.

A potential solution is the use of simultaneous multi-parametric scanning, which allows for the acquisition of both R2 and R2* maps within a single scan. This approach would eliminate inter-scan motion and improve the reliability of the resulting R2′ maps.

Dimensionality

The sequences used to create the R2′ difference map differ in dimensionality; a 2D acquisition was used for R2 mapping, while a 3D acquisition was used for R2* mapping.

Notably, when using an axial 2D sequence, there will always be limited resolution in the sagittal and coronal views. As a result, the 2D SMART2Map sequence becomes the limiting factor in generating a 3D R2′ map. Therefore, a 3D sequence for the R2 map scanning would be preferable. Additionally, 3D sequences are generally faster than 2D sequences.

Impact of Respiratory Protocol

Different breathing strategies were employed in this study: BH, FB using a surrogate signal, and FB using self-gating. One of the objectives of this study was to enable R2′ quantification under FB conditions, which was partially achieved.

Based on the included literature in Chapter 2, the recommended approach for measuring R2′ values in the liver is a MqBOLD technique utilizing a self-gated, FB acquisition strategy. However, due to limitations in the availability of acquisition methods, the breathing strategies used in this study were constrained to those compatible with the scanner protocols at our disposal. As a result, the most suitable breathing approach available for each sequence was selected.

A self-gated approach was used for the structural images through the 4DMR sequence. The image quality was rated non-inferior in comparison to conventional BH imaging. For R2 mapping, a respiratory

belt was used as a surrogate signal for FB acquisition. While this approach avoids the need for BH, it requires additional equipment and setup. Despite the relatively large respiratory-induced motion observed, the quality of the FB images using a surrogate signal was rated similar in quality to the BH images. No FB alternative was available for the R2* mapping sequence, and a single BH was required.

There are advantages to using 4D, self-gated scans when scanning the liver if you are in need to measure the breathing pattern. The 4DMR scan demonstrates this very well. The main advantage is the elimination of the need for BH or a surrogate signal obtained through a respiratory belt. This results in more comfort for the patient while maintaining image quality. The main disadvantage is the relatively long scan time. Where 3D sequences can create an image in the time of a single BH, 4D sequences can take several minutes. However, the 4DMR images have proven the potential of utilizing a self-gated, FB acquisition strategy.

Overall, this study presents a quantitative liver MRI protocol, measuring R2 and R2* values, requiring only one BH, representing a big reduction of BHs compared to previously published methods. Although a fully BH-free protocol was not achieved, this reduction marks a big advancement.

Liver Motion and Image Alignment

The SI liver displacement in this study was greater at the cranial point compared to the caudal point. This observation aligns with the findings reported by Tsai et al., who provided an overview of SI liver motion magnitudes across multiple studies. They reported a large variation in the motion, ranging from 8 mm to 24 mm [16]. The difference in displacement between cranial and caudal regions confirms that respiratory motion does not result in rigid body translation along the SI direction alone, but also induces morphological deformation of the liver.

Although no image registration techniques were applied before computing the difference maps, the resulting image alignment was considered sufficient for this study. An abdominal radiologist reviewed the image alignment and assessed liver displacement between scans to be negligible. This may be explained by the fact that both R2 and R2* mapping acquisitions were performed in one scan session at the same respiratory phase, end-of-expiration, thereby minimizing inter-scan displacement. Nonetheless, the liver is a morphologically dynamic organ, and its shape may vary slightly between scans, even within the same scan session. Simple registration methods (e.g., translation, rotation, or scaling) are inadequate to account for these variations fully. Huang et al. state: ”Much of the liver motion is cranial-caudal translation, so the rigid transformation captures much of the motion. However, there is still substantial residual deformation not accounted for by simple rigid-body motion” [17].

To address such complex deformations, advanced deformable image registration techniques are required. However, evaluating the accuracy of these methods in clinical practice remains challenging due to the lack of natural landmarks and the complex deformation patterns of the soft tissue [17]. Sen et al., provide an overview of advanced deformable registration techniques for liver imaging, reporting target registration errors of approximately 6 mm across various methods [18]. While such techniques may be beneficial for intersession alignment, their added value in intrasession settings, where misalignment is already minimal, appears limited. Therefore, although image registration could potentially enhance alignment further, its absence in this study did not affect the validity of the results.

Inhomogeneity Compensation

B0 correction was not applied in this study. However, the IDEAL-IQ sequence generates several reconstructed outputs next to an R2* map, including a B0 field map. Macroscopic magnetic field inhomogeneities contribute to R2* signal decay, but can be accounted for using the B0 map, which provides a quantitative measure of local field variation. An example of such a correction method is described by Wengler et al. [8]. Future work should therefore consider applying B0 correction to the R2* data to improve the accuracy of R2′ mapping.

Banding Artifact

The banding artifact observed in the R2′ maps originates from the underlying R2* maps. The alternating intensity between lighter and darker bands introduces a bias in the absolute R2* and R2′ values. However, comparisons of R2′ values within the same slice remain valid, as the bias is spatially consistent across the plane.

Importantly, the banding artifact is absent in the SMART2Map and 4DMR acquisitions, indicating that the issue is specific to the IDEAL-IQ protocol. This suggests that the artifact can be mitigated through further optimization of the IDEAL-IQ acquisition or reconstruction parameters.

Several strategies are available to address the banding effect:

- Post-processing: Image smoothing can be applied to reduce the visibility of the banding by averaging intensity variations across the image. However, since the bands are approximately 1 cm wide, a strong smoothing kernel would be required. This approach significantly reduces anatomical detail and leads to a loss in spatial resolution of the R2* values, making it less suitable for precise quantitative mapping.
- Sequence optimization: Modifying sequence parameters may help reduce the presence of artifacts. In this study, various settings such as resolution, voxel size, and excitation angle were tested. For the 3 T scanner, optimization led to a reduction in the visibility of the banding artifact, although it did not eliminate it. For the 1.5 T scanner, it was not managed to achieve a meaningful reduction in banding while maintaining both spatial resolution and adequate SNR. Consequently, GE's existing High-Resolution IDEAL-IQ sequence was used for this study as it provided the best trade-off between artifact suppression and image quality within the constraints of the available scanner protocols. Achieving substantial improvements would require other modifications, which demand additional time and expertise on the vendor or development side.
- Using an Alternative Sequence: It is also possible that the banding is an inherent limitation of the IDEAL-IQ sequence itself, in which case, an alternative acquisition method may be necessary to eliminate the artifact.

Patient Scanning

This patient case illustrates the feasibility of integrating the MqBOLD protocol into a routine clinical liver MRI workflow with minimal additional scan time. The results show that the method can detect measurable differences in relaxation rates between healthy and abnormal liver tissue.

Tumor tissue showed both elevated R2* and R2′ values and a reduced R2 value, relative to both the patient's healthy liver parenchyma and the reference data.

The observed reduction in R2 values within the tumor region may reflect increased water content or reduced cellular density, both common in malignant tissue. In contrast, the elevated R2* and R2′ values in the tumor suggest increased magnetic susceptibility effects, likely caused by higher concentrations of deoxyhemoglobin and abnormal microvascular architecture associated with angiogenesis. An elevation in R2* values is seen in the parenchyma of the patient's liver relative to the reference values. This is most likely due to a high iron content in the liver. This patient was diagnosed with a highly vascularized metastasis originating from a neuroendocrine tumor, which supports the observed elevations in R2* and R2′ values.

However, caution is warranted when interpreting the R2* and R2′ values. In this study, the R2* maps were affected by visible banding artifacts. Since R2′ values are calculated as the difference between R2* and R2, any inaccuracies in the R2* map directly propagate into the R2′ map, potentially compromising its reliability. As a result, the elevated R2′ values observed in the tumor may partly reflect artifact-related signal variation rather than true physiological differences.

Given these limitations, the R2 parameter appears to be the most robust and reliable metric. It is less sensitive to magnetic field inhomogeneities and was not visibly affected by artifacts in the current dataset. The consistent R2 values in the patient's healthy liver tissue, which closely matched those of the healthy volunteers, further support its stability and reproducibility. However, R2 alone does not provide information about tissue oxygenation, as it lacks sensitivity to the paramagnetic effects of deoxyhemoglobin that are captured in R2′.

While the findings in this patient case are promising, this study is limited by its single-patient design. Future work should include a diverse patient cohort with a wide variety of liver pathologies to validate the reproducibility and diagnostic value of MqBOLD-derived parameters, complemented by histopathological analysis to relate MqBOLD-derived parameters to underlying biological characteristics.

Translating Relaxometry to Functional Volume

While this research focused on accurate R2′ mapping, the ultimate goal is to estimate liver oxygenation in order to assess functional volume. Future work should aim to translate R2′ values into oxygen extraction fractions and deoxygenated blood volumes. This requires the implementation of perfusion imaging to account for non-random vessel orientation and high blood volume fractions, which influence the relationship between R2′ and oxygenation.

Fully FB / Self-Gating

Although this research minimized the number of BHs, not all sequences were yet compatible with fully FB acquisition. Further development and implementation of FB acquisition strategies, particularly for R2* mapping, would improve patient comfort and scan reproducibility. Moreover, based on the promising performance of the self-gated 4DMR sequence, future work could explore self-gating strategies for both R2 and R2* mapping.

Simultaneous Scanning

To reduce scan time and minimize possible inter-scan motion discrepancies, a future direction could be the development of sequences that enable the simultaneous acquisition of R2 and R2* maps. This can be done using MR Fingerprinting, as demonstrated by Ostenson et al. [19]. However, this method currently relies on a BH approach.

In addition to MR Fingerprinting, options involving direct R2′ mapping can also be promising. Techniques such as Asymmetric Spin Echo or Gradient Echo Sampling of Spin Echo can be used. As discussed in the literature study 2, these methods simultaneously assess multiple parameters, which can introduce variability due to their interdependent influence on the BOLD signal.

14

Conclusion

This thesis is the first to demonstrate the feasibility of R2′ mapping in the liver using a multiparametric MRI approach. It presents a short MRI protocol feasible at both 1.5 T and 3 T mostly under FB conditions. By optimizing and combining R2 and R2* mapping sequences, R2′ maps were generated in both healthy volunteers and a patient with liver metastasis, using only a single BH and with a total added scan time of under three minutes. The patient scan showed contrast between healthy liver tissue and abnormal tissue in the R2′ relaxation map, demonstrating the clinical potential of this method.

At both 1.5 T and 3 T, the measured R2 and R2* values aligned well with values reported in the literature, confirming the validity of the acquisition and processing pipeline. Although no direct reference values for R2′ exist, the values obtained in this study were consistent with estimates derived from prior studies.

While 1.5 T provided better visual image quality, 3 T yielded quantitative results in line with literature while allowing for free-breathing acquisitions. The SMART2Map FIESTA-FB sequence was identified as the preferred approach for R2 mapping at 3 T, offering a good balance between image quality, acquisition time, and patient comfort. For 1.5 T, the conventional T2 mapping BH sequence was preferred.

Limitations of the current approach include residual alignment differences between R2 and R2* acquisitions, as well as visible banding artifacts in the R2* maps. These factors affect the accuracy of the derived R2′ maps. Therefore, R2 currently remains the most robust and reliable quantitative parameter.

Looking forward, this thesis presents the first steps for non-invasive liver oxygenation imaging, with the potential to evolve into a clinically applicable tool for functional liver assessment.

References

[1] Gregory, J., Dioguardi Burgio, M., Corrias, G., Vilgrain, V., Ronot, M. Evaluation of liver tumour response by imaging. JHEP reports: innovation in hepatology. 2020 June;2(3):100100.

[2] Guglielmi, A., Ruzzenente, A., Conci, S., Valdegamberi, A., Iacono, C. How much remnant is enough in liver resection?. Digestive Surgery. 2012;29(1):6–17.

[3] Khan, A. S., Garcia-Aroz, S., Ansari, M. A., Atiq, S. M., Senter-Zapata, M., Fowler, K., et al. Assessment and optimization of liver volume before major hepatic resection: Current guidelines and a narrative review. International Journal of Surgery (London, England). 2018 Apr.;52:74–81.

[4] Muz, B., Puente, P. de la, Azab, F., Azab, A. K. The role of hypoxia in cancer progression, angiogenesis, metastasis, and resistance to therapy. Hypoxia. 2015 Dec.;3:83–92.

[5] Zou, B., Liu, X., Zhang, B., Gong, Y., Cai, C., Li, P., et al. The Expression of FAP in Hepatocellular Carcinoma Cells is Induced by Hypoxia and Correlates with Poor Clinical Outcomes. Journal of Cancer. 2018 Sept.;9(18):3278–3286.

[6] He, X., Yablonskiy, D. A. Quantitative BOLD: Mapping of Human Cerebral Deoxygenated Blood Volume and Oxygen Extraction Fraction: Default State. Magnetic resonance in medicine : official journal of the Society of Magnetic Resonance in Medicine / Society of Magnetic Resonance in Medicine. 2007 Jan.;57(1):115–126.

[7] Stone, A. J., Blockley, N. P. A streamlined acquisition for mapping baseline brain oxygenation using quantitative BOLD. Neuroimage. 2017;147:79–88.

[8] Wengler, K., Wang, J., Serrano Sosa, M., Gumus, S., He, A., Hussain, S., et al. Mapping hepatic blood oxygenation by quantitative BOLD (qBOLD) MRI. Magnetic Resonance in Medicine. 2019;81(5):3272–3282.

[9] Yablonskiy, D. A., Haacke, E. M. Theory of NMR signal behavior in magnetically inhomogeneous tissues: The static dephasing regime. Magnetic Resonance in Medicine. 1994;32(6):749–763.

[10] Bieri, O., Scheffler, K. Fundamentals of balanced steady state free precession MRI: Fundamentals of Balanced SSFP MRI. Journal of Magnetic Resonance Imaging. 2013 July;38(1):2–11.

[11] Bazelaire, C. M. J. de, Duhamel, G. D., Rofsky, N. M., Alsop, D. C. MR imaging relaxation times of abdominal and pelvic tissues measured in vivo at 3.0 T: preliminary results. Radiology. 2004 Mar.;230(3):652–659.

[12] Merkle, E. M., Dale, B. M., Paulson, E. K. Abdominal MR Imaging at 3T. Magnetic Resonance Imaging Clinics. 2006 Feb.;14(1):17–26.

[13] Kritsaneepaiboon, S., Ina, N., Chotsampancharoen, T., Roymanee, S., Cheewatanakornkul, S. The relationship between myocardial and hepatic T2 and T2* at 1.5T and 3T MRI in normal and iron-overloaded patients. Acta Radiologica (Stockholm, Sweden: 1987). 2018 Mar.;59(3):355–362.

[14] Storey, P., Thompson, A. A., Carqueville, C. L., Wood, J. C., Freitas, R. A. de, Rigsby, C. K. R2* imaging of transfusional iron burden at 3T and comparison with 1.5T. Journal of Magnetic Resonance Imaging. 2007;25(3):540–547.

[15] Bottomley, P. A., Foster, T. H., Argersinger, R. E., Pfeifer, L. M. A review of normal tissue hydrogen NMR relaxation times and relaxation mechanisms from 1–100 MHz: Dependence on tissue type, NMR frequency, temperature, species, excision, and age. Medical Physics. 1984;11(4):425–448.

[16] Tsai, Y.-L., Wu, C.-J., Shaw, S., Yu, P.-C., Nien, H.-H., Lui, L. T. Quantitative analysis of respiration-induced motion of each liver segment with helical computed tomography and 4-dimensional computed tomography. Radiation Oncology. 2018 Apr.;13(1):59.

[17] Huang, X., Ren, J., Abdalbari, A., Green, M. Deformable image registration for tissues with large displacements. Journal of Medical Imaging. 2017 Jan.;4(1):014001.

[18] Sen, A., Anderson, B. M., Cazoulat, G., McCulloch, M. M., Elganainy, D., McDonald, B. A., et al. Accuracy of deformable image registration techniques for alignment of longitudinal cholangiocarcinoma CT images. Medical Physics. 2020 Apr.;47(4):1670–1679.

[19] Ostenson, J., Damon, B. M., Welch, E. B. MR Fingerprinting with Simultaneous T1, T2, and Fat Signal Fraction Estimation with Integrated B0 Correction Reduces Bias in Water T1 and T2 Estimates. Magnetic resonance imaging. 2019 July;60:7–19.

Part V

Appendices

A

Additional Results

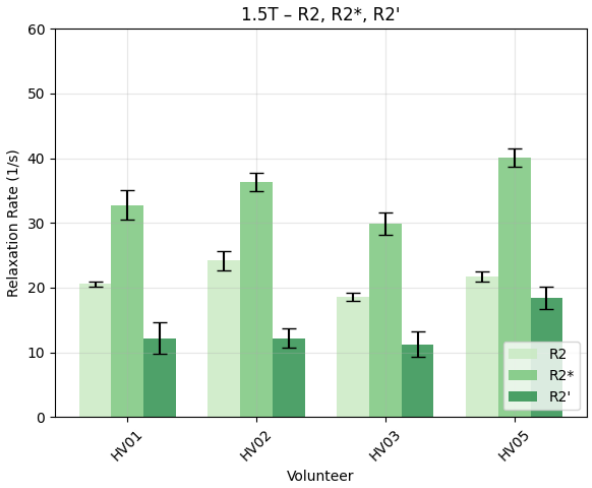

(a) Relaxation rates (SMART2Map & IDEAL-IQ), 1.5 T.

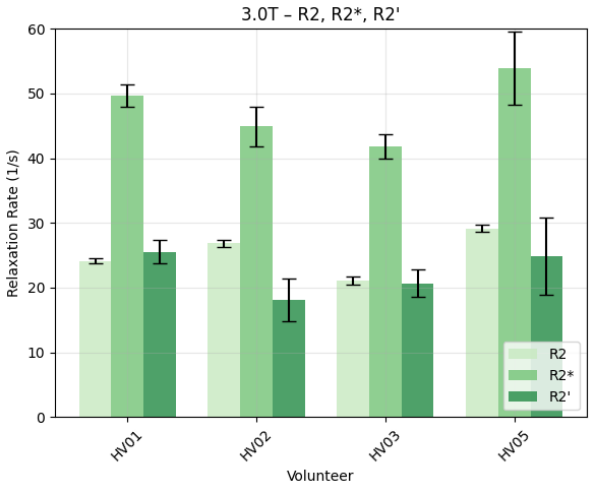

(b) Relaxation rates (SMART2Map & IDEAL-IQ), 3 T.

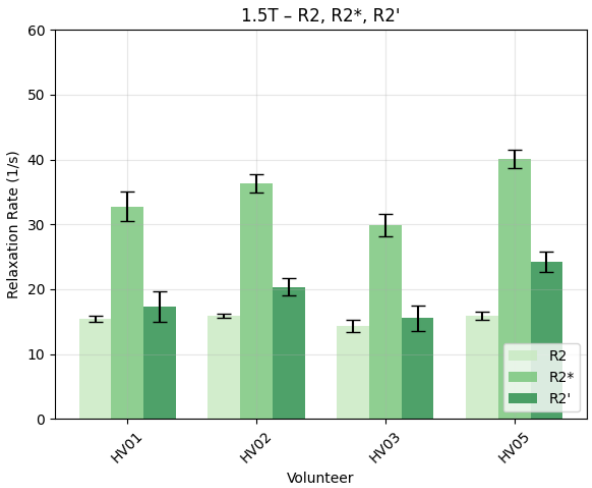

(c) Relaxation rates (T2map 4 echoes & IDEAL-IQ), 1.5 T.

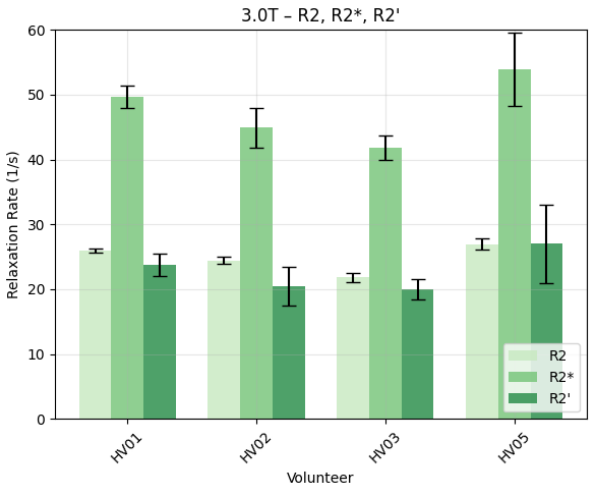

(d) Relaxation rates (T2map 4 echoes & IDEAL-IQ), 3 T.

Figure A.1: Comparison of relaxation rates between 1.5 T and 3 T in T2 weighted images within an ROI for R2 values measured with SMART2Map FIESTA-FB and T2map 4 echoes.

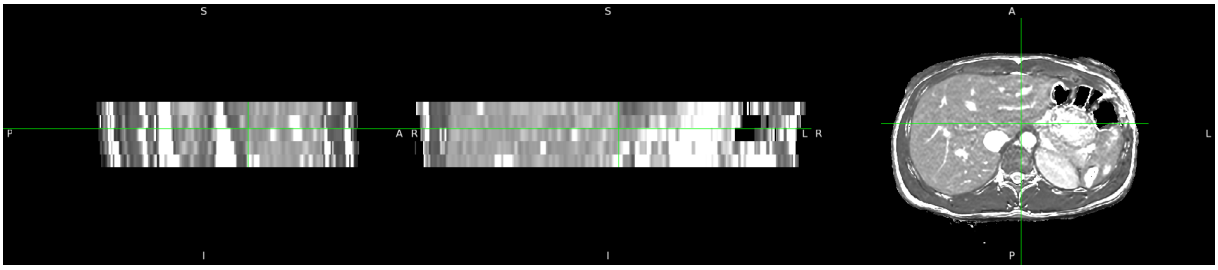

(a) All five slices acquired within a single breath-hold, showing contrast differences between the first slice and the subsequent slices.

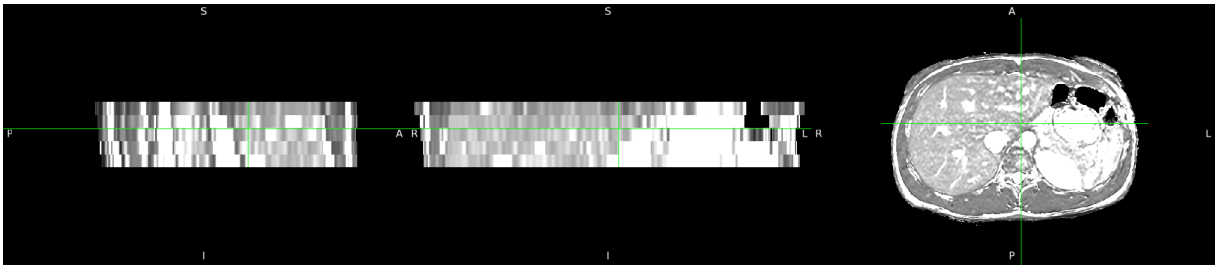

(b) Five slices acquired using five separate breath-holds, resulting in more consistent contrast across slices.

Figure A.2: Comparison of free-breathing and breath-hold acquisition strategies across five liver slices.

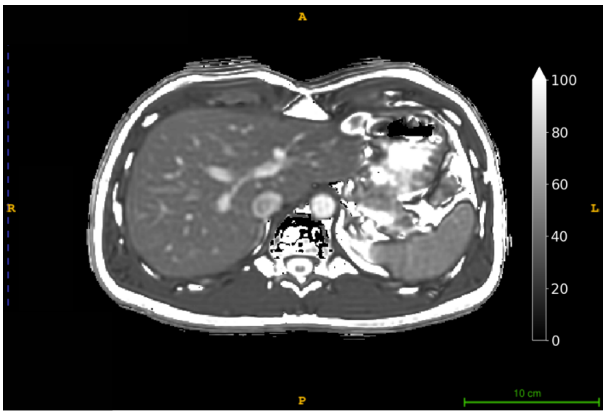

(a) FIESTA BH.

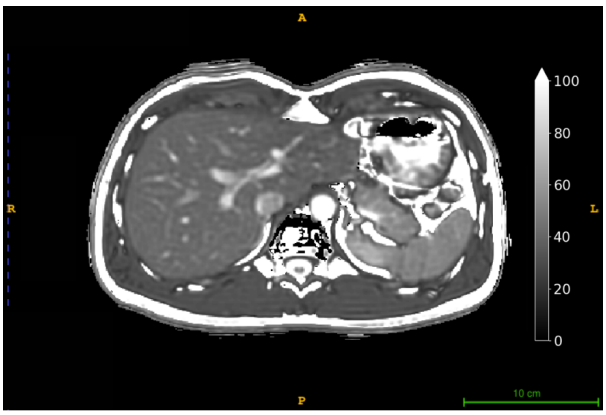

(b) FIESTA FB.

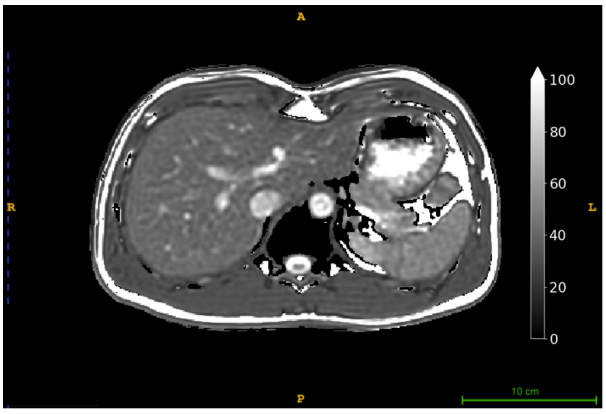

(c) FSPGR BH.

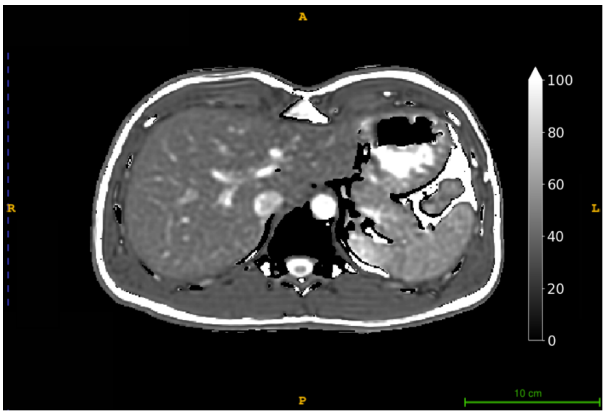

(d) FSPGR FB.

Figure A.3: Representative T2 maps across SMART2Map variants at 3 T.

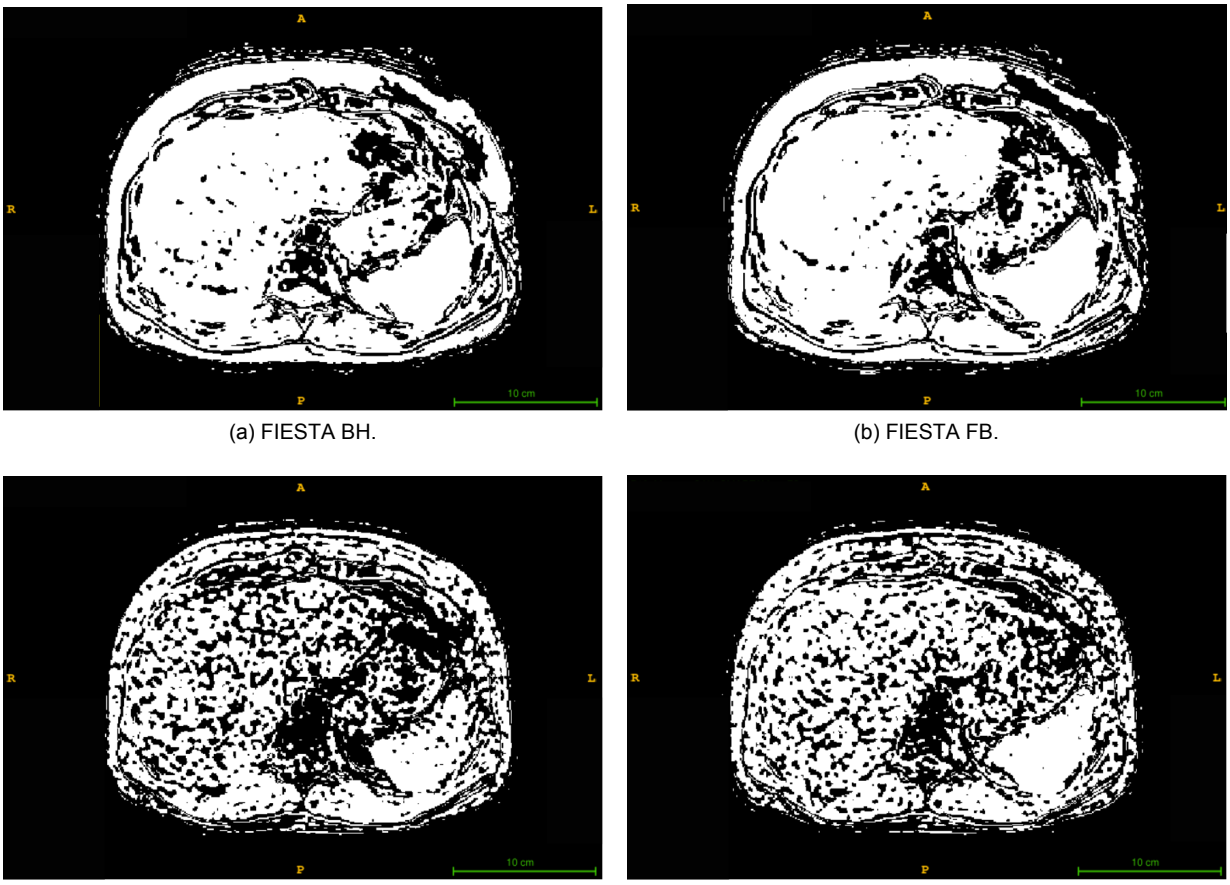

(a) FIESTA BH. (b) FIESTA FB.

(c) FSPGR BH. (d) FSPGR FB.

Note: cut-off value 0.95

Figure A.4: Comparison of R^2 binary masked goodness-of-fit maps across SMART2Map variants at 3 T.

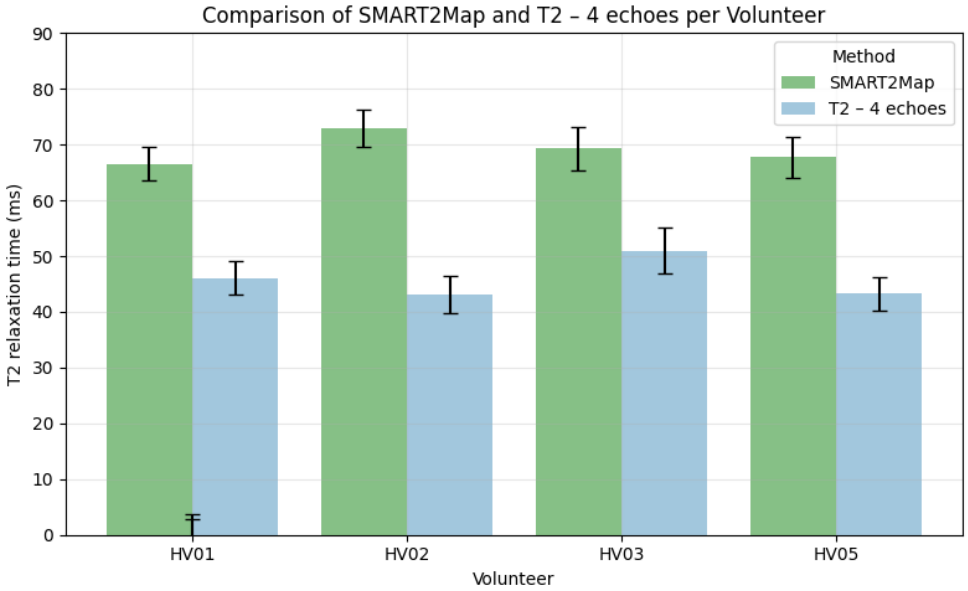

Figure A.5: Comparison of T2 relaxation times between SMART2Map- FIESTA FB sequence and the reference T2 sequence on 1.5 T within a homogeneous ROI.

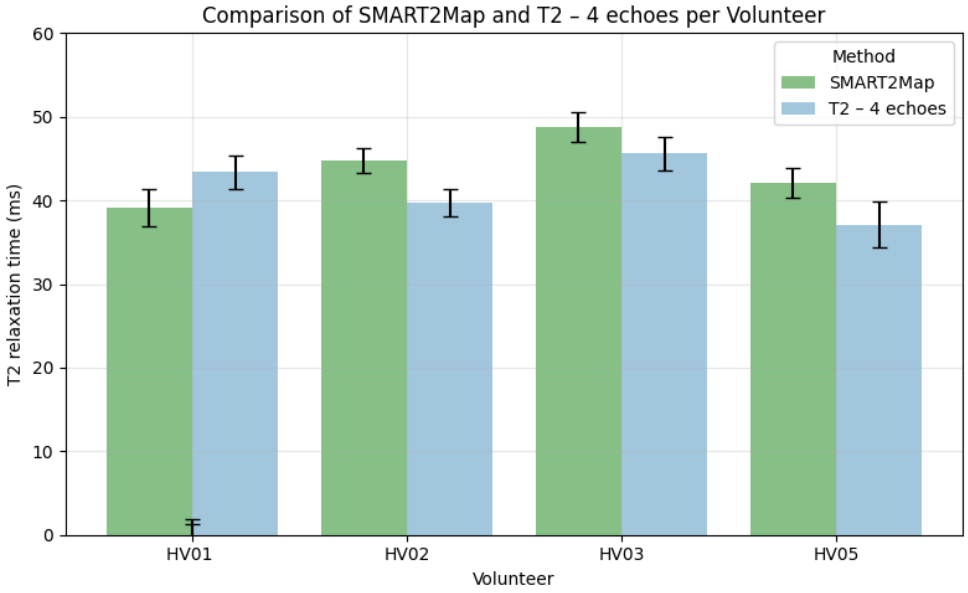

Figure A.6: Comparison of T2 relaxation times between SMART2Map- FIESTA FB sequence and the reference T2 sequence on 3 T within a homogeneous ROI.

B

Python Code

Python version: 3.10.12

B.1. Fitting

```python
import nibabel as nib
import numpy as np
from scipy.optimize import curve_fit
from joblib import Parallel, delayed
import os

def fit_T2_map(TEs, echo_files, output_path, slice_range):
    """
    Fit a T2 relaxation map voxel-wise using an exponential decay model.

    Parameters:
    TEs (array-like): Echo times in milliseconds (e.g., [0, 30, 45, 60]).
    echo_files (list of str): List of file paths to NIfTI echo images, ordered by TE.
    output_path (str): File path to save the resulting T2 map (NIfTI format).
    slice_range (range): Range of slices (in z-dimension) to process (e.g., range(0, 5)).
    """

    def signal_model(te, S0, T2):
        """Mono-exponential signal decay model."""
        return S0 * np.exp(-te / T2)

    # Load all echoes into a 4D stack: [x, y, z, echo]
    echo_vols = [nib.load(f).get_fdata() for f in echo_files]
    echo_stack = np.stack(echo_vols, axis=-1)
    x_dim, y_dim, z_dim, _ = echo_stack.shape

    T2_map = np.zeros((x_dim, y_dim, z_dim))

    def fit_voxel(x, y, z):

        signals = echo_stack[x, y, z, :]
        if np.all(signals > 0):
            try:
                popt, _ = curve_fit(
                    signal_model,
                    TEs,
                    signals,
                    p0=(signals[0], 50),
                    bounds=([0, 1], [1e5, 500]),
                    maxfev=10000
                )
                return (x, y, popt[1])  # Return T2 value only
            except:
                return (x, y, 0)
        else:
            return (x, y, 0)

    # Process selected slices
```

```
    for z in slice_range:
        print(f"Fitting slice {z}...")

        # Parallel voxel-wise fitting
        results = Parallel(n_jobs=-1, backend="loky")(
            delayed(fit_voxel)(x, y, z) for x in range(x_dim) for y in range(y_dim)
        )

        for x, y, t2 in results:
            T2_map[x, y, z] = t2

    # Save T2 map as NIfTI file
    ref_img = nib.load(echo_files[0])
    T2_nii = nib.Nifti1Image(T2_map, affine=ref_img.affine, header=ref_img.header)
    nib.save(T2_nii, output_path)

    print(f"T2 map saved to: {output_path}")
```

Listing B.1: Python script to fit the T2 map from echo images

B.2. Resampling

```

import SimpleITK as sitk
import numpy as np
import argparse
import os


def main(path, reference, resultpath, mask=None, maskout=None):
    #Load image
    img = sitk.ReadImage(path)
    ref = sitk.ReadImage(reference)

    #resample image and optionally mask
    resample = sitk.ResampleImageFilter()
    resample.SetOutputDirection(ref.GetDirection())
    resample.SetOutputOrigin(ref.GetOrigin())
    resample.SetInterpolator(sitk.sitkLinear)
    # resample.SetInterpolator(sitk.sitkNearestNeighbor)
    resample.SetTransform(sitk.Transform(3, sitk.sitkIdentity))

    resample.SetSize(ref.GetSize())
    resample.SetOutputSpacing(ref.GetSpacing())

    resample.SetNumberOfThreads(1)

    resampled_img = resample.Execute(img)
    sitk.WriteImage(resampled_img, resultpath)

    if mask is not None:
        mask_image = sitk.ReadImage(mask)
        resampled_mask = resample.Execute(mask_image)
        sitk.WriteImage(resampled_mask, maskout)

    return

if __name__ == '__main__':
    parser = argparse.ArgumentParser(description="Resample an image to 1x1x1 voxels")
    parser.add_argument('--img', type=str, required=True, help="Image path")
    parser.add_argument('--ref', type=str, required=True, help="Image path to resample to")
    parser.add_argument('--mask', type=str, required=False, help="Mask path")
    parser.add_argument('--imgout', type=str, required=True, help="Image output path")
    parser.add_argument('--maskout', type=str, required=False, help="Mask output path")
    args = parser.parse_args()
    main(args.img, args.ref, args.imgout)
```

Listing B.2: Python script to preprocess the maps by resampling

B.3. Conversion R2 Maps to T2 Maps

```python
import nibabel as nib
import numpy as np
import matplotlib.pyplot as plt

"""
Convert between R2* maps and T2* maps.
"""

def convert_r2_to_t2(r2_image, t2_output='T2map_converted.nii.gz'):
    """
    Converts an R2 map to a T2 map and saves the result.

    Parameters:
    r2_image (str): Path to the input R2* map (NIfTI file).
    t2_output (str): Path for saving the output T2* map (NIfTI file).
    """

    # Load the R2* map
    r2_img = nib.load(r2_image)
    r2_data = r2_img.get_fdata()

    # Replace zero/near-zero values with NaN to avoid division errors
    r2_data[r2_data <= 0.01] = np.nan

    # Convert R2 to T2 (in milliseconds)
    t2_data = 1 / (r2_data / 1000)

    # Save the T2* map
    t2_img = nib.Nifti1Image(t2_data, r2_img.affine, header=r2_img.header)
    nib.save(t2_img, t2_output)

    print("Conversion completed. T2* map saved as:", t2_output)


def convert_t2_to_r2(t2_image, r2_output='R2star_map_converted.nii.gz'):
    """
    Converts a T2* map to an R2* map and saves the result.

    Parameters:
    t2_image (str): Path to the input T2* map (NIfTI file).
    r2_output (str): Path for saving the output R2* map (NIfTI file).
    """

    # Load the T2* map
    t2_img = nib.load(t2_image)
    t2_data = t2_img.get_fdata()

    # Replace invalid values with NaN
    t2_data[t2_data <= 0] = np.nan
    t2_data[t2_data >= 999] = np.nan  # Exclude implausibly large values

    # Convert T2* to R2* (in /second)
    r2_data = (1 / t2_data) * 1000

    # Save the R2* map
    r2_img = nib.Nifti1Image(r2_data, t2_img.affine, header=t2_img.header)
    nib.save(r2_img, r2_output)

    print("Conversion completed. R2* map saved as:", r2_output)
```

Listing B.3: Python script to convert R2 maps to T2 maps or the other way around

B.4. Difference Map Computation

```python

import nibabel as nib
import numpy as np
import os
```

```python

def compute_r2prime_difference(base_path, r2star_filename, r2_filename, mask_filename=None):
    """
    Compute the 'R2 (R2 star minus R2) difference map.

    Parameters:
    base_path (str): Directory containing the input NIfTI files.
    r2star_filename (str): Filename of the R2* map (e.g., 'R2star_map.nii.gz').
    r2_filename (str): Filename of the R2 map (e.g., 'R2_map.nii.gz').
    mask_filename (str, optional): Optional filename of a binary mask.

    Returns:
    numpy.ndarray: The computed 'R2 difference map (3D array).
    """

    # Load R2* and R2 maps
    r2star_img = nib.load(os.path.join(base_path, r2star_filename))
    r2star_data = r2star_img.get_fdata()

    r2_img = nib.load(os.path.join(base_path, r2_filename))
    r2_data = r2_img.get_fdata()

    # Valid data mask to exclude zero or near-zero values
    valid_mask = (r2star_data > 0.05) & (r2_data > 0.05)

    # Compute 'R2 difference map
    r2prime = np.where(valid_mask, r2star_data - r2_data, 0)

    # Apply anatomical mask if provided
    if mask_filename:
        mask_img = nib.load(os.path.join(base_path, mask_filename))
        mask_data = mask_img.get_fdata()
        r2prime = r2prime * mask_data

    return r2prime
```

Listing B.4: Python script to compute the R2p difference map

C

Informed Consent

The Informed Consent below was signed by all volunteers before taking part in the study.

Proefpersoneninformatie voor deelname aan medisch-wetenschappelijk onderzoek

Ontwikkeling van MRI technologie voor verbeterde visualisatie en kwantificatie van weefsel en organen van gezonde vrijwilligers

Inleiding

Geachte heer/mevrouw,

Met deze informatiebrief willen we u vragen of u wilt meedoen aan medisch-wetenschappelijk onderzoek. Meedoen is vrijwillig. U krijgt deze brief omdat U naar aanleiding van de advertentietekst belangstelling getoond voor een wetenschappelijk onderzoek bij gezonde mensen voor het optimaliseren en evalueren van nieuwe en aangepaste MRI scan protocollen.
U leest hier om wat voor onderzoek het gaat, wat het voor u betekent, en wat de voordelen en nadelen zijn. Het is veel informatie. Wilt u de informatie doorlezen en beslissen of u wilt meedoen? Als u wilt meedoen, kunt u het formulier invullen dat u vindt in bijlage C.

Stel uw vragen
U kunt uw beslissing nemen met de informatie die u in deze informatiebrief vindt. Daarnaast raden we u aan om dit te doen:
- Stel vragen aan de onderzoeker die u deze informatie geeft.
- Praat met uw partner, familie of vrienden over dit onderzoek.
- Stel vragen aan de onafhankelijk deskundige. Voor contactgegevens zie bijlage A
- Lees de informatie op www.rijksoverheid.nl/mensenonderzoek.

1. Algemene informatie

Het Erasmus Medisch Centrum te Rotterdam heeft dit onderzoek opgezet. Hieronder noemen we het Erasmus MC steeds ‘de opdrachtgever’.

Deelnemers aan een medisch-wetenschappelijk onderzoek worden vaak proefpersonen genoemd. Zowel patiënten als mensen die gezond zijn, kunnen proefpersoon zijn.

Voor dit onderzoek zijn 1000 proefpersonen nodig.

De Medisch Ethische Toetsingscommissie van het Erasmus Medisch Centrum te Rotterdam heeft dit onderzoek goedgekeurd..

2. Wat is het doel van het onderzoek?

Het doel van het onderzoek is het optimaliseren en uittesten van nieuwe en gemodificeerde MRI- opnametechieken/technologieën. De meerwaarde van deze opnametechieken/technologieën voor gebruik bij patiënten en voor wetenschappelijk onderzoek zal worden vastgesteld.

3. Wat is de achtergrond van het onderzoek?

Magnetische Resonantie Imaging (MRI) is een techniek waarmee afbeeldingen van het menselijk lichaam worden gemaakt met behulp van een sterk magneetveld. Na het plaatsen van een persoon in dit magneetveld worden door de scanner radiogolven uitgezonden naar het lichaam. Deze worden vervolgens ook weer afgegeven en door de scanner opgevangen.

Bij een MRI-onderzoek kan het apparaat op verschillende manieren worden ingesteld, te vergelijken met de instellingen van een fotocamera, om een goed beeld te verkrijgen. Normaliter worden er tijdens het MRI-onderzoek verschillende soorten opnames gemaakt. Elke opname heeft zijn eigen instelling van de MRI scanner en elke opname heeft zijn eigen beeldcontrast. Zo is bijvoorbeeld in de ene opname vocht afgebeeld als een witte structuur, terwijl in een andere opname vocht wordt afgebeeld als een donkere structuur. Deze verschillende opnames zijn van belang voor de arts om een diagnose vast te kunnen stellen. Hoe langer een opname duurt, hoe beter de beeldkwaliteit wordt. Echter omdat een mens zich maar voor beperkte tijd stil kan houden, is het van belang deze tijd zo kort mogelijk te houden zonder dat dit de kwaliteit van de opnames verslechtert.

De techniek en de computer programma's van de MRI-scanner worden steeds verbeterd en er komen ook regelmatig nieuwe opname technieken bij. Deze nieuwe opname technieken moeten wel eerst worden getest voordat ze gebruikt kunnen worden in de patiëntenzorg of in wetenschappelijk onderzoek. Zo moet opnieuw worden vastgesteld wat de beste instellingen is van de scanner. Optimaal is die opname die in zo kort mogelijk tijd de beste afbeeldingen maakt. Het gaat hier om optimalisatie van scan protocollen voor MRI onderzoek van hoofd, nek, borstkas, buik, armen of benen.

Het aanpassen van de instellingen van de scanner wordt in eerste instantie gedaan met behulp van testobjecten . Op een zeker moment is het echter nodig om verschillende instellingen van een opname te vergelijken bij personen. Het optimaliseren van de MRI instelling kan ook worden uitgevoerd bij patiënten, maar zij zouden dan aansluitend aan hun eigenlijke onderzoek langer in de MRI scanner zou moeten liggen. Een goede manier om deze optimalisatie uit te voeren is het gebruik van vrijwilligers. Bij deze vrijwilligers is het MRI-onderzoek volledig gericht op het testen van deze nieuwe instellingen. Na de optimalisatie van de instelling van de scanner volgen vergelijkende studies waarin de nieuwe of aangepaste opnametechiekenopnametechnieken worden vergeleken met bestaande opnametechiekentechnieken. Hierbij wordt gekeken naar beeldkwaliteit, maar ook naar de mogelijkheden van de nieuwe opnametechnieken om structuren af te beelden die eerder niet konden worden afgebeeld. De meerwaarde van de nieuwe of gemodificeerde opnametechieken wordt zo duidelijk.

Een aantal nieuwe of aangepaste MRI kenopnametechieken zijn specifiek ontwikkeld om bloedvaten af te beelden, de weefsel doorbloeding te meten of de aankleuring van weefsels te beoordelen. Bij het optimaliseren of uittesten van deze opnametechieken zal contrastvloeistof worden toegediend. Dit gebeurt via een infuusnaald die voorafgaand aan het MRI-onderzoek in een ader in uw arm wordt gebracht. Bij het testen van sommige opnametechieken zal tevens één buisje bloed uit het infuus worden afgenomen. U wordt hiervoor niet extra geprikt. In het bloed zal het hematocriet worden bepaald (relatieve maat voor hoeveelheid rode bloedcellen in uw bloed). Voor het testen van opnametechieken waarbij het toedienen van contrastmiddel en/of afnemen van bloed nodig is vragen wij u specifiek om toestemming. Indien u hiervoor geen toestemming geeft, kunt u alleen meedoen aan het testen van opnametechieken waarbij geen contrastmiddel en/of bloedafname nodig is. We zullen u niet vaker dan 4 keer per jaar vragen mee te doen aan een MRI studie die in totaal 4 jaar zal duren. Als u toestemming geeft voor het testen van opnametechieken waarbij contrastmiddel wordt toegediend, dan zult u hiervoor niet vaker dan 2 keer per jaar worden gevraagd..Wanneer u deelneemt aan het onderzoek dan betekent dit dat wij uw (medische) gegevens verzamelen en gebruiken. Welke gegevens dat zijn en hoe wij deze gegevens verzamelen, gebruiken en beschermen leest u in paragraaf 7 en 8.

Daarnaast verzamelen en gebruiken wij uw lichaamsmateriaal. Welk lichaamsmateriaal dat is, hoe en waarom wij dit verzamelen, gebruiken en beschermen, leest u hieronder in paragraaf 7 en 8.

4. Hoe verloopt het onderzoek?

Hoelang duurt het onderzoek?
Doet u mee met het onderzoek? Dan duurt dat maximaal 90 minuten per bezoek. Het is mogelijk meerdere keren per jaar te worden uitgenodigd voor dit onderzoek.

Stap 1: bent u geschikt om mee te doen?

Let op: het kan voorkomen dat u gezond bent, maar dat u toch niet geschikt bent om mee te doen. De onderzoeker zal u daar meer over vertellen

Voor aanvang van de MRI scan zal de onderzoeker het volgende doen:

- doorspreken van vragen uwerzijds en ondertekenen van het toestemmingsformulier;
- controle op veiligheid voor het MRI-onderzoek;
- uitleg over de MRI-scan;
- indien nodig een infuusnaald laten aanbrengen voor het toedienden van contrast en/of het afnemen van een kleine hoeveelheid bloed.

Stap 2: De MRI scan

Voor het onderzoek is het nodig dat u maar de afdeling Radiologie &nucleaire Geneeskunde in het ErasmusMC komt. Een bezoek duurt maximaal 90 minuten.

We doen de volgende onderzoek:

- Een MRI scan
- In sommige gevallen wordt er contrastvloeistof toegediend. Dit wordt vooraf aan u gevraagd. Uw toestemming wordt hiervoor gevraagd.
- In sommige gevallen wordt er bloed afgenomen voor het bepalen van het Hematocriet.
- Dit wordt vooraf aan u gevraagd. Uw toestemming wordt hiervoor gevraagd. Daarvoor neemt de onderzoeker per keer 1 buisje bloed af.

Wij nemen maximaal 15 ml bloed bij u af. Deze hoeveelheid geeft bij volwassenen geen problemen.
Ter vergelijking: iemand die bloed geeft bij de bloedbank, geeft per keer 500 ml bloed.

Voor de standaard MRI-scans hoeft u niets anders te doen dan stil te liggen in de scanner en eventueel uw adem gedurende korte periodes in te houden.

5. Welke afspraken maken we met u?

We willen graag dat het onderzoek goed verloopt. Daarom maken we de volgende afspraken met u

- U komt op tijd naar de afspraak

of contact op te nemen met de onderzoeker wanneer:

- U niet meer in de gelegenheid bent op de afspraak te komen;
- U niet meer wenst mee te doen aan het onderzoek;
- Uw telefoonnummer of e-mailadres verandert.

Vrouwen die zwanger zijn kunnen niet meedoen aan dit onderzoek.

6. Van welke bijwerkingen, nadelige effecten of ongemakken kunt u last krijgen?

Bij een aantal studies zal contrastmiddel worden toegediend en bloed worden afgenomen. Hiervoor wordt apart toestemming gevraagd.

De bijwerkingen van het contrastmiddel zijn zeldzaam en zijn o.a. het optreden van hoofdpijn, misselijkheid, jeuk en huiduitslag. In ernstige gevallen kunnen een allergische reactie en/of shock optreden na gebruik van contrastmiddel.

De bijwerkingen treden in veel gevallen direct na het toedienen van het contrasttoediening op.

Daarom dient u na de toediening van het contrasttoediening nog een half uur in het ziekenhuis te blijven ter controle.

Het gebruik van het contrastmiddel is echter relatief veilig aangezien een allergische reactie of shock zelden worden waargenomen, namelijk in minder dan 0.02% van alle onderzoeken waarbij een contrastmiddel gebruikt wordt.

Op de plaats waar u de injectie met het contrastmiddel heeft gehad kan een tijdelijke gevoelige plek ontstaan, met soms wat zwelling of het ontstaan van een blauwe plek. Zeer sporadisch ontstaat hier een ontsteking.

7. Wat zijn de voordelen en de nadelen als u meedoet aan het onderzoek?

Meedoen aan het onderzoek kan voordelen en nadelen hebben. Hieronder zetten we ze op een rij. Denk hier goed over na, en praat erover met anderen.

U heeft zelf geen voordeel van deelname aan dit onderzoek. Door uw deelname levert u echter wel een belangrijke bijdrage aan het verbeteren van MRI onderzoek ten behoeve van patiëntenzorg en wetenschappelijk onderzoek

De MRI-scan is volledig onschadelijk, er wordt geen gebruik gemaakt van straling. Wel is het zo, dat de MRI scanner zelf een vrij nauwe tunnel is waarin u 90 minuten ligt, waardoor deze niet geschikt is voor mensen die last hebben van engtevrees (claustrofobie).

Ook maakt de MRI scanner tijdens de opnamen veel lawaai. U moet hierom ook oordoppen in doen of een koptelefoon opzetten. Een nadeel van dit onderzoek is, dat deelname aan dit onderzoek in totaal ongeveer 2 uur van uw tijd zal kosten (naast eventuele reistijd). Als u daarna besluit opnieuw mee te willen doen, zal dit elke keer 2 uur van uw tijd vragen. Wanneer u besluit niet deel te nemen aan dit onderzoek, zal dit op geen enkele manier uw eventuele toekomstige behandeling in ons ziekenhuis benadelen.

8. Wanneer stopt het onderzoek?

De onderzoeker laat het u weten als er nieuwe informatie over het onderzoek komt die belangrijk voor u is.

In deze situaties stopt voor u het onderzoek:

- Na het voltooien van de MRI scan.
- U wilt zelf stoppen met het onderzoek. Dat mag op ieder moment. Meld dit dan meteen bij de onderzoeker. U hoeft er niet bij te vertellen waarom u stopt
- Een van de volgende instanties besluit dat het onderzoek moet stoppen:
    - ErasmusMC
    - de overheid, of
    - de medisch-ethische commissie die het onderzoek beoordeelt.

Wat gebeurt er als u stopt met het onderzoek?
De onderzoekers gebruiken de gegevens en het lichaamsmateriaal (het bloed indien van toepassing die tot het moment van stoppen zijn verzameld. Als u wilt, kan verzameld lichaamsmateriaal worden vernietigd. Geef dit door aan de onderzoeker.

9. Wat gebeurt er na het onderzoek?

Krijgt u de resultaten van het onderzoek?
De onderzoeker zal u niet verder informeren over het verloop van het onderzoek.

10. Wat doen we met uw gegevens en lichaamsmateriaal?

Doet u mee met het onderzoek? Dan geeft u ook toestemming om uw gegevens en lichaamsmateriaal te verzamelen, gebruiken en bewaren.

Welke gegevens bewaren we?
We bewaren deze gegevens:
- uw naam
- uw geslacht
- uw geboortedatum
- beelden van het MRI-onderzoek
- (medische) gegevens die we tijdens het onderzoek verzamelen

Welk lichaamsmateriaal bewaren we?
We verzamelen en gebruiken, indien nodig voor het onderzoek, een buisje bloed. Het verzamelde bloed wordt na gebruik niet bewaard maar direct vernietigd.

Waarom verzamelen, gebruiken en bewaren we uw gegevens en lichaamsmateriaal?
We verzamelen, gebruiken en bewaren uw gegevens en uw lichaamsmateriaal om de vragen van dit onderzoek te kunnen beantwoorden. En om de resultaten te kunnen publiceren. Gegevens en/of lichaamsmateriaal kunnen worden gebruikt door de opdrachtgever voor het uitvoeren van de studie.

Hoe beschermen we uw privacy?
Om uw privacy te beschermen geven wij uw gegevens en uw lichaamsmateriaal een code. Op al uw gegevens en lichaamsmateriaal zetten we alleen deze code. De sleutel van de code bewaren we op een beveiligde plek in het ziekenhuis. Als we uw gegevens en lichaamsmateriaal verwerken, gebruiken we steeds alleen die code. Ook in rapporten en publicaties over het onderzoek kan niemand terughalen dat het over u ging.

Wie kunnen uw gegevens zien?
Sommige personen kunnen wel uw naam en andere persoonlijke gegevens zonder code inzien. Dit kunnen gegevens zijn die speciaal voor dit onderzoek zijn verzameld, maar ook gegevens uit uw medisch dossier.

Dit zijn mensen die controleren of de onderzoekers het onderzoek goed en betrouwbaar uitvoeren. Deze personen kunnen bij uw gegevens komen:

- Leden van de commissie die de veiligheid van het onderzoek in de gaten houdt.
- Een controleur die door de onderzoeker is ingehuurd
- Nationale en internationale toezichthoudende autoriteiten
- De medewerkers van het onderzoeksteam

Deze personen houden uw gegevens geheim. Voor inzage door deze personen vragen wij u toestemming te geven. De Inspectie Gezondheidszorg en Jeugd kan zonder uw toestemming uw gegevens inzien.

Hoelang bewaren we uw gegevens en lichaamsmateriaal?
We bewaren uw gegevens 15 jaar in het ziekenhuis.
Uw lichaamsmateriaal bewaren we in het ziekenhuis. Het wordt 15 jaar bewaard om daarop in de loop van dit onderzoek nog nieuwe bepalingen te kunnen doen die te maken hebben met dit onderzoek. Zodra dit niet meer nodig is, vernietigen we uw lichaamsmateriaal.

Mogen we uw gegevens en lichaamsmateriaal gebruiken voor ander onderzoek?
Uw verzamelde gegevens en uw (overgebleven) lichaamsmateriaal kunnen ook van belang zijn voor ander wetenschappelijk onderzoek op het gebied van het ontwikkelen van nieuwe MRI technieken . Daarvoor zullen uw gegevens en lichaamsmateriaal 15 jaar worden bewaard in het ziekenhuis. In het toestemmingformulier geeft u aan of u dit goed vindt. Geeft u geen toestemming? Dan kunt u nog steeds meedoen met dit onderzoek.

Wat gebeurt er bij onverwachte ontdekkingen?
Bij een MRI-scan kunnen we toevallig iets vinden dat niet direct van belang is voor het onderzoek maar wel voor uw gezondheid. De onderzoeker neemt dan contact op met uw huisarts. U bespreekt dan met uw huisarts of specialist wat er moet gebeuren. De kosten hiervan vallen onder uw eigen zorgverzekering.

Een normale scan betekent dus niet dat er zeker geen afwijkingen aanwezig zijn. Wanneer u niet wilt dat toevalsbevindingen van de MRI-scan of bloedafname aan uw huisarts worden medegedeeld, kunt u niet meedoen aan het onderzoek.

Kunt u uw toestemming voor het gebruik van uw gegevens weer intrekken?
U kunt uw toestemming voor het gebruik van uw gegevens op ieder moment intrekken. Zeg dat dan tegen de onderzoeker. Dit geldt voor het gebruik in dit onderzoek en voor het gebruik in ander onderzoek. Maar let op: trekt u uw toestemming in, en hebben onderzoekers dan al gegevens verzameld voor een onderzoek?
Dan mogen zij deze gegevens nog wel gebruiken. Voor uw lichaamsmateriaal geldt dat de onderzoekers dit vernietigen nadat u uw toestemming intrekt. Maar zijn er dan al metingen gedaan met uw lichaamsmateriaal? Dan mag de onderzoeker de resultaten daarvan blijven gebruiken.

We sturen uw gecodeerde gegevens naar landen buiten de Europese Unie
In dit onderzoek sturen we uw gecodeerde gegeven ook naar landen buiten de Europese Unie. In die landen gelden niet de privacyregels van de Europese Unie. Maar uw privacy zal op een gelijkwaardig niveau worden beschermd of wij vragen hiervoor uw toestemming.

Het betreft hier de fabrikant van de MRI scanner en de nieuwe en aangepaste software en met onderzoekers van een samenwerkende universiteit die de gemaakte MRI beelden verwerken, beide in de Verenigde Staten
Als u toestemming geeft kunnen we uw geanonimiseerde gegevens delen met andere onderzoeksinstituten, non-profit en of industriële partners in Nederland of in andere landen binnen of buiten de Europese Unie (EU) waar we mee samen werken.

Dit doen we bijvoorbeeld om meer gegevens te verzamelen voor het onderzoek of om de uitkomsten van behandelingen of manier van beeldvorming te vergelijken en mogelijk te optimaliseren.

Wij vragen u op het toestemmingsformulier apart toestemming voor het doorsturen van uw geanonimiseerde beelden. Wanneer u die toestemming niet geeft, kunt u toch meedoen met dit onderzoek

Wilt u meer weten over uw privacy?

- Wilt u meer weten over uw rechten bij de verwerking van persoonsgegevens? Kijk dan op www.autoriteitpersoonsgegevens.nl.
- Heeft u vragen over uw rechten? Of heeft u een klacht over de verwerking van uw persoonsgegevens? Neem dan contact op met degene die verantwoordelijk is voor de verwerking van uw persoonsgegevens. Voor uw onderzoek is dat:
    - ErasmusMC Zie bijlage A voor contactgegevens, en website.
- Als u klachten heeft over de verwerking van uw persoonsgegevens, raden we u aan om deze eerst te bespreken met het onderzoeksteam. U kunt ook naar de Functionaris Gegevensbescherming van het EerasmusMC gaan. Of u dient een klacht in bij de Autoriteit Persoonsgegevens.

Waar vindt u meer informatie over het onderzoek?
Op de volgende website(s) vindt u meer informatie over het onderzoek.
www.ClinicalTrials.gov Na het onderzoek kan de website een samenvatting van de resultaten van dit onderzoek tonen.

11. Krijgt u een vergoeding als u meedoet aan het onderzoek?

De MRI scan voor het onderzoek kost u niets. Voor het meedoen aan dit onderzoek krijgt u een onkostenvergoeding van €10 per 30 minuten doorgebracht in de MRI scanner. Daarnaast krijgt u een vergoeding van de reiskosten.

12. Bent u verzekerd tijdens het onderzoek?

Voor iedereen die meedoet aan dit onderzoek is een verzekering afgesloten. De verzekering betaalt voor schade door het onderzoek. Maar niet voor alle schade. In **bijlage B** vindt u meer informatie over de verzekering en de uitzonderingen. Daar staat ook aan wie u schade kunt melden.

13. Heeft u vragen?

Vragen over het onderzoek kunt u stellen aan de onderzoeker Wilt u advies van iemand die er geen belang bij heeft? Ga dan naar de onafhankelijk deskundige, voor contactgegevens zie bijlage A. Hij weet veel over het onderzoek, maar werkt niet mee aan dit onderzoek. Heeft u een klacht? Bespreek dit dan met de onderzoeker of de arts die u behandelt. Wilt u dit liever niet? Ga dan naar de klachtenfunctionaris. In bijlage A staat waar u die kunt vinden.

14. Hoe geeft u toestemming voor het onderzoek?

U kunt eerst rustig nadenken over dit onderzoek. Daarna vertelt u de onderzoeker of u de informatie begrijpt en of u wel of niet wilt meedoen. Wilt u meedoen? Dan vult u het toestemmingsformulier in dat u bij deze informatiebrief vindt. U en de onderzoeker krijgen allebei een getekende versie van deze toestemmingsverklaring.

Dank voor uw tijd.

Met vriendelijke groet,
Mede namens het onderzoeksteam.

Prof. dr. E.H.G Oei

16. Bijlagen bij deze informatie

A. Contactgegevens
B. Informatie over de verzekering
C. Toestemmingsformulier
D. Algemene MRI informatiefolder

Bijlage A: contactgegevens

Hier de gegevens van de hoofdonderzoeker, andere onderzoekers, de klachtenfunctionaris en de Functionaris Gegevensbescherming vermelden met de contactgegevens, zoals e-mailadres en telefoonnummer.

Hoofdonderzoeker:	Prof. dr. E.H.G. Oei
Telefoonnummer:	010-7042006
Onafhankelijk deskundige	Dr. H. Ahmad
Telefoonnummer:	010-7032886

Klachten:

Indien u niet tevreden bent over het onderzoek of de behandeling, kunt u terecht bij de onafhankelijke klachtenopvang/klachtenfunctionaris van het Erasmus MC.

Op de website van het Erasmus MC is een Digitaal klachtenformulier beschikbaar via https://www.erasmusmc.nl/nl-nl/patientenzorg/klachtenopvang-en-klachtenbemiddeling

Na het invullen wordt het formulier automatisch verzonden naar de klachtenfunctionaris.

Als het niet lukt om het digitale klachtenformulier in te vullen, dan kunt u uw klacht ook per post versturen: Erasmus MC, Secretariaat Klachtenopvang (GK-745), Antwoordnummer 55, 3000 WB Rotterdam.

Vermeld in de brief uw naam, patiëntnummer (indien van toepassing), naam van het onderzoek en contactgegevens.

Na ontvangst van de brief zal de klachtenfunctionaris contact met u opnemen

Functionaris Gegevensbescherming:

De Functionaris voor de Gegevensbescherming van het Erasmus MC is bereikbaar via het secretariaat van de afdeling Juridische Zaken. E-mail:
functionaris.gegevensbescherming@erasmusmc.nl Tel: 010-703 4986

Uw rechten:

Voor meer informatie over uw rechten:
Voor meer informatie of bij vragen over uw rechten kunt u contact opnemen met de functionaris voor de Gegevensbescherming of met de Autoriteit Persoonsgegevens.

Bijlage B: informatie over de verzekering

Het ErasmusMC heeft een verzekering afgesloten voor iedereen die meedoet aan het onderzoek.
De verzekering betaalt de schade die u heeft doordat u aan het onderzoek meedeed. Het gaat om schade die u krijgt tijdens het onderzoek, of binnen 4 jaar na het einde van uw deelname aan het onderzoek.

U moet schade binnen 4 jaar melden bij de verzekeraar.

Heeft u schade door het onderzoek? Meld dit dan bij deze verzekeraar:

De verzekeraar van het onderzoek is:

Naam verzekeraar: Centramed B.A.
Adres: Postbus 7374 2701 AJ Zoetermeer
Telefoonnummer: 070 301 70 70
E-mail: schade@centramed.nl
Polisnummer: 624.100.042

De verzekering betaalt maximaal €650.000 per proefpersoon en €5.000.000 voor het hele onderzoek en €7.500.000 per jaar per jaar voor alle onderzoeken van dezelfde opdrachtgever.

Let op: de verzekering dekt de volgende schade **niet**:

- Schade door een risico waarover we u informatie hebben gegeven in deze brief. Maar dit geldt niet als het risico groter bleek te zijn dan we van tevoren dachten. Of als het risico heel onwaarschijnlijk was.
- Schade aan uw gezondheid die ook zou zijn ontstaan als u niet aan het onderzoek had meegedaan.
- Schade die ontstaat doordat u aanwijzingen of instructies niet of niet goed opvolgde.
- Schade aan de gezondheid van uw kinderen of kleinkinderen.
- Schade door een behandelmethode die al bestaat. Of door onderzoek naar een behandelmethode die al bestaat.

Deze bepalingen staan in het 'Besluit verplichte verzekering bij medisch-wetenschappelijk onderzoek met mensen 2015'. Dit besluit staat in de Wettenbank van de overheid (https://wetten.overheid.nl).

Bijlage C: toestemmingsformulier proefpersoon

Behorende bij
Ontwikkeling van MRI technologie voor verbeterde visualisatie en kwantificatie van weefsels en organen van gezonde vrijwilligers

- Ik heb de informatiebrief gelezen. Ook kon ik vragen stellen. Mijn vragen zijn goed genoeg beantwoord. Ik had genoeg tijd om te beslissen of ik meedoe.
- Ik weet dat meedoen vrijwillig is. Ook weet ik dat ik op ieder moment kan beslissen om toch niet mee te doen met het onderzoek. Of om ermee te stoppen. Ik hoef dan niet te zeggen waarom ik wil stoppen.
- Ik geef de onderzoeker toestemming om mijn huisarts of specialist informatie te geven over onverwachte bevindingen uit het onderzoek die van belang zijn voor mijn gezondheid.
- Ik geef de onderzoekers toestemming om mijn gegevens te verzamelen en te gebruiken. De onderzoekers doen dit alleen om de onderzoeksvraag van dit onderzoek te beantwoorden.
- Ik weet dat mijn bloed niet zal worden opgeslagen in een biobank.
- Ik weet dat voor de controle van het onderzoek sommige mensen al mijn gegevens kunnen inzien. Die mensen staan in deze informatiebrief. Ik geef deze mensen toestemming om mijn gegevens in te zien voor deze controle.
- Ik weet dat mijn gecodeerde gegevens naar landen buiten de EU worden gestuurd waar privacyregels van de EU niet gelden. Ik weet dat er voor mijn gegevens een gelijkwaardig beschermingsniveau is afgesproken.
- **Wilt u in de tabel hieronder ja of nee aankruisen?**

Ik geef toestemming om mijn gegevens te bewaren om dit te gebruiken voor ander onderzoek, zoals in de informatiebrief staat.	Ja ☐	Nee☐
Ik geef toestemming om mijn geanonimiseerde gegevens te delen met andere onderzoeksinstituten, non-profit en of industriële partners in Nederland of in andere landen binnen of buiten de Europese Unie (EU) waar wij mee samenwerken.	Ja ☐	Nee☐
Ik geef toestemming om contrastmiddel toe te dienen	Ja ☐	Nee☐
Ik geef toestemming om bloed uit het infuus af te laten nemen voor bepaling van het hematocriet.	Ja ☐	Nee☐
Ik geef toestemming om mij eventueel na dit onderzoek te vragen of ik wil meedoen met een vervolgonderzoek.	Ja ☐	Nee☐

- Ik wil meedoen aan dit onderzoek.

Mijn naam is (proefpersoon): ……..
Handtekening: …… Datum : __ / __ / __

Ik verklaar dat ik deze proefpersoon volledig heb geïnformeerd over het genoemde onderzoek.

Wordt er tijdens het onderzoek informatie bekend die die de toestemming van de proefpersoon kan beïnvloeden? Dan laat ik dit op tijd weten aan deze proefpersoon.

Naam onderzoeker (of diens vertegenwoordiger):…….
Handtekening:…… Datum: __ / __ / __

D

Screening Form

Screeningsformulier MRI onderzoek (voor patiënten en begeleiders).
Het sterke magneetveld van het MRI is, voor zover bekend, in de meeste gevallen onschadelijk. I sommige gevallen kan het echter schadelijk zijn. Om eventuele risico's uit te sluiten en i.v.m. de voorbereiding voor het onderzoek verzoeken wij u onderstaande lijst zorgvuldig in te vullen, te ondertekenen, mee te nemen, en in te leveren bij de laborant. Wanneer u één of meerdere vrage met ja heeft beantwoord of bij twijfel neemt u dan contact op met de MRI-kamer. Telefoonnumme 010 - 70 4 20 06 (op werkdagen tussen 08:00-16:30 uur). Kruis ja aan bij twijfel.

Bent u:

in de afgelopen 6 weken geopereerd	O Ja	O Nee
Zo ja, waar aan		
in het verleden geopereerd waarbij metaal is achtergelaten	O Ja	O Nee
Zo ja, waaraan en wat		
ergens overgevoelig voor(bv. antibiotica, contrastmiddelen)?	O Ja	O Nee
Zo ja, waarvoor		
Wat voor reactie heeft u gehad?		

Heeft u:?

een medische behandeling ondergaan in het buitenland, waarbij metaal is ingebracht?	O Ja	O Nee
Zo ja, in welk ziekenhuis en wat is er ingebracht?		
clips(bv. in het hoofd)/stents na operatie van de bloedvaten	O Ja	O Nee
Zo ja, wat, wanneer en in welk ziekenhuis is het geplaatst?		
een kunsthartklep	O Ja	O Nee
Zo ja, wanneer en in welk ziekenhuis is het geplaatst?		
(mogelijk) metaalsplinters in uw ogen bv. door werkzaamheden met metaal?	O Ja	O Nee
een pacemaker, pacemakerdraden of een ICD	O Ja	O Nee
één of meer metalen oorbuisjes	O Ja	O Nee
een kunstlens waarbij metalen clips gebruikt zijn	O Ja	O Nee
een gehoorapparaat dat niet te verwijderen is	O Ja	O Nee
een niet te verwijderen apparaat in of op het lichaam (bv. insulinepomp, neurostimulator, hydrocephaluspomp, tissue-expander)?	O Ja	O Nee
gebitsprothesen met magnetisch kliksysteem en prothesen met slotje	O Ja	O Nee
metaal (bv. kunstgewrichten, fixatiepennen, metalen tube, halovest) in of op het lichaam zitten?	O Ja	O Nee
Zo ja, wat en waar?		
last van nierinsufficiëntie(slechte nierfunctie)	O Ja	O Nee
Zo ja, maakt u gebruik van nierdialyse?	O Ja	O Nee
last van COPD (astma,ed.)?	O Ja	O Nee
een piercing die niet te verwijderen is	O Ja	O Nee
een tatoeage	O Ja	O Nee
last van claustrofobie (angst voor kleine ruimtes)	O Ja	O Nee

Wat is Uw gewicht	kg
Wat is uw lengte (alleen bij een MRI-hart)	m

Alleen voor vrouwen

Bent u zwanger of bestaat er een kans dat u zwanger bent?	O Ja	O Nee
Zo ja, hoeveel weken		
Geeft u momenteel borstvoeding?	O Ja	O Nee

Naam en handtekening van de persoon die dit formulier heeft ingevuld
Naam + voorletters:
Geboortedatum:
Relatie tot de patiënt:
Datum + Handtekening:

Voor de onderzoeker
Formuliergegevens gecontroleerd door:
□ MRI-Laborant □ Student □ Radioloog Datum: